STRAY LOAD LOSSES IN INDUCTION MACHINES

By

A. A. JIMOH, B. Eng., M. Eng., MIEEE

A Thesis

Submitted to the School of Graduate Studies

in Partial Fulfilment of the Requirements

for the Degree

Doctor of Philosophy

March 1986

STRAY LOAD LOSSES IN INDUCTION MACHINES

DOCTOR OF PHILOSOPHY (1986) McMASTER UNIVERSITY

(Electrical & Computer Engineering) Hamilton, Ontario

TITLE: Stray Load Losses in Induction Machines

AUTHOR: Abdul-Ganiyu Adisa Jimoh, B. Eng. (Ahmadu Bello University)
M. Eng. (Ahmadu Bello University)

SUPERVISOR: Dr. R. D. Findlay

NUMBER OF PAGES: xxi, 223

ABSTRACT

Understanding and minimizing loss are the main objectives of seeking solutions to the problems of stray loss in induction machines. This thesis contributes towards this objective by addressing the various problems of stray load loss. These problems include the questions of definition, origin, components, and effects; theoretical and experimental means of evaluation; and loss reduction.

Insights into these problems are achieved through a comprehensive review of the state of the art of the subject. We have established that some commonly used terminologies in the subject area formed major obstacles to progress in definition.

A conceptually simple and general theory of squirrel cage induction machines is presented. The theory results in a set of linear periodic differential equations, which has an infinite number of possible solutions. A suitable solution procedure is developed.

Means for accounting for slot openings and saturation are developed. These have enabled various field waveforms in a practical machine to be generated and analyzed. The analysis produced insights into the interactions of harmonics and how harmonics contribute to stray load losses. Through this, an approximate means of separating a saturated non-sinusoidal waveform of an air gap flux density waveform into its fundamental, saturation, and other space harmonics is developed.

An expression for determining the machine torque is derived. This torque expression, the ideas for manipulating and analyzing the field waveforms, and the presented theory are structured into an algorithm, modeling the behaviours of squirrel cage induction machines. The algorithm enabled the torque-speed characteristic of a practical machine to be predicted.

The predicted characteristic is compared with that measured by means of accelerometer. The fact that it compares very well validates the theory and the developed model. The new steady state model has several advantages, including its easy application to the study and the evaluation of stray load losses. A brief study of how harmonics influence the developed torque is also conducted using the new model.

Two theoretical methods are developed for predicting stray load loss at the design, manufacturing, or utilization stage of a machine. These methods, which employ the developed model, are applied to a practical machine.

The predicted stray losses are compared with the measured, and that predicted using the nominal assignation technique. This draws attention to the need for experimental investigation of the subject. Consequently, two experiments, calorimetric method and novel experiment to study inter-bar current problem, are developed. Due to technical and economic problems, however, their implementation are not yet completed.

ACKNOWLEDGEMENTS

I would like to express my appreciation to my supervisor Dr. R. D. Findlay for his support and encouragement. I would like to thank the other members of my supervisory committee; Drs. R. T. H. Alden and B. Latto.

I have been very fortunate in having an informal association with a distinguished and humble intellectual Professor Michel Poloujadoff. His encouragement and many suggestions have contributed greatly to the success of this work. Mr. Grant Neal of the Motor Division of Westinghouse (Canada) Limited is gratefully acknowledged for his co-operation and encouragement. I would also like to thank a very good friend, Prof. Raymond Xu for his contributions.

The financial supports of Ahmadu Bello University, Zaria, Nigeria, through an award of a study fellowship; Canadian Government, through Canadian Commonwealth Scholarship and Fellowship Program; and McMaster University are deeply appreciated. I would like to thank Dr. Jennifer Conners, Miss Edna Menzies, Miss Elsie Lavery, Marion and Perry Wilson, Mr. Derrick Folbigg, the Philpott Memorial Church, and the organizers of the International Student Fellowship activities for making my family and I feel at home in Canada. Their friendship and love will forever be remembered.

Special thanks should go to Mrs. Maureen McCracken for making the beautiful drawings, and Mr. Dan McCracken, Dr. Jennifer Conners, and

Mr. Francis Omani for proof reading this thesis. The friendship of close associates Mr. Rajeev Krishnamurthi, Mr. Francis Omani, Dan and Maureen McCracken, Mr. Pierre Gauthier, and Mr. Gerry Brown are deeply appreciated. I would like to thank Mrs. Lynda Chapple for her diligence and cheerful co-operation in typing this manuscript. Last, but definitely not the least, I would like to thank my children, Bukola and Ademola, and my Wife, Gbemisola, for their patience and support.

TABLE OF CONTENTS

ABSTRACT iii

ACKNOWLEDGEMENTS v

LIST OF PRINCIPAL SYMBOLS xi

LIST OF FIGURES xvi

LIST OF TABLES xix

LIST OF PLATES xxi

CHAPTER 1: INTRODUCTION 1

1.1 General Description of the Problem 2
1.2 Organization of the Thesis 4

CHAPTER 2: COMPREHENSIVE REVIEW OF THE PHENOMENA ASSOCIATED WITH STRAY LOAD LOSS 8

2.1 Background 8
2.1.1 Definition 8
2.1.2 Origin and Components 9
2.1.3 Effects of Stray Load Losses 11

2.2 Present Methods of Measurement of Stray Load Losses 18
2.2.1 Full-Load Tests 18
2.2.2 Light Load Tests 24

2.3 Calculation of Stray Load Losses: A Review of the State of the Art 26
2.3.1 Stray Load Losses in the Windings 26
2.3.2 End-Leakage Losses 31
2.3.3 Additional Losses in the Tooth Body, Surface and the Core 37
2.3.4 Skew-Leakage Losses 38
2.3.5 Stray Load Losses Due to Interbar Currents 38
2.3.6 Saturation

2.4 Other Approaches to the Study of Stray Load Losses 40

2.5 Current Methods for Reduction of Stray Load Losses 41
2.5.1 Reduction of Losses in Conductors 42
2.5.2 Reduction of Losses in the End Region 43
2.5.3 Reduction of Harmonics and their Magnitudes 45
2.5.4 Industrial Imperfection 47
2.5.5 Others 48

CHAPTER 3 MODEL DEVELOPMENT 50

3.1 Introduction 50
3.1.1 Definition of the Problem 51

3.2 Stator 54

3.3 Rotor 60
3.3.1 Induced E.M.F. in a Rotor Mesh by the Stator Fields 60
3.3.2 Induced E.M.F. in a Rotor Mesh by the Rotor Fields 63
3.3.3 Induced Currents in the Rotor Winding 64
3.3.4 An Alternative Formulation 73

3.4 Solution of the Machine Equation 79

3.5 Effects of Slot Openings 87

3.6 Effects of Saturation 88
3.6.1 Effects of Saturation of the Core 89
3.6.2 Effects of Saturation of the Teeth Body 89
3.6.3 Effects of Saturation of the Teeth Tips 94

3.7 The Machine Equations 99

CHAPTER 4 WAVEFORMS AND HARMONICS: THEIR INFLUENCE ON STRAY LOAD LOSS 104

4.1 Magnetic Field of Stator 104
4.1.1 Stator Fields with Effect of Slot Openings 111
4.1.2 Stator Fields with Effects of Saturation 121

4.1.3 Stator Fields with Effects of Both Stator and Rotor Slot Openings and Saturation 129

4.2 Magnetic Fields of the Rotor 131
4.2.1 The Rotor Impedances 131
4.2.2 Magnetic Field of the Rotor 133

4.3 Overall Resultant Air-Gap Field 134

4.4 Discussions: Harmonics and Stray Load Losses 140

CHAPTER 5: PREDICTION AND MEASUREMENT OF TORQUE 149

5.1 Derivation of an Expression for Electromagnetic Torque 150

5.2 Torque-Time, and Torque-Speed Characteristics 153

5.3 Effects of Harmonics 157
5.3.1 Analysis of the Torque Equation 163

5.4 The Measurement of Torque-Speed Characteristics 169
5.4.1 Comparison of Predicted and Measured Torques 173

CHAPTER 6: PREDICTION TECHNIQUES FOR STRAY LOAD LOSS 174

6.1 General Concept of Losses in Squirrel-Cage Induction Machine 175

6.2 Method 1 for Predicting Stray Load Loss 179
6.2.1 A Criticism of the Conventional Method of Estimating Total Load Loss 179
6.2.2 The Proposed Method 181

6.3 Method 2 for Predicting Stray Load Loss 182
6.3.1 Estimation of Rotor Conductor Loss 182
6.3.2 The Proposed Method 184

6.4 Measurement of Stray Load Loss 188
6.4.1 Results and Comparison 192

CHAPTER 7: CONCLUSIONS 196

7.1 Suggestions for Further Works 202

REFERENCES 204

APPENDIX A A FAST FOURIER TRANSFORM ALGORITHM 212

APPENDIX B CALCULATION OF THE ROTOR BAR IMPEDANCE PARAMETERS 214

B.1 Resistance 214

B.2 Reactances 215

B.3 Skin-Effect 216

APPENDIX C A BRIEF DISCUSSION OF THE DEVELOPED EXPERIMENTS 218

LIST OF PRINCIPAL SYMBOLS

A	Cross-sectional area
B	Flux density
$B_{m\nu}$	Maximum νth harmonic flux density
D	Rotor diameter
e	Instantaneous electromotive force (e.m.f.)
f	supply frequency
F	Magneto-motive force (m.m.f.)
H	Magnetic field intensity
i	Instantaneous current
i_{sm}	Stator's mth phase instantaneous current
I_1	Stator r.m.s. current per phase
I_s	Maximum value of stator current
I_m	Magnetizing current
I_c	Conductor current
J	Rotor inertia
J_R	Skin effect factor for resistance
J_x	Skin effect factor for leakage reactance
k_c, ξ	Carter's factor or slot permeance factor
k_s	Saturation factor
K_s	Slot leakage constant
l	Axial length of machine bore
l', l_c	Length of lamination stack

l_b	Length of bar
L	Self inductance
m	Number of phase
m_1	Number of stator phases
M	Mutual inductance
n	Order of harmonic
n_s	Synchronous speed in r.p.s.
N_b	Number of turns per bar
N_c	Number of turns per coil
N_{sc}	Number of conductor per slot
p	Number of poles
P_c	No load core loss
P_{c1}, P_{cus}, P_{scu}	Stator copper loss
P_{c2}, P_{cur}, P_{rcloss}, P_{rcu}	Rotor conductor loss
P_{fw}, P_{f+w}	Friction and windage loss
P_i, P_{in}	Input power
P_m	Mechanical input power or shaft input power
P_o, P_{out}	Output power
P_r	Rotational power
P_{rs}	Rotor stray load power loss
P_{rfe}	Rotor iron loss
P_{sfe}	Stator iron loss
P_{scl}	Stator core loss
P_{seg}	Total power loss for the method of segregation
$P_{rotorff}$	Rotor fundamental frequency loss

$P_{strayff}$	Stator stray loss due to fundamental frequency components
P_{ss}	Stator stray load power loss
P_{stray}	Stray load loss
P_{tl}	Total power loss
Q	Number of slots
Q_1	Number of stator slots
Q_2	Number of rotor slots
r	Mean air gap radius
R_1, r_1	Resistance of a stator winding phase
s	slip
t	Time
T	Torque (chapter 2 only)
T	Time period (1/f)
T_s	Stray load loss torque (chapter 2 only)
u	Order of rotor harmonics
v	Instantaneous applied voltage
w_o	Slot width opening
w_{10}	Stator slot width opening
w_{20}	Rotor slot width opening
x_{es}	Stator end leakage reactance
x_{1s}	Stator leakage reactance
$x_{m\nu}$	Magnetizing reactance
$z_{b\nu}$	νth harmonic bar impedance
$z_{e\nu}$	νth harmonic end-ring segment impedance
α_d	Squirrel-cage winding pitch

β_ν	Phase angle of the νth harmonic component
γ	Electrical conductivity
δ	Air gap length
ϑ	Angular position
μ_o	Permeability of free space
ν	Order of stator harmonics
τ_p	Pole-pitch
τ	Torque
ϑ, φ	Flux
λ	Flux linkage
λ_1	Stator tooth pitch
λ_2	Rotor tooth pitch
ω	Angular velocity
ω_s	Stator angular velocity
ω_r	Rotor angular velocity

SUBSCRIPTS

a, b, c	Stator phases
b	Bar
c	Coil side
e	End-region
ee	Eddy-current in end-region
em	Electromagnetic
fl	Full-load
g	Air-gap
(h+e)	Hysteresis and eddy-current loss components

l	Leakage
nl	No-load
pf	Power factor
r	rotor
r	radial
s	stator
t	turn
t	tangential
u	Rotor harmonic order
ν	Stator harmonic order

LIST OF FIGURES

FIGURE		PAGE
2.1	Torque-Speed Characteristic of a Polyphase Induction Machine	14
3.1	A Simplified conventional equivalent circuit of an induction machine	52
3.2	The chain equivalent circuit	52
3.3	Classification of induction machines parameters and variables	56
3.4	Flux linkages of rotor mesh with air gap flux due to a stator sinusoidal component of the mmf	62
3.5	Circular ladder equivalent network for the squirrel-cage winding	66
3.6	A network model of the squirrel cage winding	74
3.7(a)	Network of squirrel-cage winding: illustration of the flow of current	76a
3.7(b)	Network of squirrel-cage winding: calculation of current in the bars	76a
3.8	Calculation of fictitious opening of a semi-closed slot	96
3.9	Calculation of fictitious opening of a closed slot	98
4.1	Layout of the stator's full-pitch concentric winding	106
4.2	Step distribution of the stator's air-gap flux density distribution	108
4.3	Spectrum of three phase field waveform of figure 4.2(a)	109
4.4	Stator punching	112
4.5	The rotor punching	113

4.6	Stator current vs. effective slot openings	114
4.7	Slots permeance factor distributions and spectral	115
4.8	Stator air gap flux density with slot ripples	117
4.9	B-H magnetization curves	122
4.10	Saturation factor versus MMF	123
4.11	Stator air-gap flux density waveforms with saturation, and their spectral	124
4.12	A study of how saturation influences the air gap field waveforms	126
4.13	Stator air-gap flux density waveforms with saturation and stator and rotor slot ripples	130
4.14	A typical shape of a double cage rotor slot	133a
4.15	An equivalent circuit for the double cage of figure 4.14	133a
4.16	The waveform, and its spectrum, of the rotor air gap flux density with saturation and stator and rotor slot ripples	135
4.17	Saturation factor distribution	138
4.18	The stator, rotor, and the overall resultant air gap flux density waveforms with their spectral	139
4.19	Classification of harmonics in induction motors	141
5.1	Torque versus time	156
5.2	Torque-speed characteristics	158
5.3	Torque vs. time	161
5.4	Block diagram of accelerometer connections	171
6.1	Generalized real power flow in induction motors	185
6.2	Real power flow at no-load	185
6.3	Actual real power flow at full-load	186
6.4	Apparent real power flow at full-load	186

6.5 Set-up for no-load test 189

6.6. Set-up for D.C. test 189

6.7 Set-up for full-load test 190

C.1 Instrumenting machine laminations for the calorimetric method experiment 219

C.2 Instrumenting a rotor lamination for a study of the inter-bar current problem 222

LIST OF TABLES

TABLES		PAGE
2.1	Components of stray load losses as given by Schwarz [4]	12
2.2	Classification of methods for measuring stray load losses	17
2.3	Comparison of measurement approaches	19
3.1	List of Parameters and variables participating in the phenomenon of induction machines	55
4.1	Typical details of a practical squirrel-cage induction machine	105
4.2	Significant harmonics of stator air gap waveforms (Amplitude > 0.1 Tesla)	110
4.3	Effects of non-smooth air-gap on stator air-gap fields	119
4.4	Magnitudes of some harmonics of stator slot ripple	120
4.5	Effects of saturation on stator air gap field	128
4.6	Stator fields and effects of both stator and rotor slot ripples and saturation	132
4.7	Significant harmonics of rotor air gap waveforms (Amplitude > 0.1 Tesla)	136
4.8(a)	Full-load case (I_1 = 26.7A, s=0.0)	143
4.8(b)	Locked-rotor case at locked-rotor current (I_1 = 133.97A, s=1.0)	144
4.8(c)	Locked-rotor case at full-load current (I_1 = 26.7A, s=1.0)	145
4.8(d)	No-load case (I_1 = 7.21A, s=0.0005)	146
5.1	Effects of harmonics	159

5.2 Typical predicted values of some parameters for some harmonics 162

6.1 Comparison of calculated and measured stray load loss 194

LIST OF PLATES

PLATES		PAGE
5.1	Set up for the measurement of torque-speed characteristic	172
6.1	Set up for the full-load test of a squirrel-cage induction motor	191
C.1	Instrumented machine laminations for the calorimetric method experiment	220
C.2	Instrumented rotor lamination for a study of the inter-bar current problem	223

CHAPTER 1

INTRODUCTION

The marketability of an electric machine is now primarily determined by its efficiency. The ruggedness, cheapness, and optimistic possibility of making an induction machine speed and torque variant are responsible for its common usage in most industrial and domestic appliances. Unfortunately these excellent qualities are marred by generally poorer efficiency, in comparison with other types of electric machines. One of the factors responsible for this reduced efficiency of induction machines is stray load loss.

Around the turn of the century, various works were published on the subject of determining the efficiency of a rotating machine accurately and with ease. Two methods, input-output, and loss separation, were often compared. The former is precise but difficult to perform in order to obtain an accurate result; the latter is easy to perform accurately for conventional losses, but the overall result, taking into consideration only these conventional losses, is less accurate. The difference in the results of these two methods came to be known as stray losses.

It was discovered that stray losses are related most closely to the loading of a machine. Hence, they are called stray load losses, or load loss, or unknown losses.

In this chapter the various problems associated with this loss are generally introduced.

1.1 General Description of the Problem

One of the primary problems that confront the machine designer is the predetermination of losses. The losses must be kept low, not only to achieve high efficiency, but also to keep the size of the machine to a minimum. This being the case, the designer is in need both of some means of predicting losses, and of a dependable method for loss measurement. Furthermore, the development of easy and accurate methods of prediction and measurement would permit these losses to be studied more intensively, with the objective of reducing them.

The problems of evaluation of stray load loss in induction machines have long attracted researchers and have been the subject of much literature [1, 2]. The problems have so far not been adequately solved. In 1912, Olin [3] suggested accounting for these losses by empirically relating no-load to load losses. This would have been an appropriate approach if the origin of the losses was distinct, and the phenomena leading to them were linear. But previous works to date have shown that it is difficult enough understanding the origin of these losses in induction machines, let alone comprehending the theory of the process that led to them. Schwartz [4] noted this. In his paper published in 1965, he said that 'there is still considerable confusion on various aspects of stray losses, particularly with regard to their definition and origin'.

Naturally, a knowledge of the definition of what it is to be evaluated is desirable prior to determining a suitable technique for this evaluation. The question of definition as a stray load loss problem arose out of lack of success in developing a direct method for determining this loss. In fact the lack of adequate understanding of the origins and definition of stray losses has resulted in a number of published works which do not give satisfactory results, and which can be definitely misleading unless interpreted correctly.

As reported in the literature, there is a significant difference between the numerical calculation of stray load loss in induction machines and measured results. This difficulty with the problems of evaluation is often considered to lie in the theoretical comprehension of the loss processes in iron: the magnetic induction has components of varying transient frequencies which result in a variation of the permeability with time and locality. While this may be true, it may lead to the conclusion that these problems are generally complicated. It is simpler to ask very fundamental questions of lesser complication: why are the existing models which preclude the consideration of harmonics, or which base the consideration of harmonics on assumptions, inadequate for an accurate prediction of the behaviour of a machine? How much is based on intuition rather than facts?

The failure, so far, in developing a simple, accurate, and reliable means of measurement of stray load loss in induction machines has raised doubt among some researchers of whether at all such measurement techniques exist. Such pessimism is too early to express in

light of the development of modern instrumentation. Furthermore the lack of a clear understanding of the origin and definition of the loss makes it difficult to pursue the development of a measurement technique that is simple and at the same time accurate.

In summary, the problems of stray loss in induction machines are basically:

(i) Addressing and contributing to the questions of definition, origin, components and effects of stray load loss in induction machines.

(ii) Addressing and solving the problems of theoretical or analytical means of evaluation.

(iii) Addressing and solving the problem of measurement.

(iv) Based on the achievements in the foregoing, addressing the questions of understanding and hence loss reduction.

This thesis addresses these problems with particular emphasis on (i) and (ii).

1.2 Organization of the Thesis

An investigative probe into the state of the art of stray loss prediction, with consideration of some questions involving the various aspects of stray load loss in induction machines, is addressed in chapter 2. This chapter starts with background materials, reviewing and addressing the questions of definition, origin, components and effects of stray loss in induction machines. This is followed by an investigation of the present methods of measurement of this loss, then a

review of the state of the art of calculating stray loss in induction machines. Subsequent sections in this chapter are devoted, respectively, to a discussion of other approaches to the study of stray loss, and a review of the current methods of reduction of this loss.

Chapters 3 to 6 address the problems of analysis and solution of the problems of prediction and study of some aspects of machine behaviour. Chapter 3 commences with an explicit analysis of the standard definition. This leads to the realization of the origins of the problem, and hence, forms the basis for the development of a new model of a squirrel-cage induction machine. The development of a new model and the derivation of the associated theory and necessary components for solutions form the subject of discussion later in the chapter. The remainder of the chapter is devoted to a discussion of how the effect of non-smooth air gap and non-linear effects may be accounted for in the model.

In chapter 4, with the aid of the proposed model, some waveforms are generated and their harmonics are studied to determine the behaviours of the waveforms in order to study how the harmonics contribute to stray load loss. Stator air gap magnetic field waveforms, with and without the effects of non-smooth air gap and saturation, are generated and studied at the early part of the chapter. This task is repeated for the rotor and the resultant field waveforms later in the chapter. The chapter concludes with a discussion on harmonics and stray load losses.

Chapter 5 starts with a presentation of the derivation of expressions for the instantaneous and time-average electromagnetic torque of a machine. This is followed by a presentation of an algorithm which simulates the behaviour of an induction machine. This algorithm, which results from the work in chapters 3 and 4 and the derived torque expressions, forms the basis of a technique to obtain the electromagnetic torque - speed and torque - time characteristics, and the parasitic torques of a practical machine. This is followed by an analysis of the torque expression in order to establish an insight into the development of synchronous and asynchronous torques in a machine. The remainder of the chapter is devoted to a discussion of an experimental technique that was performed to verify the predicted torque-speed characteristic. Also included is a comparison of results.

In chapter 6 two new methods which employ the new model for predicting the amount of stray load loss in an induction machine, either at the design, manufacturing or utilization stage, are proposed. Before presenting these, however, the concept of losses in squirrel cage induction machines is generally discussed. The presentation of the proposed ideas for prediction is followed by a presentation of an input-output experiment which was performed to evaluate the amount of stray load loss in a machine, for comparison with results predicted by the newly proposed methods. This chapter concludes with a comparison of results.

Although not yet implemented, two additional sets of experiments were developed in cooperation with Westinghouse (Canada) Limited. These

experiments and the preliminary works which were carried out for their implementation form the main subject of discussion under suggestions for further work in chapter 7. This concluding chapter begins with a discussion of the achievements in this work and how they contribute to the problems of understanding and reduction of stray loss.

CHAPTER 2

COMPREHENSIVE REVIEW OF THE PHENOMENA ASSOCIATED WITH STRAY LOAD LOSS

In this chapter, the current understanding of the various aspects of stray load loss in induction machines is discussed in four parts. The historical search for a definitive evaluation technique for these losses is discussed, together with the recognized criticisms of each approach. The definition, origin, components and effects of these losses are discussed in the first part. These are followed by a review of the various methods of measuring stray load losses in induction machines. In subsequent sections, the current art of predicting stray losses is discussed along with practical means for reducing them in a machine. Most of this work was covered in somewhat less detail by the author in two papers presented at the Summer Power meeting of 1984 [1, 2].

2.1 Background

2.1.1. Definition

A survey of the literature on stray load losses in induction machines reveals that there is considerable disagreement on the definition of these losses. Some definitions, like those given by Alger, et al [5], Olin [3], and Bird [6] are similar to that given in Christofides' paper [7], which essentially is embodied in both American

and British Standards. Christofides gives: "The load losses of an induction motor are defined as the difference between the total power loss of the machine on load and the losses determined by the loss-segregation method. The segregated losses are

(i) friction and windage loss P_{fw} and Stator-Core loss P_{scl} deduced from the no-load test

(ii) stator I^2R loss P_{c1}

(iii) rotor-conductor loss $P_{c2} = s(P_i - 3I_1^2R_1 - P_{scl})$, where s is the slip at full load, P_i the stator input power, and I_1 the stator phase current and R_1 the resistance per phase of the stator winding".

Some authors gave the definition from a particular aspect of the subject. For example, that by Morgan et al [8] reflects the measurement aspect, Schwarz's [4] definition is in terms of the origin of these losses; and Odok's [9] and Christofides' [7] are from the calculational or prediction point of view.

A general observation, however, indicates that each author made his definition compatible with his contributions. This is imperative as most of the problems due to these losses remain relatively unsolved.

2.1.2. Origin and Components

There is general agreement that the following constitute the physical origins of stray load losses in induction machines:

(a) The magnetic property limitations of iron that lead to saturation at load current.

(b) The geometrical structure, i.e. slots, windings, and air gap, around the active region of the machine that lead to (i) space harmonics due to such effects as ripple and tooth pulsation, and (ii) leakage flux.

(c) Industrial imperfection - the most prominent of which is cross-bar currents due to imperfect insulation of the squirrel cage rotor bars.

The components of stray load losses are reasonably well established. However, the different ways which they are presented are often confusing, and hence it may seem as if the implications are different too. Three major reasons can be immediately associated with this:

1. The confusion that arises from the use of the terms 'leakage flux' and 'harmonics'.
2. The confusion that arises from the inter-usage of the terms 'differential leakage', 'zig-zag and phase-belt leakage', and 'air gap leakage' even though they are the same [6, 10].
3. The confusion in identifying the components that constitute differential leakage, or zig-zag and phase-belt, or air gap leakage fluxes - i.e. the difficulties in identifying with their physical concepts.

No standard list of the components of load losses in induction machines exists, but an example as given by Schwarz [4] is as shown in

table 2.1. Chalmers and Williamson [11] give:

"Fundamental-frequency components:

(a) Eddy-current losses in stator conductors owing to stator slot-leakage flux.

(b) Losses in end-region copper, steel and other metallic parts owing to end-region leakage fluxes.

(c) In machines with skewed rotor slots, a small loss at the ends of the stator core owing to skew leakage flux produced by the relative phase displacement of stator and rotor fundamental m.m.f. waves.

High-frequency components:

(a) Induced losses in the rotor due to m.m.f. harmonics produced by the stator load current. Note that pulsations in the main flux due to slot openings are produced on no-load and their effect is included in the iron loss measured running light. These losses are therefore not included in the stray load losses.

(b) Induced losses in the stator due to rotor m.m.f. harmonics".

2.1.3. Effects of Stray Load Losses

Stray losses have five detrimental effects on the performance of an induction machine:

(i) heating

(ii) torque loss

(iii) acceleration and retardation effects

(iv) efficiency

(v) rating

Table 2.1: Components of Stray Load Losses as Given by Schwarz [4]

Components	Origin	Type and Location
1. surface losses	gap leakage (harmonic) flux	stator and rotor core losses
2. tooth-pulsation losses	gap leakage (harmonic) flux	stator and rotor core losses
3. tooth-pulsation, squirrel-cage, circulating current losses	gap leakage (harmonic) flux	rotor I^2R loss
4. stator-harmonic, squirrel-cage, circulating current losses	gap leakage (harmonic) flux	stator I^2R loss
5. stator-slot eddy-current losses	slot leakage flux	stator I^2R loss
6. rotor-slot eddy-current losses	slot leakage flux	abnormal rotor I^2R loss at high slip only
7. stator-overhang eddy-current losses	overhang leakage flux	stator core loss
8. rotor-overhang eddy-current losses	overhang leakage flux	abnormal rotor core loss at high slip only

(i) Heating

Stray load losses contribute to increased heating of the various components of the machine. There is very little literature to suggest that any major effort has been made to correlate heating effects with the amount of stray load loss. Schwarz [4], however, noted that doubling the conventional 1/2% stray load losses allocation (British Standards) in a modern high efficient machine would have a marked effect on the heating performance.

(ii) Torque Loss

Asynchronous torques are produced by the stator m.m.f. harmonics in the same manner as by the main field. These, as shown in the torque-speed curves in Figure 2.1 for the main and actual fields, affect the machine output. In a squirrel cage motor with poorly insulated rotor bars the dips on the actual field curve can assume such values as to prevent the motor from reaching the normal operating speed.

Barton and Ahmad [12] observed that for small and medium size induction machines stray losses greatly affect the pull-out torque, but do not affect the starting torque as much. Some researchers, [4, 7, 9] noting the relationship between torques (parasitic torques) and stray load losses, considered the analysis of torque as the most appropriate channel through which stray load losses could be studied and best understood.

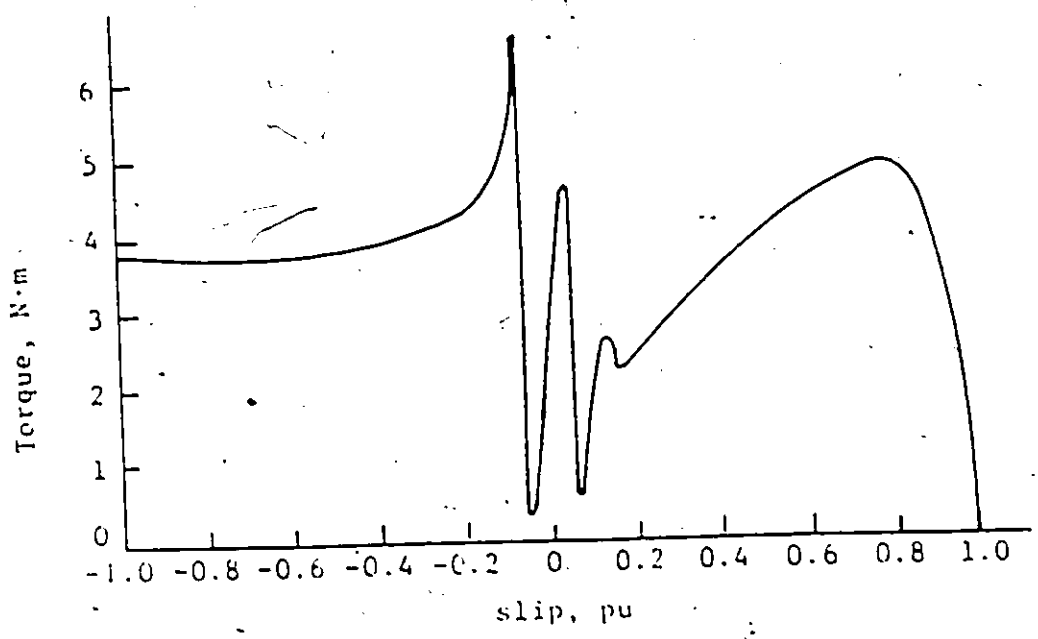

Machine: 3 phase squirrel cage;

5.7 kW, 400 V, 50 Hz, 1500 rpm, tested at 100 V, [7].

Figure 2.1: Torque-Speed Characteristic of a Polyphase Induction Machine.

(iii) Acceleration and Retardation

In applications, such as centrifuge drives, where the principal duty is to start and stop a load, stray load losses will increase the duration of the accelerating period while decreasing the time of retardation. Barton and Ahmed carried out some experimental works to support this hypothesis.

(iv) Efficiency

Although some authorities assume a nominal value for stray load losses of 0.5%, experiments reported in the literature suggest that for some machines, these losses could be as high as twenty times [6] that value. Even though a large body of literature exists on the subject, it is by no means clear either quantitatively or qualitatively just what factors contribute to stray load losses. However, it is obvious that machine efficiencies can be improved by the reduction of these effects; and if the reports are to be believed, savings can amount to as much as 9% in efficiency.

Increasing machine efficiency is a modern idea. For example, Diamant [13], observed that in those days of low electricity cost, when there was little apparent need for energy conservation, productivity efforts of motor manufacturers were generally directed toward lower initial costs to users, at the expense of efficiency. And very recently, Bonnett [14] presented the following expression to illustrate the effect of efficiency on operating costs:

$$S_{av} = KW \times C \times N \times \left(\frac{100}{E_B} - \frac{100}{E_A}\right) \qquad (2.1)$$

where

S_{av} – savings in dollars per year

KW – kilowatt rating of the specified load

C – energy cost in dollars per kilowatt hour

N – running time in hours per year

E_A & E_R – efficiencies of two similar motors, A and B respectively, which operate at the same specified load and having different efficiencies

(v) Rating

Derating is the practical consequence of the preceding effects. If the stray load losses in a completed motor are larger than predicted, heating under rated conditions will be increased beyond design tolerances. Thus, to avoid destruction due to excessive heating, some of the rated quantities must be reduced, for example slip and output power.

2.2. Present Methods of Measurement of Stray Load Losses

Various methods have been suggested for measuring stray load losses of an induction machine. They can be classified as shown in Table 2.2. For one reason or another, none of these methods gained world-wide acceptance.

In America, there are three recognized tests to obtain stray load loss estimates: input-output, pump-back, and the reverse rotation test, all of which are documented in the ANSI/IEEE standards [15]. Each of these methods suffer either due to lack of confidence in the results

Table 2.2: Classification of Methods for Measuring Stray Load Losses

Full-load	Light load
(I) Input - Output	(I) AC/DC Short-Circuit Test
(II) Pump back	(II) Reverse rotation test
(III) Calorimetric	
(IV) Differential dynamometer	
(V) Mechanical differential	
(VI) Back-to-back	

arising from inherent inaccuracies in measurement, or from impossible conditions of implementation, like obtaining two machines identical in every respect. In Britain, the practice is different. Instead of accepting any of these tests, a nominal value of 0.5% is approved as a standard limit by the British Standards. This also has shortcomings. For example, Alger observed that this practice does not give a designer any latitude, nor encourage development work on this subject [16]. Each of these tests is briefly described below with remarks. Table 2.3 summarizes the methods discussed.

2.2.1. Full-load Tests [4, 6, 9, 15, 17, 18]

(I) Input-Output Method

In this method the rotor output (P_o) is measured directly on a dynamometer. The input (P_i) is also found by measurement. The total loss is thus

$$P_{tl} = P_i - P_o \tag{2.2}$$

No-load core (P_c), and friction and windage (P_{fw}) losses are then determined from a no-load test. The stator copper (P_{cus}), and the rotor copper (P_{cur}) losses are determined at rated output power. Then the total power losses from this loss-segregation method is

$$P_{seg} = P_{cus} + P_{cur} + P_c + P_{fw} \tag{2.3}$$

The stray load losses are then determined as

$$P_{stray} = P_{tl} - P_{seg} \tag{2.4}$$

Table 2.3: Comparison of Measurement Approaches

Category	Method of Test	Expression for Stray Load Losses (P_{stray})	Remarks	General Remarks
Full-Load Tests	Input/Output	$P_i - P_o - P_{seg}$	1, 2	Complicated
	Pump Back	$0.5(P_{t12} - P_{seg})$	1, 2, 3	Non-economical
	Calorimetric	$P_{t1} - P_{seg}$	4, 5	Direct
	Differential Dynamometer	$f(P_{t12} - P_{seg2})$	1, 2	Prone to inaccuracies due to measurement difficulties
	Mechanical Differential	$0.5(P_{t1s} - P_{segs})$	3, 6	
	Back-to-Back	$P_{ac} - (P_{sc1} - P_{cus})$	7, 8, 9	
Light-Load Tests	AC/DC Short Circuit	$P_{strayff} + P_r - P_{rotorff}$	Section 5 (i), (ii), (iii), (iv)	Simple Economical Indirect
	Reverse Rotation	$P_m - P_{fw} - P_i + 3I^2R_1 + 2P_{strayff}$	Section 5 (i), (ii), (iii), (iv)	Based on too many assumptions with questionable validity

Notes:
1. Sensitive to inaccuracies.
2. Difficult to perform.
3. 'Totally identical' machines are impossible.
4. Limited to some machines.
5. Inaccurate.
6. Mechanical losses are difficult to determine precisely.
7. Loss value obtained is an approximation.
8. Losses shared equally bewteen non-identical machines is questionable.
9. Not suitable for larger machines.

This method requires the subtraction of two nearly equal numbers in order to obtain the relatively small value of stray losses. Hence, a very high degree of accuracy is required, as a slight error in either of the large quantities will be significant to the final result. For example [41, for a machine with 90% efficiency, a measurement inaccuracy of only 1% will produce an error of about 100% in the determination of the value of stray losses.

This method is almost impracticable, especially for large high efficient machines.

(II) <u>Pump Back Method</u> [15, 17, 18]

This is similar to (I) except that the output power is measured electrically by coupling an identical machine, which is used as a generator. Readings are taken of watts, amperes, and volts at both input and output terminals and also of the slip and winding temperature of both machines. From these data, the copper losses can be calculated and the no-load losses of the two machines can be measured while they are coupled together. The stray load losses are the difference between these losses, P_{seg2}, and the total loss, P_{t12}.

This method has the same numerical disadvantage as that of the input-output method. As well, the stray losses measured are for two machines. It is almost impossible to get two absolutely identical machines; nor is it likely that the stray losses will be equal under the operating conditions at which the measurements are made.

(III) **Calorimetric** [4, 18]

The calorimetric method is implemented by measuring the amount of heat carried away from the machine by the cooling gas, usually air.

This method can only be applied practically to large machines and those in which cooling gas is forced through specific passages. There are measurement problems which result in reduced accuracy, since a numerical procedure similar to that of previous method must be used.

(IV) **Differential Dynamometer** [15, 17]

The differential dynamometer test is a modified form of the pump-back test (section (II)) which utilizes a dynamometer as a load and driving device in place of a duplicate machine. The first part of the test is conducted by having the motor drive the dynamometer and taking readings for various load points exactly as described for the input-output method (section (I)). In the second portion, the dynamometer drives the motor which now operates as an induction generator. The output at each load point is adjusted to be equal to the motor input during the first portion of the test.

The total losses for the machine operating as both a motor and generator can be calculated from the difference in dynamometer scale readings and subtracting the known losses, P_{seg2}, from the total loss, P_{t12}, leaves the stray load losses. The total stray loss is divided between motor and generator operation in the same proportion, f, as the secondary I^2R losses during the motor and generator tests.

Even though this method eliminates some of the problems suffered

by the pump back method, it still suffers from the numerical problems noted in section (I).

(V) **Mechanical Differential** [6, 16]

Two 'identical' induction machines are coupled to the main shafts of a mechanical differential. Both machines are connected to a common electrical supply in such a way that they rotate in opposite directions. When both machines rotate at the same speed the differential cage remains stationary. If this cage is rotated, one of the induction machines accelerates and begins to act as an induction generator, while the other reduces its speed and commences to supply mechanical power to the induction generator through the differential gearbox. By adjusting the speed of rotation of the differential cage, it is possible to vary the loading of both motor and generator from no load to full load.

The electrical supply provides all the losses in the system, except the combined rotor losses: these are obtained from the mechanical drive to the differential cage. Hence, if the sum of all the losses in the system, P_{segs}, (with the exception of the stray load losses and the rotor losses) is subtracted from the total electrical input power to the system, P_{tls}, it is possible to obtain a value for the combined stray load loss.

The main difficulty with this method is that the mechanical losses in the differential are difficult to determine precisely. The requirement of two identical machines is again difficult to satisfy.

(VI) Back-to-back Test [19]

Two induction machines (not necessarily identical) are each coupled to a dynamometer. The dynamometers are fixed on a stationary bedplate, while the stators of the two induction machines are strapped together and are free to rotate on their own bearings. One induction machine operates as a generator, and is driven at a speed n_g, while the other operates as a motor and it runs at speed n_m (r.p.s.), i.e. $n_g > n_{sync} > n_m$. The two speeds n_m and n_g can be adjusted until the two stator frames have no tendency to rotate, which means that the torques in the two couplings are equal. If at this point of balance, the electrical input to the two induction machines is P_{ac}, the total electrical loss P_{u2} of both machines is given by

$$P_{u2} = P_{ac} + 2\pi(n_g - n_m)T \qquad (2.5)$$

The load loss P_{stray} is approximately

$$P_{stray} = P_{ac} - (P_{scl} - P_{cus}) \qquad (2.6)$$

where P_{scl} and P_{cus} are stator core and stator copper losses respectively.

The stray loss obtained by this method is approximate because the method assumes the load loss component $2\pi(n_g - n_m)T$ is equal to rotor copper losses in the two machines. Also the fact that stray losses obtained have to be shared equally between two non-identical machines operating in different modes is questionable [20]. The arrangement may not be suitable for larger machines.

2.2.2. Light Load Tests

As the name implies these methods do not require any load for carrying them out. They are based on the following assumptions:

(i) The fundamental frequency component of stray load loss occurs only in the stator.

(ii) Tooth-ripple, and pulsation are the main sources of high frequency components of stray losses.

(iii) The stray losses can only be supplied by mechanical power.

(iv) The values of the high frequency losses is the same for both full-speed forward and reverse rotations.

(v) These losses (high frequency) are independent of the type of supply, dc or ac, under short circuit condition as long as the magnitude of the supply is that of the rated.

These assumptions have generated considerable controversy [4, 6, 11, 21] and have constituted a major setback for these methods. The point often made against light-load tests is that the flux conditions during test conditions are different from that existing under full-load conditions. A particular advantage over the previous category of test is that these methods are readily and economically implemented.

(I) **AC/DC Short-Circuit Test** [4, 6, 17, 18, 22]

This consists of three separate tests

(i) rotor-removed test

(ii) dc or synchronous short-circuit test, and

(iii) ac or synchronous short-circuit test.

(i) **Rotor-Removed Test**: Stray loss in the stator is measured with the rotor removed by applying balanced polyphase current to the terminals of the stator winding. The value of input power minus the stator I^2R loss is considered as the stray load loss in the stator due to fundamental frequency, $P_{strayff}$.

Ware [22], suggested that this loss be measured at current

$$I = \sqrt{(I_1^2 - I_m^2)} \qquad (2.7)$$

where I_1 is the stator load current and I_m is the magnetizing curent.

(ii) **DC (synchronous) Short-Circuit Test**: This test, suggested by Koch, consists of passing direct current through the stator of the induction motor while the rotor is driven at synchronous speed. The net increase in the mechanical power required to drive the rotor under these circumstances is measured and is termed the 'rotational watts', P_r. The 'rotational watts' contain the fundamental-frequency rotor losses, plus high-frequency losses caused by the rotation of the rotor. The direct current must be chosen to correspond to the peak value of the corresponding alternating load current.

(iii) **AC (Asynchronous) Short-Circuit Test**: This is basically the normal blocked rotor test. The net power input, $P_{rotorff}$, is assumed to be entirely rotor-fundamental-frequency loss.

The stray load loss is thus

$$P_{stray} = P_{strayff} + P_r - P_{rotorff} \qquad (2.8)$$

(II) **Reverse Rotation Tests** [4, 6, 8, 11, 15, 17, 18, 22]

This consists of two separate tests:

(i) Rotor removed as described in (I) above, and

(ii) Reverse rotation test.

Reverse Rotation Test [8]: Balanced polyphase voltages are applied to the stator of the machine, and the rotor is driven at synchronous speed in a direction opposite to that of the airgap rotating m.m.f.. The stator input P_i and the shaft input P_m are measured at the current of equation (2.7).

With the stator power removed the mechanical power P_{fw} required to drive the rotor at synchronous speed in the same direction is measured.

The stray load loss is then found as

$$P_{stray} = P_m - P_{fw} - P_i + 3I^2R_1 + 2P_{strayff} \qquad (2.9)$$

2.3. Calculation of Stray Load Losses: A Review of the State of the Art

2.3.1. Stray Load Losses in the Windings

This component originates as an increased resistance of the stator conductors, due to skin effect, caused by slot leakage flux. The flux results in eddy current losses at the central portion of the conductor, leading to non-uniform current density and magnetic field intensity distributions across the conductor. There are other components of this loss such as the additional I^2R loss due to heat.

2.3.1.1. Eddy-current Losses in Conductors

The importance of the determination and limitation of the eddy current losses in conductors was realized early. The problem was investigated by A. B. Field [23] and later by many other authors. Field observed that these eddy currents were produced by flux crossing the slot transversely from tooth to tooth through the body of the conductor. The net result in the conductor was a current varying in density and phase throughout the conductor. Field summarized his work with the aid of plots of the loss versus the conductor-slot parameter. His description of the physical phenomena of eddy currents in slot embedded conductors is considered a classic work in the area. It may be regarded as the best comprehensive review of the problem. However, the limitations imposed in his work are two-fold; that the conductors are either solid or infinitely laminated, and that the currents of all conductors in the same slot are in phase.

The novel idea of critical height of conductor for which the losses in the slot are minimum was first suggested by A. B. Field [24]. He argued that since an increase of copper section increases the eddy current losses while decreasing the normal ohmic losses, there must exist an optimum depth of conductor for which the total losses is a minimum. He also showed that in a multi-layer coil, the total losses could be still further reduced, for the same total depth of copper, by grading the conductor section in different layers, larger depths being used in the bottom layers than in the top ones.

Shortly, after this, Taylor [25] developed expressions for the excess loss factor for various types of winding and stranding arrangements. Taylor also considered the case of minimum intensity of heat dissipation, assuming that most of the heat was dissipated from the sides of the conductors. At about the same period as Taylor, Gilman [26, 27] studied the effect on copper losses of a finite number of strands in a conductor, together with the case of conductors in the same slot carrying currents of different time phases. He developed formulas for the calculation of the density in any point of a current-carrying wire, for the total loss ratio for the general case in a solid bar, for the hypothetical case of an infinitely stranded conductor with various arrangements of groupings and twistings of the end windings, and for the practical cases of conductors with two and three strands. He then developed a general law for any number of strands in a slot and at the end region.

Lyon [28, 29] made a much more compact, elegant, and detailed derivation of the eddy current formulas by the use of hyperbolic functions using complex angles. His derivations include expressions to account for complex power loss, slot-leakage impedance, and the impedance to direct current resistance ratio. His contributions enabled investigations of the effect of eddy currents in a slot in the reactance of the winding, an aspect which was better presented in a more recent book by Lammeraner and Stafl [30].

Other notable contributions were made by Summers [31] whose method of reduction of eddy current losses in conductors had many

advantages over the previously existing ones. Alger [10] has obtained expressions for the effective resistance and reactance of deep squirrel-cage rotor bars. Lammeraner and Stafl [30] effectively treated the case of conductors with specific cross-sections in slots; hollow conductors, conductors of combined materials in a slot, and wedge-shaped conductors.

Characterizing all the major contributions which have so far been discussed are some simplifying assumptions. Mukherji [32] observed that the justification for some of these assumptions may be questionable: (a) that there is no component of field strength parallel to the side of a slot (this is true only if the conductor completely fills the slot); (b) that there is negligible skin-effect in the end-conductors; (c) that the effect of the saturation of the iron material around the slot is negligible; (d) that the neglect of the reluctance of the iron part of the path of the slot-leakage flux, and the assumption that eddy current and hysteresis losses in that part of the iron due to this leakage flux are also negligible. In order to include some of these points in conductor eddy current loss analyses some nondirect methods were developed. For example the synthetic procedure of Taylor [25] was developed into an iterative method [30]. Lammeraner and Stafl [30] also developed a flux plotting method which allows for variability of permeance and the effect of hysteresis. This latter method is sufficiently accurate for practical cases.

The advent of the computer and especially the recent advancements on the numerical solution of partial differential equations have led to contributions such as those by Anderson [33], Chari and

Csendes [34], Weiss and Csendes [35], and Chari and Bedrosian [36]. Their works have demonstrated that the problem of eddy currents in the conductor can be solved as either a two-dimensional or three-dimensional one.

2.3.1.2. Other Components of Stray Load Losses in Conductors

Generally, the additional I^2R loss due to temperature rise in the conductor is not considered a serious component of stray load losses in the conductor. This may be true for a short duty in a well-designed machine. Such losses assume greater importance for less efficient machines or those which are poorly ventilated.

The I^2R losses in the stator winding due to the harmonic components of the current induced by the non-sinusoidal air gap field has received little attention. This is due to the general assumption [5, 7] that the stray load losses in the stator winding are small for small machines, and that they are negligible in large machines. These losses are largely comprised of fundamental frequency eddy current losses. Hence this component, high frequency copper losses in the stator winding, is negligible.

On the other hand, the high frequency conductor losses in the rotor winding of a squirrel cage induction machine have been well treated, usually in the analysis of inter-bar currents. The first such comprehensive treatment was by Rossmaier [37]. Later, his theoretical work was extended and interpreted by Odok [9], whose neatly presented theoretical work resulted in an expression for the stray load losses in

a squirrel cage rotor. However, Odok's treatment was primarily concerned with the losses due to inter-bar currents.

Alger's equivalent circuit for the machine [38] includes the effects of air gap harmonics. His model also includes expressions for rotor conductor losses arising out of voltages induced by slot permeance and mmf, and phase belt harmonics. These expressions are stated in terms of stator currents, rotor bar resistance and the circulating current loss factor. By using the ratio of leakage reactance to magnetizing reactance, he developed a set of curves for the circulating loss factor for both the permeance and mmf harmonics as a function of slot ratio and slot opening over air gap ratio for the number of stator slots per pole.

Christofides [7] extended Odok's work to show, by means of graphs, how the losses vary with skew and slot combination. Subba Rao and Butler [39] included the effects of finite end-ring impedance in their analytical model. They also developed some expressions for the rotor bar harmonic frequency losses, as well as a number of curves for the loss factors.

2.3.2. End-Leakage Losses

These are losses due to the eddy-current which are induced in the end region of the machine, by fluxes which enter the lamination in the axial direction and penetrate the end-region metal parts. The losses vary not only with the design of the end winding but also with distance of the ventilating shields and other metal parts to the end

windings. They are difficult to evaluate precisely, because the end-winding regions of an induction machines are electromagnetically complex. However, there is a substantial body of literature to show that this component has been well treated from various angles. Even though most of the works which are mentioned in this section were concerned with the end regions of large synchronous generators, the results are generally applicable, with slight modifications, to induction machines.

2.3.2.1. Analogue Techniques

The first practical method for solving this problem was the field-plotting method (Dreyfus [40]). The electrolytic analogue model described by Winchester [41] has the merit that complex boundary shapes can be dealt with reasonably accurately. Kant [42] outlined an interesting method of obtaining the 3-dimensional end field with the aid of an electrolytic-tank analogue.

Hawley et al. [43] observed that in general the analogue technique has two useful purposes: (i) it can give designers a 'feel' for the way in which a magnetic field behaves and yield qualitative results of a temporary nature; and (ii) it can act as a useful check during the development of a mathematical method. It is, however, a slow and tedious process. Hawley used a conducting-paper analogue to solve the end-region problem. This technique yielded a reasonable result, though it is prone to human errors.

2.3.2.2. Analytical Methods

Douglas presented three methods of approach for solving end-leakage problems [44]. One of them is to make use of the virtual-image principle as a means of replacing the iron or other boundary surfaces by equivalent circuits in air, so that the entire field problem is reduced to one of integration. These methods of approach were later employed, together with other analytical methods, by Caldwell [45], and Harrington [46]. Image circuits are valid for only one type of boundary. As well, they fail to satisfy the principle of continuity of current flow. Carpenter [47], later extended the image principle to circuits which are partly embedded in one of the reflecting surfaces, and in particular to end-winding problems in which the surface is broken by an air gap. His method of approach was to consider first a semi-infinite circuit protruding from an infinite, flat, iron block without an air gap, and then to take into account the more important of the complexities of the end-region boundaries which are met in practice. This was illustrated by calculating the end-winding inductance of a 2-layer induction-motor winding.

Another analytical approach, which has been widely applied to the problem of losses in the end zone, involves the simplification of the end structure in order to facilitate the use of a purely mathematical method. Smith [48], and Honsinger [49] treated this problem as a boundary value problem, solving Laplace's equation so as to obtain an expression for the magnetic scalar potential in the end region. Both papers made allowances for boundaries, which are defined

by surfaces at which the flux is either normal or tangential. Honsinger's paper [49] addresses the end region problem of an induction machine, and in the companion paper [50] his results were used to correlate actual measurements of end-winding reactance. Ashworth and Hammond [51] used the magnetic vector potential instead, and confined their attention to the field in the air of an end-winding, subdivided into cylindrical current sheets to isolate the effect of the winding. Their solution completely neglected the effect of iron surfaces. Lawrenson [52] obtained the field at a point in the end structure as the sum of the contributions of small elements of the coil end, using the Biot-Savart law. His technique allows the coil-end shape to be treated accurately: but it is difficult to take account of boundaries other than the plane formed by the core end surfaces. The method is essentially a computer method, as detailed calculations have to be made for every surface on which the field is required. The current sheet method of Tegopoulos [53] is often considered as the most effective. He used the vector magnetic potential and allowed approximately for all containing boundary surfaces. Reece and Pramanik [54] believed that the works of Smith [48] and Honsinger [49] contained some important errors. Their work [54] served to correct these errors, and further refined the treatment of the core surfaces and the representation of the windings.

The work of Ashworth and Hammond [51] was later extended by Stoll and Hammond [55] to include the effect of nonmagnetic core end plates and of the iron surrounding the end region. The major draw back was the omission of the air gap fringing field. Myerscough [56] used a

Green's function expansion for the magnetic field of end windings completely enclosed in a region bounded by material of finite permeability. He stated that an allowance can be made, by perturbation methods, for additional magnetic and conducting parts within the region.

2.3.2.3. **Numerical Techniques**

The first substantial work which applied numerical methods to the end zone problem was that of Okuda [57]. By using Maxwell's equations he derived partial differential equations in the cylindrical coordinate system to relate the three-dimensional current densities and magnetic vector potentials in the end region of a machine. He also described how these equations can be solved by finite difference techniques. A couple of years later Sarma et al. [58] published a similar work in which a three-dimensional cartesian coordinate system is employed instead. The problems involved in the solution of three-dimensional finite difference equations are highlighted. The work of Jacobs et al [59] simplified some of these problems by formulating the problem as a 2-scalar potential 3-dimensional non-linear boundary value problem.

Chari and Silvester [60] indicated that the end-region problem in a.c. machines is also amenable to solution through finite element techniques. The results were later confirmed by Chari, Sharma and Kudlacik [61], and Okuda, Kawamura, and Nishi [62]. The latter described a vector potential solution of the end-field problem of a turbogenerator in cylindrical polar coordinates. They formulated the field problem as a diffusion equation employing three components of

vector potential and one scalar potential. Howe and Hammond [63] also applied the finite element analysis, which included eddy currents, to end field problems of simplified geometry in a two-dimensional cartesian system.

2.3.2.4. Other Works

In 1954, Baird [64] presented a method of calculation for the eddy current loss in induction motor end-turn clamping rings of solid copper. The currents in the end-turns were resolved into axial and circumferential components, the former producing a rotating field and the latter a time-varying circumferential field. Eddy currents were shown to be set up in the ring due to the higher harmonics in the armature mmf wave. The power loss in the clamping ring has then calculated separately for the axial and the circumferential portions of the eddy current paths. Test results were used to confirm the theory. Alger et al. [10] considered it satisfactory to assume that the stray load loss in the end-region of an induction machine is equal to the portion of the end-winding power which is caused by flux entering the stator laminations, axially, multiplied by an empirical constant.

The works of Howe and Hammond [63, 65] and Tavner et al. [66] are also important, especially to the issue of end stray losses reduction, while that of Tavner, Hammond and Penman [67] is important because of its synethetic approach. Very recently an important practical contribution was made by Ming-Zheng and McPherson [68] who carried out an experimental investigation of stray losses in the end

bells of an induction motor. They concluded that the magnetic field and losses in the end bells are so small as to have a negligible effect on the efficiency or temperature rise of a machine.

2.3.3. Additional Losses in the Tooth Body, Surface and the Core

There are eddy current and hysteresis losses in the rotor and stator tooth bodies and surfaces adjacent to the air gap, and cores, due to stator and rotor harmonics respectively. These losses may also include additional eddy current and hysteresis losses due to slot mmf and permeance harmonics. The work of Dreyfus [69] was the first comprehensive theoretical treatment of this component of stray losses. Since after his work some other authors have made some significant contributions. Alger et al [10] discussed these losses and gave some semi-empirical expressions for them. In order to remove the empiricism that characterized some of the previous works Christofides [7] carried out an analytical study of these losses. He came up with some expressions and curves which describe the variation of these losses with skew and slot combinations. Subba Rao and Butler [39] carried out further analytical work and considered the effect of linear versus saturation conditions. They represented the B-H magnetization characteristic by a polynomial expression. An exhaustive mathematical treatment was carried out by Heller and [illegible]mata [17].

None of these works yields results which are entirely satisfactory. This is primarily due to the difficulty of modelling the non-linear processes in iron.

2.3.4. Skew-Leakage Losses

These are losses, particularly at the ends of the stator core [70], owing to skew leakage flux produced by the relative phase displacement of stator and rotor mmf waves. It has been found [7, 39, 71] in squirrel cage machines, that skew (and hence skew leakage losses) depends on the bar-iron insulation. A rotor with imperfect bar-iron insulation requires small effective skew, and hence reduces skew-leakage losses.

Alger et al. [10] formulated an expression, suitable only for a rotor with perfect bar-iron insulation. The formulation is based on the assumption that the load component of the stator mmf exactly offsets the rotor mmf at the centre of the core. As the core length increases the phase difference of stator and rotor mmfs increases to give a corresponding increase in radial flux density. Additional work was carried out by Heller and Joki [71], who considered skew-leakage losses in a squirrel cage rotor.

2.3.5. Stray Load Losses Due to Interbar Currents

When a squirrel cage machine is running on load a net induced voltage exists which acts across the iron between adjacent bars. If the insulation between bars and iron is imperfect, this voltage will cause circulating currents from bar to bar across the rotor iron, resulting in losses and reducing motoring torque. A pair of rotor bars with distributed resistance is analogous to a transmission line: the first thorough analytical treatment, using the analogy in terms of a

distributed-parameter problem was made by Rossmaier [37]. His work was later interpreted and extended by Odok [9], who concluded that simplified expressions could be obtained based on the assumptions that the end-ring resistance is negligible, and that the impedance between adjacent bars is practically an ohmic resistance. He observed that for very low bar-iron resistances the losses increase linearly with better bar-iron insulation. For higher bar-iron resistance the losses decrease hyperbolically with better insulation.

Simplified expressions for losses due to interbar currents, together with descriptions on their origins for design purposes, have been given by Christofides [7], and Subba Rao and Butler [39]. The simplified expressions devised by the latter considered both linear and saturated cases.

Another issue which has been investigated by some authors [7, 39, 71] is the effectiveness of skew in a machine with imperfect bar-iron insulation. Heller and Joki [71] carried out an extensive work, formulating the hypothesis that losses are directly proportional to the square of skew for small bar-iron insulation resistance and inversely proportional to the square of skew for high resistance.

The work of Behdashti and Poloujadoff [72] represents an important contribution on appropriate models for the analysis of these losses, and it also includes a comprehensive bibliography of other works on this aspect. Butler and Mohammed [73] treat the case when interbar resistance is not equal along the axial length.

2.3.6. Saturation

Saturation is an important physical origin of no-load stray losses. It is established from past analyses, that when the magnetic flux paths of the machines are saturated by the main flux, the harmonic mmf and flux density waves are appreciably reduced, with the result that there is a reduction in the stray load losses. Since the non-linearity which saturation introduces is usually ignored, this component was often left out in analyses. This is because, with saturation, the principle of superposition is no longer valid, hence losses are lower than predicted.

Generally, the effects of saturation of the main magnetic flux paths on the stray load losses are assumed fully accounted for by increasing the effective air gap by some factor, and reducing the effective incremental permeability of the rotor iron. Christofides and Adkins [19] used a weighted factor averaged over a pole-pitch, then selected a suitable value of incremental permeability. Their method, which can be considered a discretized linearization of the non-linear problem, enables the use of the superposition principle. A brief review of other works can be found in reference [39].

2.4. Other Approaches to the Study of Stray Load Losses

The seeming lack of agreement between the practical and analytical results on stray load losses of induction machines necessitates the consideration of different approaches to the study of this subject. Such approaches are:

(a) Empirical Modelling - this involves empirically relating a measureable effect of stray load loss to some measureable variables in the device. An example is that which relates the parasitic torque, or stray load loss torque, to the current and speed of the machine:

$$T_s = kI^b\omega^c \tag{2.10}$$

Lindsay [74] investigated this approach by using parameter optimization techniques.

(b) Circuit Modelling - this involves deriving appropriate thermal, magnetic, or electric circuit models and hence, by using the parameter identification method described in reference [75], determining the components of the model. The first major difficulty in this approach is that the complex stucture and the nonlinear phenomena in induction machines precludes the establishment of an accurate model. This is why this approach has not attracted much attention. However, a notable work on a thermal equivalent network is given by Bates and Tustin [76]. An equivalent electric circuit for the harmonic fields in an induction machine has been used in some other works [5, 7, 9, 39].

2.5. Current Methods for Reduction of Stray Load Losses

The greatest challenge posed by stray load losses is the difficulty encountered in developing adequate methods for reducing them in an induction machine. Techniques for reducing stray load losses usually result in some other inadequacy of design. Hence most machines still suffer from relatively low overall efficiencies. For example,

Diamant [77] noted that 'the practically realizable efficiency improvement increases the evaluated motor value by more than 80%, occasionally doubling the value of the normal efficiency motor'. The challenge, therefore, is in coming up with a method to reduce stray load losses without creating any new, or amplifying any of the existing, technical or economic problems.

Most of the suggestions for achieving a highly efficient induction machine with low stray load losses can be grouped as follows:

1. Reduction of losses in conductors.
2. Reduction of losses in the end region.
3. Reduction of harmonics.
4. Reduction of losses due to industrial imperfection.
5. Others.

2.5.1. Reduction of Losses in Conductors

2.5.1.1. Due to Skin Effect

Early works, for example Summers [31], showed that skin effects can be held down in large machines, where such losses are significant, by suitable transposition and stranding of the conductors. The use of critical height, artificial bars (where the critical height needs to be exceeded), and special conductors, such as hollow conductors, conductors of several materials, and wedge shaped conductors, are discussed by Lammeraner and Stafl [30].

2.5.1.2. Due to Other Effects

Temperature build up in the conductor can be controlled by suitable ventilation. Cases of use of special conductors, like water cooled conductors, in large a.c. machines have been reported.

Circulating currents are induced in the rotors of an induction machine by tooth-pulsation fluxes, and by the low-order harmonics of the gap leakage flux. The I^2R losses due to these currents are dependent on the impedance of the winding as well as the parameters determining the flux. Hence, to reduce these losses Schwartz [4] suggested the use of current displacement rotor designs where considerable control can be exercised over the effects of tooth-pulsation fluxes by varying the resistances of the squirrel cage. Such a rotor is also good for high starting torque drives. This method alone does not ensure a reduction of these losses (see sections 2.5.3, 2.5.4 and 2.5.5 below).

2.5.2. Reduction of Losses in the End Region

Baird [64] suggested the following methods for reducing the losses in the clamping rings:

(i) Laminating the rings in the axial direction on both sides of the end turns;

(ii) Reducing the radial thickness of the rings without decreasing the distance between the clamping ring backing and the end-turns;

(iii) Using equal radial thickness of low-resistance solid ring on either side of the end-regions;

(iv) Sectioning the ring into cylindrical segments by means of axial cuts.

Winchester [41] observed that slotting the end teeth of large turbine generators accomplishes, to a lesser degree, the same effect as laminating the core in a direction parallel to the magnetic flux. He also noted that bolting a copper shield in place over the stator frame flange allows the currents which otherwise flow in the flange to flow in the low-resistance shield, reducing the losses.

Lawrenson [52] analyzed the magnetic field of turbo-generators, and noted some points which could be of value to an optimal reduction of the losses in the end structures.

Stoll and Hammond [55] remarked that the reduction of the end loss can be achieved by reducing the stator-winding cone angle, and using a lower resistivity material for the clamping plates themselves in large machines where, for mechanical strength, the plates have to be thicker than the eddy current skin depth of the material. Howe and Hammond [63] observed that intense local concentrations of axial flux are associated with sharp corners in the magnetic parts of turbogenerators as well as with edge effects near conducting screens. Hence, rounding of the stator profile seems to offer an effective method of reducing the axial component of fringing flux. They also suggested that axial flux levels at the stator surface are better reduced by making the rotor shorter than the stator. Some additional comments were made about use of conducting screens in turbogenerators, to reduce end losses. In their companion paper [65], on axial flux in

turbogenerators, they observed that axial flux is a very local phenomenon which cannot be eliminated, but which can be reduced by careful design of those regions where it is likely to be troublesome.

Tavner et al. [66] noted, from measurements, that the axial flux impinging on the core end falls as the winding overhang is reduced, or as the winding radius is reduced, irrespective of the winding design; and that an overhanging helical winding will produce less core-end leakage than a conventional diamond winding of similar size and loading even if the latter has zero cone angle. They further observed that the internal axial flux produced by a winding, whose end does not project beyond the core end, is always less than if the winding were overhanging, again regardless of the winding design.

2.5.3. Reduction of Harmonics and Their Magnitudes

Some common means of reducing harmonics are well known, among them the use of slot wedges, and large air gaps.

2.5.3.1. Use of Slot Wedges

The ripples of the air gap flux distribution are caused by non-uniformities by air gap due to open stator slots. Flux ripples constitute harmonics which are mainly responsible for load losses. The smaller the air gap and the wider the open stator slot, the greater are the fundamental mmf and pulsation losses [77]. Therefore, high stray load losses may occur in machines where, for production reasons open slots must be used for inserting the windings. This may be improved if, after insertion of the winding, the slots are closed by wedges.

The magnetic slot wedges, are usually made of low-permeability and high resistivity magnetic material. Their use aids in reducing stray load losses. As well, it is widely held that they aid in reducing (1) the electromagnetic noise due to the decrease of equivalent width of stator slot; (2) the excitation current due to the reduction of air gap length; and (3) the starting current due to the increase of stator leakage reactance [77, 78]. However, the increase of stator leakage reactance reduces the starting torque and power factor. Kato et al. [78], did not consider these problems significant in large capacity machines, as in practice the magnetic slot wedges are saturated in the starting condition. Hence, there is little starting torque reduction. They also believed that the decrease of power factor is partly offset by the decrease of excitation current. Heller and Hamata [17], on the other hand, noted that including magnetic wedges in a machine results in high production costs, and more rapid aging. The aging causes faster deterioration of magnetic and mechanical material's properties. Reference [78] includes an analysis of the effect of magnetic slot wedges on the losses. The requirements necessary for the design of an ideal magnetic slot-wedge are very well stated in reference [79].

Anazawa, Kaga and others [80, 81] developed a new wedging material, the soft ferrite wedge. They noted that the efficiency of an induction machine with soft ferrite wedges increases by about 4% at rated output, and 11% at a quarter output. They also noted that the starting torque of an induction motor with soft ferrite wedges was unchanged, while, due to saturation of the wedges, the leakage reactance

at starting was reduced. The effects of soft ferrite wedges on the asynchronous and synchronous torques were reported in reference [81].

2.5.3.2. Large Air Gap

The use of a larger air gap can help to reduce stray load losses because it provides leeway for leakage flux to smooth over the ripples. A reduction in losses of 56% was recorded by Christofides and Adkins [19], when the air gap of a squirrel cage induction motor was increased from the design value by about 55%. More recently Spooner [82] observed, from a series of tests on solid-rotor induction machines, that the large gap approach is more effective than slot opening reduction in decreasing stray losses.

Lengthening the air gap is not an ideal solution because the larger the gap the lower the air gap permeance, and hence lowered power transfer across the air gap. Methods relating stray load loss reduction to air gap length increment have been derived; both the works of Christofides and Adkins [19] and Spooner [82] contain graphs that relate these two variables for squirrel cage and solid rotor induction motors respectively.

2.5.4. Industrial Imperfection

Industrial imperfections fall into two categories: (i) those due to manufacturing and (ii) those due to design. One possible consideration from modern research is that losses are reduced by insulating rotor bars. This obviously includes some design compromise. It has, however, been claimed that the losses due to industrial

imperfection resulting from poor rotor bar insulation can be counteracted by making the effective rotor tooth face approximately equal to the stator tooth pitch, by using closed slots in the rotor and by segmenting the rotor into two or three sections by means of thin common end-rings, each section having a skew of one stator tooth-pitch.

2.5.5. Others

Additionally, there is a variation of load losses with skew and slot combinations making these important considerations for an optimal reduction of stray load losses at the design stage. Schwartz [4] and Alger et al. [5] noted that losses due to circulating currents induced by tooth-pulsation flux represent one of the severest limitations in the choice of rotor-slot numbers. The variations of load losses with skew and slot combinations were realized by Christofides, whose paper [7] represented a major contribution in this respect. Subba Rao and Butler [39] and Heller and Joki [71] also discuss these aspects.

Oberettl suggested 13 rules [83] which he claims, when observed, make it possible to reduce the stray load losses to 1% of the power input. The rules refer to the number of stator and rotor slots, slot skewing, coil pitch, parallel winding paths, slot opening, transverse rotor resistance, influence of working and aging. These rules are:

1. $Q_1 > Q_2$
2. Number of stator slots as high as possible
3. Non-skewed stator and rotor slots, especially if $Q_1 < Q_2$
4. Two-layer chorded stator winding with a chord 5/6

5. With a delta connection: $|Q_1 - Q_2| \neq p, 2p, 4p$
6. With parallel paths: a connection making the secondary armature reaction impossible
7. Ratio of slot opening w_o to segment height h: rotor; $w_o \geq 1$; stator $w_o/h \leq 3$.
8. Re-turn rotor surface to prevent sheets to be short-circuited, stator bore better not re-turned
9. Use of sharp press-tools if sheets are not annealed
10. Use of annealed sheets, particularly for small motors
11. Small stator and rotor slot openings
12. With skewed machines transverse resistance either very small or very large
13. Storage of the motors because, due to aging, the stray losses are reduced after six months to 0.6 of their original value.

Rules 3 and 12 are contradictory to the existing notions on skewing and their importance towards minimizing core loss. They most probably results from the many studies that have been carried out on the subject of inter-bar currents. These studies which are mainly theoretical have little experimental works to support them. Hence, these rules and many others above require experimental verification.

CHAPTER 3

MODEL DEVELOPMENT

3.1 Introduction

This chapter commences with a presentation of a conceptual background to a definition of stray load loss in induction machines, as stated in section 2.1.1. Hence it gives an explicit definition of the phenomenon, culminating in the behaviour of a machine. This gives an insight into the origins of this problem and hence forms the basis for a new approach. The approach involves the development of a model for a squirrel cage induction machine.

In contrast to some other approaches, this model, which takes account of harmonics, precludes the introduction of the notions of belt and zig-zag reactances, or differential reactance. It does not view the air gap flux as the sum of linkage and leakage components. The end product of the derivations presented in this chapter can be developed into an algorithm which can be viewed as simulating the steady state behaviour and operation of a machine. The principal assumptions are that the stator terminal voltages are sinusoidal and balanced and that speed is constant. Any changes in speed are considered to be very slow: no transient phenomena are considered.

In section 3.2 the stator aspects of the model are described. This is followed, in the next section, by the derivation of a theory of

squirrel cage induction machines. This theory, which culminates in an equation of the machine, forms the basis of the model, especially the rotor aspects. Solving the machine equation which results from the theory is the subject of discussion in section 3.4. How actual and fictitious slot openings can be accounted for in the model are discussed in the section that follows. The question of the effects of saturation is addressed in section 3.5. Finally, the machine equations are analyzed and discussed in the last section.

3.1.1 Definition of the Problem

In section 2.1.1 a definition of stray load loss, which is embodied in both the American and British Standards; and which also has its roots in the historical origin of this loss, was presented. Essentially the definition implies that stray load loss occurs as a result of the differences between the phenomenon implied by the method of segregation (which essentially is the conventional equivalent circuit, figure 3.1, under no-load, locked rotor, and load conditions) and the actual phenomenon in a device under the load operation. Explicitly, this suggests that there are some differences between the ideas behind the conventional equivalent circuit, which gives the apparent load loss, and the actual phenomenon, which gives the actual load loss.

Analytically, it is difficult enough comprehending the actual phenomenon in an induction machine let alone accurately modelling it. Hence, it was in order to overcome the difficulties involved in this

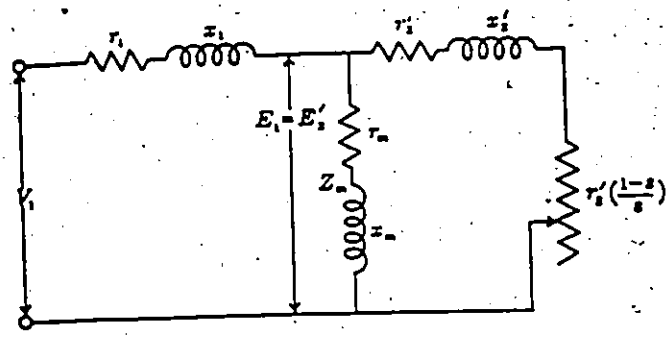

Figure 3.1: A Simplified Conventional Equivalent Circuit of an Induction Machine

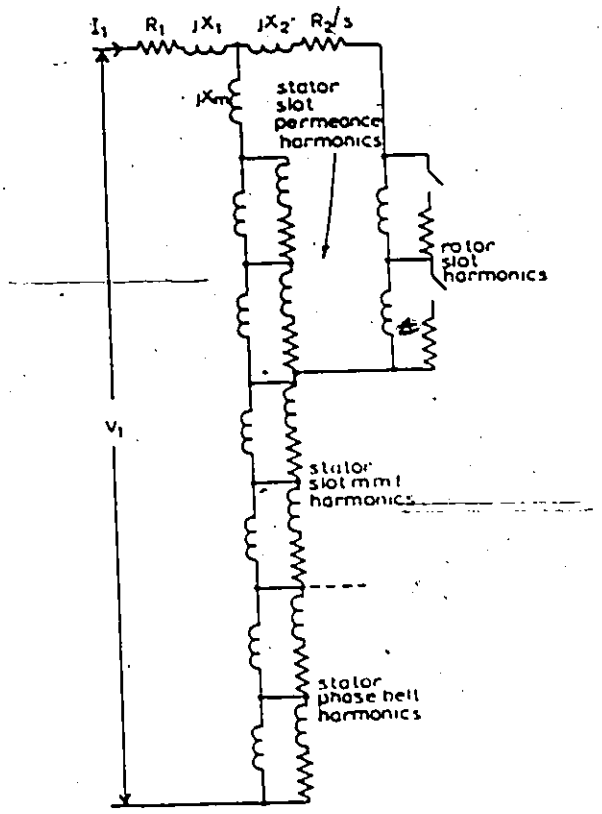

Figure 3.2: The Chain Equivalent Circuit

problem of accurate modelling that led to the development of the conventional equivalent circuit based on the following simplifying assumptions:

1) The core losses resulting from the leakage fluxes and the harmonics are negligible. An extension of the conventional equivalent circuit, which accounts for harmonics by neglecting the non linear interactions among all the field sinusoidal components is the chain equivalent circuit, figure 3.2.

2) The rotor core loss varies with rotor frequency, and hence with the slip. Under running conditions the rotor frequency is normally in the order of 2 Hz and the rotor core loss is high and decreasing with increasing speed, while the friction and windage start at zero and increase. As a result, the sum of the friction and windage, and core losses is roughly constant.

3) Armature reaction does not contribute significantly to losses in an induction machine.

4) The only source in the device is explicit. Implicit sources are either assumed absent or their effects are negligible.

5) Perfect insulation is assumed to exist between the bars and the iron materials of a squirrel-cage rotor.

6) Such distributive phenomena as saturation, the effects of tooth ripple and pulsation, and temperature rise, are assumed accountable by factors or lumped parameters.

Within certain limits, some of these assumptions are justifiable, but others are not. It is this latter group which account for the origin

and components of stray load losses in an induction machine.

To put the measurement problem in perspective: at any instant the parameters and variables participating in the phenomenon in the device may be classified as listed in table 3.1 and as illustrated in figure 3.3, under the following three main headings: input, device and output. The device parameters and variables can further be grouped into four categories: geometric, materials constants, field quantities, and device variables. The input, device, and output variables are indeed independent quantities with respect to which the performance of the machine can be determined. The actual phenomenon culminating in the behaviour of the device is dictated by the remaining device parameters and quantities. Hence, the phenomenon culminating in stray load losses in an induction motor is a function of a complex geometry, defined by those parameters listed in table 3.1, material properties, some of which are non-linear, and the distributive field quantities.

3.2 Stator

Assuming that there is supply current only in the stator winding and that it is sinusoidal, then the instantaneous current in phase m of the stator winding of a three-phase induction machine can be written as

$$i_{sm}(t) = I_s \cos\left(2\pi ft - \frac{2}{3}\pi(m-1)\right); \quad m = 1,2 \text{ or } 3 \qquad (3.1)$$

If this current flows in a coil made of N_c turns, then, by Ampere's law, the magnetic intensity is related to the current in the coil by

$$\oint H dl = N_c i(t) \qquad (3.2)$$

Table 3.1: List of Parameters and Variables Participating in the Phenomenon of Induction Machines

Input Quantities		1) Time 2) Stator Current (Supply Current) 3) Supply Voltage 4) Power Factor 5) Frequency
Device Parameters and Quantities	Geometric	1) Rotor slots; number, pitch, and shape 2) Stator slots; number, pitch, and shape 3) Air-gap length 4) Laminations thickness and insulation 5) Stack length 6) Number of poles 7) Number of phases 8) Winding; type, chording, etc. 9) End-region geometries 10) Skew
	Material Constants	1) Permeability; for both stator and rotor materials 2) Mass densities 3) Specific heats 4) Thermal conductivities 5) Electrical resistivities 6) Thermal diffusivities
	Field Quantities	1) Magnetic flux density 2) Magnetic field strength 3) Electric field strength 4) Temperature; rise from ambient, gradient 5) Current density
	Device Variables	1) Time 2) Induced Currents 3) Induced Voltages 4) Slip (speed) 5) Electromagnetic Torque
Output Quantities		1) Time 2) Speed (slip) 3) Torque 4) Angular Velocity 5) Acceleration, Retardation

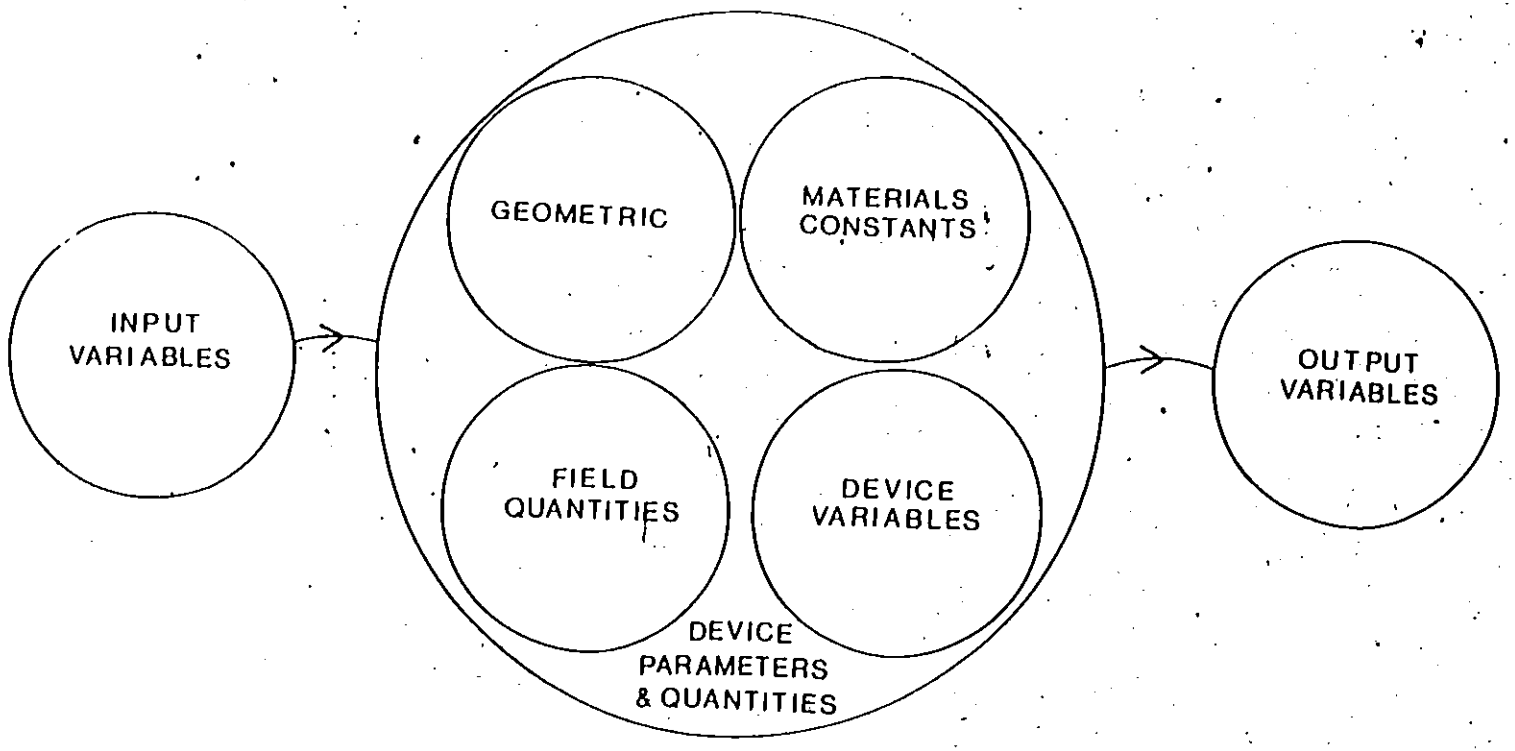

Figure 3.3: Classification of Induction Machines Parameters and Variables

If, for now, the effect of saturation is neglected, by assuming that for steel the permeability is infinite, then the magnetic flux density in the steel is zero. Furthermore, since the air gap length δ is small in comparison with the pole pitch, we can assume that the magnetic lines cross the air gap radially and the field strength along the gap is constant, varying only in direction.

Hence, as in some standard works [9, 17, 84], in the air gap

$$\oint H dl = 2\delta H(t) = N_c i(t)$$

Therefore,

$$H(t) = \frac{N_c i(t)}{2\delta} \tag{3.3}$$

and consequently, the instantaneous value of the magneto- motive force (mmf) of the flux in the gap at a given point will be

$$F(t) = \delta H(t) = \frac{N_c i(t)}{2} \tag{3.4}$$

This is equivalent to saying that the air gap mmf due to a single conductor carrying the current i(t) varies along the circumferential path of the air gap in the manner:

$$F(\vartheta,t) = \frac{N_c i(t)}{2}\left(1 - \frac{\vartheta}{\pi}\right); \quad (0 \leq \vartheta \leq 2\pi) \tag{3.5}$$

where ϑ is the angular position with respect to the conductor, in radians.

If the conductor is situated at a point ϑ_o with respect to a

fixed reference then (3.5) can be written in a more general way as

$$F(\vartheta,t) = \frac{N_c i(t)}{2} \begin{cases} (1 - \frac{\vartheta - \vartheta_o}{\pi}; & (\vartheta_o \leq \vartheta \leq 2\pi) \\ (\frac{\vartheta_o - \vartheta}{\pi} - 1); & (0 \leq \vartheta \leq \vartheta_o) \end{cases} \tag{3.6}$$

For a conductor carrying the same current but in the opposite direction and situated at a point ϑ_1,

$$F(\vartheta,t) = \frac{-N_c i(t)}{2} \begin{cases} (1 - \frac{\vartheta - \vartheta_1}{\pi}) ; & (\vartheta_1 \leq \vartheta \leq 2\pi) \\ (\frac{\vartheta_1 - \vartheta}{\pi} - 1) ; & (0 \leq \vartheta \leq \vartheta_1) \end{cases} \tag{3.7}$$

A coil will appear as two conductors carrying equal currents in opposite directions, with one coil side situated at ϑ_o and the other at ϑ_1. For the two possible cases, using equations (3.6) and (3.7), the following can be written:

case 1: if $\vartheta_1 > \vartheta_o$.

$$F_c(\vartheta,t) = \frac{N_c i(t)}{2} a(\vartheta) = \frac{N_c i(t)}{2} \begin{cases} \pm \frac{|\vartheta_o - \vartheta_1|}{\pi} ; & (\vartheta_1 \leq \vartheta \leq 2\pi) \\ - \frac{|\vartheta_o - \vartheta_1|}{\pi} ; & (0 \leq \vartheta \leq \vartheta_o) \\ (2 - \frac{|\vartheta_o - \vartheta_1|}{\pi}); & (\vartheta_o \leq \vartheta \leq \vartheta_1) \end{cases} \tag{3.8}$$

Case 2: if $\vartheta_o > \vartheta_1$

$$F_c(\vartheta,t) = \frac{-N_c i(t)}{2} a(\vartheta) = \frac{N_c i(t)}{2} \begin{cases} \dfrac{|\vartheta_o - \vartheta_1|}{\pi} ; & (\vartheta_o \leq \vartheta \leq 2\pi) \\ \dfrac{|\vartheta_o - \vartheta_1|}{\pi} ; & (0 \leq \vartheta \leq \vartheta_1) \\ -(2 - \dfrac{|\vartheta_o - \vartheta_1|}{\pi} ; & (\vartheta_1 \leq \vartheta \leq \vartheta_o) \end{cases} \quad (3.9)$$

where, the angular positional factor,

$$a(\vartheta) = \begin{cases} \dfrac{-|\vartheta_o - \vartheta_1|}{\pi} ; & (\vartheta_1 \text{ (or } \vartheta_o) \leq \vartheta \leq 2\pi) \\ \dfrac{-|\vartheta_o - \vartheta_1|}{\pi} ; & (0 \leq \vartheta \leq \vartheta_o \text{ (or } \vartheta_1) \\ (2 - \dfrac{|\vartheta_o - \vartheta_1|}{\pi} ; & (\vartheta_o \text{ (or } \vartheta_1) \leq \vartheta \leq \vartheta_1 \text{ (or } \vartheta_o) \end{cases} \quad (3.10)$$

Therefore, for a three phase winding with N coils per phase, the air gap mmf is a step distribution defined by

$$F_s(\vartheta,t) = \frac{N_c}{2} \sum_{m=1}^{3} i_{sm}(t) \sum_{n=1}^{N} \pm a_n(\vartheta) \quad (3.11)$$

With the assumption of no saturation and smooth air gap, the corresponding air gap flux density distribution is

$$B_{gs}(\vartheta,t) = \frac{\mu_o}{\delta} F_s(\vartheta,t) \quad (3.12)$$

For, if we assume for now that the effects of saturation and a non-smooth air gap can be accounted for by factors k_s and k_c respectively, then

$$B_{gs}(\vartheta,t) = \frac{\mu_o}{\delta k_s k_c} F_s(\vartheta,t) \qquad (3.13)$$

3.3 Rotor

3.3.1 Induced E.M.F. in a Rotor Mesh by the Stator Fields.

If equation (3.13) is expanded into a Fourier series, then for the νth harmonic (where $\nu = 1$ corresponds to the fundamental for a machine with p poles), the sine component of the flux density is $B_{m\nu} \sin(\beta_\nu)$ and the cosine component in $B_{m\nu}\cos(\beta_\nu)$. If

$$s_\nu = 1 \pm (1-s)\nu \qquad (3.14)$$

then the νth harmonic component of air gap flux density as seen on the rotor peripheral is

$$B_{gs\nu}(\vartheta,t) = B_{m\nu}\cos\beta_\nu \cos\left(s_\nu\omega_s t - \nu p\frac{\vartheta}{2}\right) + B_{m\nu}\sin\beta_\nu \sin\left(s_\nu\omega_s t - \nu p\frac{\vartheta}{2}\right)$$

$$= B_{m\nu}\cos\left(s_\nu\omega_s t - \nu p\frac{\vartheta}{2} - \beta_\nu\right) \qquad (3.15)$$

where $\omega_s = 2\pi f$

The rotor has Q_2 bars which define Q_2 meshes (see figure 3.5). The differential area through which the fluxes linking a rotor mesh pass is

$$dA = \frac{lD}{2}\, d\vartheta$$

The flux through this differential area is

$$d\Phi = B_{gs\nu}(\vartheta,t)dA$$

$$= B_{gs\nu}(\vartheta,t)\,\frac{lD}{2}\,d\vartheta$$

Then, from figure 3.4, the total flux linking a mesh or coil whose axis is situated at $\vartheta = \vartheta_k$ (i.e. ϑ_k denotes the abscissa of the center of the mesh) is:

$$\Phi_{bs\nu} = \int_{\vartheta_k - \pi/Q_2}^{\vartheta_k + \pi/Q_2} B_{gs\nu}(\vartheta,t)\,l\frac{D}{2}\,d\vartheta$$

Substituting for $B_{gs\nu}(\vartheta,t)$ from equation (3.15), then

$$\Phi_{bs\nu} = B_{m\nu}\,l\frac{D}{2}\int_{\vartheta_k - \pi/Q_2}^{\vartheta_k + \pi/Q_2} \cos(s_\nu\omega_s t - \nu p\frac{\vartheta}{2} - \beta_\nu)\,d\vartheta$$

$$= -\frac{B_{m\nu}\,lD}{\nu p}\left[\sin(s_\nu\omega_s t - \nu p\frac{\vartheta}{2} - \beta_\nu)\right]_{\vartheta_k - \pi/Q_2}^{\vartheta_k + \pi/Q_2}$$

$$\therefore \Phi_{bs\nu} = 2\frac{B_{m\nu}\,lD}{\nu p}\cdot\sin\frac{\nu p\pi}{2Q_2}\cos(s_\nu\omega_s t - \nu p\frac{\vartheta_k}{2} - \beta_\nu) \qquad (3.16)$$

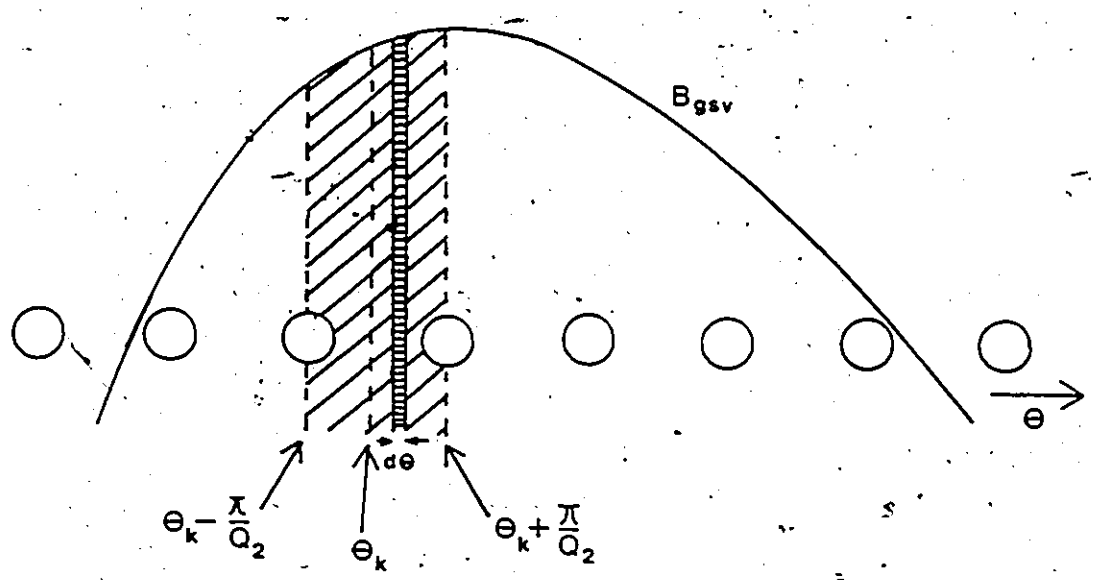

Figure 3.4: Flux linkages of a rotor mesh with air gap flux due to a stator sinusoidal component of the mmf.

The induced electro-motive force (e.m.f.) in a squirrel cage winding mesh is

$$e_{bs\nu} = -\frac{d\lambda_{bs}}{dt}$$

where the flux linkage

$$\lambda_{bs} = N_b \Phi_{bs}$$

But the number of turns $N_b = 1$,

Therefore,

$$e_{bs\nu k} = \frac{4\pi f s_\nu B_{m\nu} lD}{\nu p} \cdot \sin\frac{\nu p \pi}{2Q_2} \sin(s_\nu \omega_s t - \frac{\nu p \vartheta_k}{2} - \beta_\nu) \qquad (3.17)$$

3.3.2 Induced E.M.F. in a Rotor Mesh by the Rotor Fields

It was shown, in section 3.2, that the distribution of the mmf in the air gap, produced by a single turn with one coil side situated at $\vartheta_o = \pm\frac{\alpha_d}{2}$ and the other at $\vartheta_1 = \mp\frac{\alpha_d}{2}$ and carrying a current i(t), is given by equation (3.8) or (3.9). It can also be shown that when this is developed into a fourier series it is

$$F(\vartheta,t) = \frac{2N_c i(t)}{\pi} \sum_{u=1}^{\infty} \frac{1}{u} \sin\frac{u\alpha_d}{2} \cos u\vartheta \qquad (3.18)$$

If the stator νth harmonic air gap field causes currents $i_{\nu 12}, i_{\nu 23}, \cdots i_{\nu Q_2 1}$ in the rotor winding meshes (see figure 3.5), then the air gap mmf distribution due to current in the nth mesh is

$$F_{r\nu n} = \frac{2i_{\nu n(n+1)}}{\pi} \sum_{u=1}^{\infty} \frac{1}{u} \sin \frac{u\alpha_d}{2} \cos u(\vartheta - (n-1)\alpha_d)$$

where $\alpha_d = 2\pi/Q_2$ is the angle between the centers of two adjacent meshes and is equivalent to the angle with which bars are mutually displaced in space. The corresponding flux density distribution, like equation (3.13), is

$$B_{gr\nu n} = \frac{2\mu_o i_{\nu n(n+1)}}{\pi\delta k_c k_s} \sum_{u=1}^{\infty} \frac{1}{u} \sin \frac{u\alpha_d}{2} \cos u(\vartheta - (n-1)\alpha_d) \qquad (3.19)$$

The total air gap flux density distribution due to currents in all meshes is therefore

$$B_{gr\nu} = \frac{2\mu_o}{\pi\delta k_c k_s} \sum_{n=1}^{Q_2} i_{\nu n(n+1)} \sum_{u=1}^{\infty} \frac{1}{u} \sin \frac{u\alpha_d}{2} \cos u(\vartheta - (n-1)\alpha_d) \qquad (3.20)$$

By following the same procedure as in section 3.3.1 it can be shown that the e.m.f. induced by this field in a rotor mesh whose center is situated at $\vartheta = \vartheta_k$ is

$$e_{br\nu k} = \frac{4\mu_o lD}{\pi\delta k_c k_s} \sum_{n=1}^{Q_2} \frac{di_{\nu n(n+1)}}{dt} \sum_{u=1}^{\infty} \frac{1}{u^2} \sin^2 \frac{u\alpha_d}{2} \cos u(\vartheta_k - (n-1)\alpha_d) \qquad (3.21)$$

3.3.3 Induced Currents in the Rotor Winding

The squirrel cage winding has Q_2 bars which define Q_2 meshes which are numbered: 12, 23, 34, ... $Q_2 1$. A mesh therefore is defined by two adjacent bars and the two end-ring segments which link them at either ends. If a bar is viewed as a branch of a lumped impedance

$$z_{b\nu} = r_{b\nu} + jx_{b\nu} \qquad (3.22)$$

representing the νth harmonic resistance and slot leakage reactance, in which the effects of heat and skin effect have been duly accounted, and an end-ring segment is viewed as a branch of a lumped impedance

$$z_{e\nu} = r_{e\nu} + jx_{e\nu} \tag{3.23}$$

representing the νth harmonic end-ring segment resistance and end-leakage reactance. Then a squirrel-cage winding can be represented by a circular ladder network of figure 3.5. The network therefore is exactly as the squirrel cage winding is configured except that the physical bars and end-rings are represented by equivalent impedances.

For any νth harmonic the total voltage induced in the kth mesh is the sum of the induced e.m.f.s in that mesh by the νth harmonic component stator (section 3.3.1) and rotor (section 3.3.2) air gap fields. Hence,

$$e_{\nu k(k+1)} = e_{bs\nu k} + e_{br\nu k} \tag{3.24}$$

where $e_{bs\nu k}$ and $e_{br\nu k}$ are as in equations (3.17) and (3.21) respectively. These two e.m.f.s can be simplified as follow:

$$e_{bs\nu k} = E_{m\nu} \sin(s_\nu \omega_s t - \frac{\nu p \vartheta_k}{2} - \beta_\nu) \tag{3.25}$$

where

$$E_{m\nu} = \frac{4\pi f s_\nu B_{m\nu} l D}{\nu p} \cdot \sin \frac{\nu p \pi}{2Q_2} \tag{3.26}$$

and

$$e_{br\nu k} = G \sum_{n=1}^{Q_2} H_{kn} \frac{di_{\nu n(n+1)}}{dt} \tag{3.27}$$

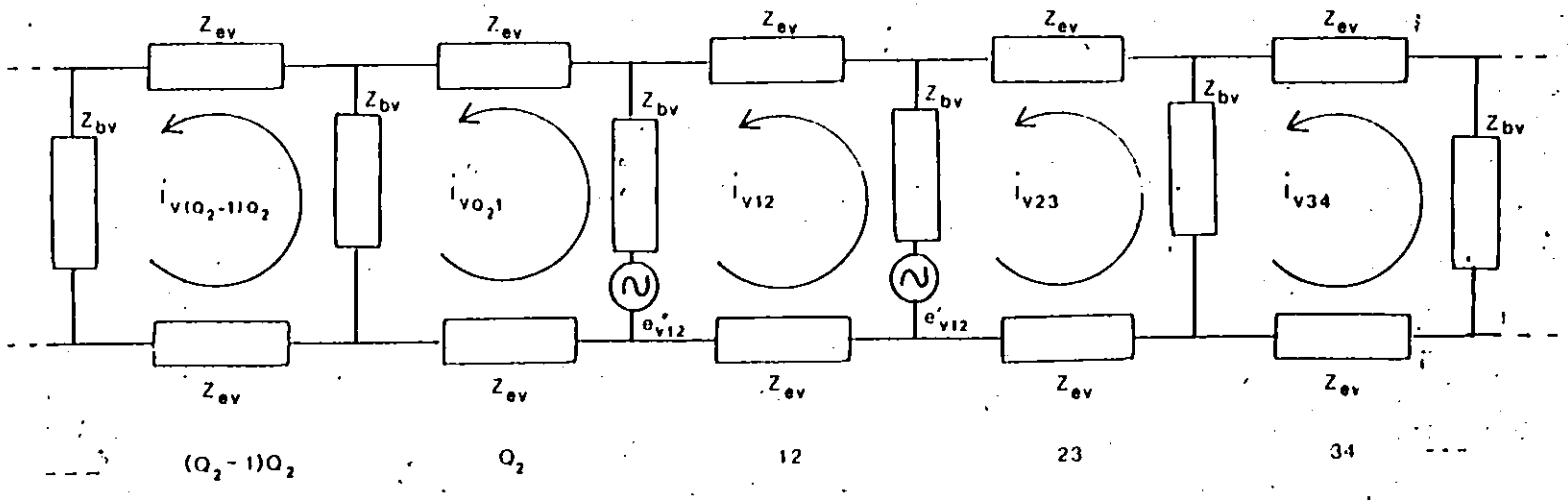

Figure 3.5: Circular ladder equivalent network for the squirrel-cage winding

where

$$G = \frac{4\,\mu_o' l D}{\pi \delta k_c k_s} \tag{3.28}$$

and

$$H_{kn} = \sum_{u=1}^{\infty} \frac{1}{u^2} \sin^2 \frac{u\alpha_d}{2} \cos u(\vartheta_k - (n-1)\alpha_d) \tag{3.29}$$

If we assume that e.m.f. is induced only in the bars but not in the end-rings then the total voltage induced in the kth mesh can be expressed in terms of the voltages induced in the two bars comprising the mesh thus

where

$$e_{\nu k(k+1)} = e'_{\nu k(k+1)} + e''_{\nu k(k+1)} \tag{3.30}$$

$$e'_{\nu k(k+1)} = e'_{bs\nu k} + e'_{br\nu k} \tag{3.31}$$

and

$$e''_{\nu k(k+1)} = e''_{bs\nu k} + e''_{br\nu k} \tag{3.32}$$

$e'_{bs\nu k}$ and $e'_{br\nu k}$ are the induced e.m.f.s, by the stator and rotor air gap fields respectively, in one bar of the mesh, and $e''_{bs\nu k}$ and $e''_{br\nu k}$ are those in the other bar. These voltages can be determined from the general fact that the complex or vector voltage in one coil-side of a turn is related to the complex or vector voltage of a mesh (or turn) by the following expressions:

$$\dot{e}'_c = \frac{\dot{e}_t \exp[j(-\frac{\alpha_d}{2} + \frac{\pi}{2})]}{2 \sin \frac{\alpha_d}{2}} \tag{3.33a}$$

and

$$\dot{e}_c'' = \frac{-\dot{e}_t \exp[j(\frac{\alpha_d}{2} + \frac{\pi}{2})]}{2 \sin \frac{\alpha_d}{2}} \tag{3.33b}$$

where $\dot{e}_t$ is the complex mesh voltage, and $\dot{e}_c'$ and $\dot{e}_c''$ are the complex coil side voltages. α_d is the pitch of the mesh in mechanical angle. For any νth harmonic and p poles the pitch in electrical angle is $\frac{\nu p \alpha_d}{2}$.

For example, if the complex form of $e_{bs\nu k}$ is defined as

$$\dot{e}_{bs\nu k} = E_{m\nu} \exp[j(s_\nu \omega_s t - \frac{\nu p \vartheta_k}{2} - \beta_\nu) \tag{3.34}$$

such that

$$e_{bs\nu k} = \mathrm{Im}\ [\dot{e}_{bs\nu k}]$$

where Im refers to imaginary component.

Then, by applying equation (3.33) and substituting for pitch in electrical angle, it can be shown that

$$e_{bs\nu k}' = \mathrm{Im}\ [\dot{e}_{bs\nu k}']$$

$$= \frac{E_{m\nu}}{2 \sin(\frac{\nu p \alpha_d}{2})} \cos(s_\nu \omega_s t - \frac{\nu p \vartheta_k}{2} - \beta_\nu - \frac{\nu p \alpha_d}{2}) \tag{3.35}$$

It can similarly be shown that

$$e_{bs\nu k}'' = \frac{-E_{m\nu}}{2 \sin(\frac{\nu p \alpha_d}{2})} \cos(s_\nu \omega_s t - \frac{\nu p \vartheta_k}{2} - \beta_\nu + \frac{\nu p \alpha_d}{2}) \tag{3.36}$$

By following a similar procedure as above it can be shown that

$$e'_{br\nu k} = G \sum_{n=1}^{Q_2} H'_{kn} \frac{di_{\nu n(n+1)}}{dt} \tag{3.37}$$

where

$$H'_{kn} = \frac{1}{2} \sum_{u=1}^{\infty} \frac{1}{u^2} \sin \frac{u\alpha_d}{2} \cos u(\vartheta_k - (n-1)\alpha_d + \frac{\alpha_d}{2}) \tag{3.38}$$

$$e''_{br\nu k} = G \sum_{n=1}^{Q_2} H''_{kn} \frac{di_{\nu n(n+1)}}{dt} \tag{3.39}$$

where

$$H''_{kn} = -\frac{1}{2} \sum_{u=1}^{\infty} \frac{1}{u^2} \sin \frac{u\alpha_d}{2} \cos u(\vartheta_k - (n-1)\alpha_d - \frac{\alpha_d}{2}) \tag{3.40}$$

If we assume that e.m.f. is induced only in the mesh 12, figure 3.5, but not in any other mesh, then the following set of equations is true for the network of figure 3.5:

$$\begin{aligned}
-e_{\nu 12} + 2(z_{b\nu} + z_{e\nu})i_{\nu 12} - z_{b\nu} i_{\nu 23} - z_{b\nu} i_{\nu Q_2 1} &= 0 \\
e''_{\nu 12} - z_{b\nu} i_{\nu 12} + 2(z_{b\nu} + z_{e\nu})i_{\nu 23} - z_{b\nu} i_{\nu 34} &= 0 \\
-z_{b\nu} i_{\nu 23} + 2(z_{b\nu} + z_{e\nu})i_{\nu 34} - z_{b\nu} i_{\nu 45} &= 0 \\
- \quad - \quad - \quad - \quad - \quad - \quad - \quad & \qquad (3.41) \\
e'_{\nu 12} - z_{b\nu} i_{\nu 12} - z_{b\nu} i_{\nu (Q_2-1)Q_2} + 2(z_{b\nu} + z_{e\nu})i_{\nu Q_2 1} &= 0
\end{aligned}$$

If the first equation in (3.41) is multiplied by −1 and the

whole equations in (3.41) are summed together we obtain:

$$e_{\nu 12} + e'_{\nu 12} + e''_{\nu 12} - 2(2z_{b\nu} + z_{e\nu})i_{\nu 12} + 2(z_{b\nu} + z_{e\nu})i_{\nu 23}$$

$$+ 2z_{e\nu}i_{\nu 34} + 2z_{e\nu}i_{\nu 45} + \dots + 2z_{e\nu}i_{\nu(Q_2-1)Q_2} + 2(z_{b\nu} + z_{e\nu})i_{\nu Q_2 1} = 0 \tag{3.42}$$

Substituting equation (3.30) into equation (3.42) and simplifying we obtain

$$(2z_{b\nu} + z_{e\nu})i_{\nu 12} - (z_{b\nu} + z_{e\nu})i_{\nu 23} - z_{e\nu}i_{\nu 34} - z_{e\nu}i_{\nu 45}$$

$$- \dots - z_{e\nu}i_{\nu(Q_2-1)Q_2} - (z_{b\nu} + z_{e\nu})i_{\nu Q_2 1} = e_{\nu 12} \tag{3.43}$$

Generalizing equation (3.43) to the case in which e.m.f. is induced only in mesh k(k+1), not in any other mesh, we can write

$$- z_{e\nu}i_{\nu 12} - z_{e\nu}i_{\nu 23} - \dots - (z_{b\nu} + z_{e\nu})i_{\nu(k-1)k}$$

$$+ (2z_{b\nu} + z_{e\nu})i_{\nu k(k+1)} - (z_{b\nu} + z_{e\nu})i_{\nu(k+1)(k+2)} - \dots$$

$$- z_{e\nu}i_{\nu Q_2 1} = e_{\nu k(k+1)} \tag{3.44}$$

Writing equation (3.44) for each mesh and arranging the resulting set of equations in matrix form we obtain

$$\begin{bmatrix} e_{\nu 12} \\ e_{\nu 23} \\ - \\ e_{\nu Q_2 1} \end{bmatrix} = \begin{bmatrix} (2z_{b\nu} + z_{e\nu}) & -(z_{b\nu} + z_{e\nu}) & -z_{e\nu} & \dots & -z_{e\nu} & -(z_{b\nu} + z_{e\nu}) \\ -(z_{b\nu} + z_{e\nu}) & +(2z_{b\nu} + z_{e\nu}) & -(z_{b\nu} + z_{e\nu}) & \dots & -z_{e\nu} & -z_{e\nu} \\ - & - & - & - & - & - \\ -(z_{b\nu} + z_{e\nu}) & - & -z_{e\nu} & -z_{e\nu} \dots & -(z_{b\nu} + z_{e\nu}) & (2z_{b\nu} + z_{e\nu}) \end{bmatrix} \begin{bmatrix} i_{\nu 12} \\ i_{\nu 23} \\ - \\ i_{\nu Q_2 1} \end{bmatrix} \tag{3.45}$$

which in compact form is

$$e_\nu = z_\nu i_\nu \tag{3.46}$$

where the Q_2 elements vector of the induced e.m.f. in the meshes is

$$e_\nu = [e_{\nu 12} \quad e_{\nu 23} \cdots \quad e_{\nu Q_2 1}]^T \tag{3.47}$$

and the corresponding vector of the induced mesh currents is

$$i_\nu = [i_{\nu 12} \quad i_{\nu 23} \cdots \quad i_{\nu Q_2 1}]^T \tag{3.48}$$

and the $Q_2 \times Q_2$ impedance matrix is

$$z_\nu = \begin{bmatrix} (2z_{b\nu} + z_{e\nu}) & -(z_{b\nu} + z_{e\nu}) & -z_{c\nu} & \cdots & -z_{c\nu} & -(z_{b\nu} + z_{e\nu}) \\ -(z_{b\nu} + z_{e\nu}) & (2z_{b\nu} + z_{e\nu}) & -(z_{b\nu} + z_{c\nu}) & \cdots & -z_{e\nu} & -z_{e\nu} \\ - & - & - & - & - & - \\ -(z_{b\nu} + z_{e\nu}) & -z_{e\nu} & -z_{e\nu} & \cdots & -(z_{b\nu} + z_{e\nu}) & (2z_{b\nu} + z_{e\nu}) \end{bmatrix} \tag{3.49}$$

From equation (3.24) we can write

$$e_\nu = e_{bs\nu} + e_{br\nu} \tag{3.50}$$

where

$$e_{bs\nu} = [e_{bs\nu 1} \quad e_{bs\nu 2} \cdots \quad e_{bs\nu Q_2}]^T \tag{3.51}$$

and from equation (3.27)

$$e_{br\nu} = \begin{bmatrix} e_{br\nu 1} \\ e_{br\nu 2} \\ - \\ e_{br\nu Q_2} \end{bmatrix} = G \begin{bmatrix} H_{11} & H_{12} & \cdots & H_{1Q_2} \\ H_{21} & H_{22} & \cdots & H_{2Q_2} \\ - & - & - & - \\ H_{Q_2 1} & H_{Q_2 2} & \cdots & H_{Q_2 Q_2} \end{bmatrix} \frac{d}{dt} \begin{bmatrix} i_{\nu 12} \\ i_{\nu 23} \\ - \\ i_{\nu Q_2 1} \end{bmatrix} \tag{3.52}$$

which in compact form is

$$e_{br\nu} = G\,H\,d/dt\;i_\nu \tag{3.53}$$

substituting equations (3.50) and (3.53) into (3.46) we have

$$e_{bs\nu} = z_\nu i_\nu - e_{br\nu}$$

$$= z_\nu i_\nu - G\,H\,\frac{d}{dt}\,i_\nu \tag{3.54}$$

Equation (3.54) relates the rotor mesh currents with the stator quantities. This equation therefore implies that with the knowledge of the stator currents, and hence the stator air gap field, the rotor mesh currents of a squirrel-cage induction machine, and hence the rotor air gap field, can be determined. Hence, it can be said that (3.54) is the equation of the machine which needs to be solved.

Equation (3.54) may alternatively be expressed in terms of the bar quantities, instead of the mesh quantities, thus

$$e'_{bs\nu} + e''_{bs\nu} = z_\nu c^{-1} i_{b\nu} - GHc^{-1}\,\frac{d}{dt}\,i_{b\nu} \tag{3.55}$$

where

$$e'_{bs\nu} = [e'_{bs\nu 1}\quad e'_{bs\nu 2}\quad \cdots\quad e'_{bs\nu Q_2}]^T \tag{3.56}$$

and

$$e''_{bs\nu} = [e''_{bs\nu 1}\quad e''_{bs\nu 2}\quad \cdots\quad e''_{bs\nu Q_2}]^T \tag{3.57}$$

The elements of these vectors, equations (3.56) and (3.57), are as

defined by equations (3.35) and (3.36) respectively. The bar currents vector is

$$i_{b\nu} = [i_{b\nu 1} \quad i_{b\nu 2} \quad \cdots \quad i_{b\nu Q_2}]^T \tag{3.58}$$

and it is related to the mesh currents vector, equation (3.48), by the relation

$$i_{b\nu} = c i_{\nu} \tag{3.59}$$

where the $Q_2 \times Q_2$ transformation matrix is

$$c = \begin{bmatrix} -1 & 0 & 0 & \cdots & 0 & 1 \\ 1 & -1 & 0 & \cdots & 0 & 0 \\ 0 & 1 & -1 & \cdots & 0 & 0 \\ - & - & - & - & - & - \\ 0 & 0 & 0 & \cdots & -1 & 0 \\ 0 & 0 & 0 & \cdots & 1 & -1 \end{bmatrix} \tag{3.60}$$

3.3.4 An Alternative Formulation

An alternative formulation of the machine equation relating the rotor currents to the stator quantities may be derived using the method of superposition and equivalent network to the network of figure 3.5 instead of the mesh currents method as in the last section. If it is assumed that e.m.f. is induced by the air gap fields, only in the kth bar of a squirrel cage winding, and not in any other bar, then for any harmonic the circular ladder equivalent network of figure 3.5 can be

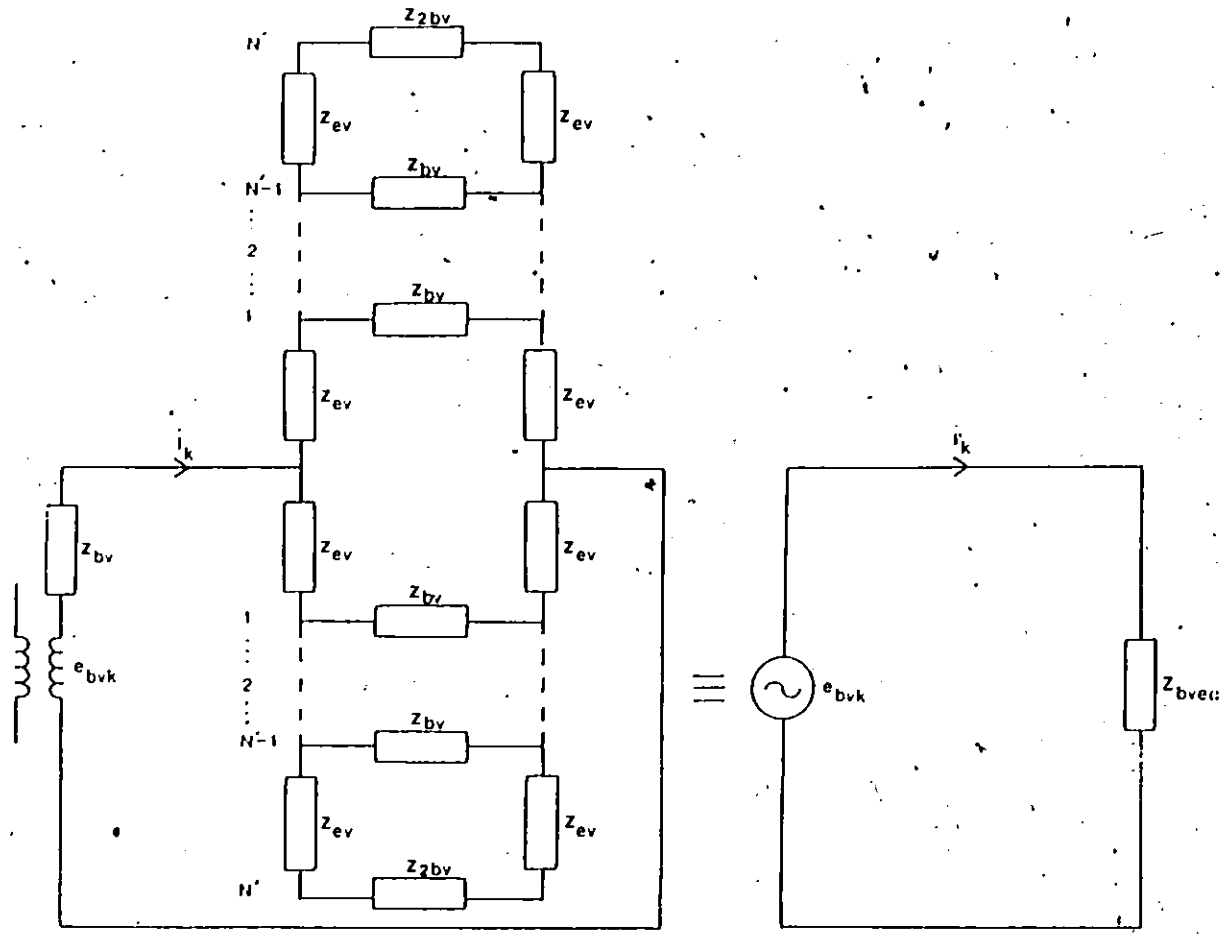

Figure 3.6: A network model of the squirrel cage winding.

developed into the form shown in figure 3.6. N' in the figure is defined by

$$N' = \begin{cases} \dfrac{Q_2-1}{2} \text{ ; if } Q_2 \text{ is odd} \\ \\ \dfrac{Q_2}{2} \text{ ; if } Q_2 \text{ is even} \end{cases} \tag{3.61}$$

and the impedance

$$z_{2b\nu} = \begin{cases} z_{b\nu} \text{ ; if } Q_2 \text{ is odd} \\ \\ 2z_{b\nu} \text{ ; if } Q_2 \text{ is even} \end{cases} \tag{3.62}$$

The induced e.m.f. in the kth bar by the stator and rotor air gap field is

$$e_{b\nu k} = e'_{\nu k(k+1)} - e''_{\nu(k+1)(k+2)} \tag{3.63}$$

which from equations (3.31) and (3.32) can be written as

$$e_{b\nu k} = e'_{bs\nu k} + e'_{br\nu k} - e''_{bs\nu(k+1)} - e''_{br\nu(k+1)}$$

$$= e_{bs\nu k1} + e_{br\nu k1} \tag{3.64}$$

where

$$e_{bs\nu k1} = e'_{bs\nu k} - e''_{bs\nu(k+1)} \tag{3.65}$$

Substituting equations (3.35) and (3.36) into (3.65) and taken $\vartheta_k = (k-1)\alpha_d$ and $\vartheta_{k+1} = k\alpha_d$ we found

$$e_{bs\nu k1} = \frac{E_{m\nu}}{\sin(\frac{\nu p\alpha_d}{2})} \cos(s_\nu \omega_s t - \frac{\nu p}{2}(k-\frac{1}{2})\alpha_d - \beta_\nu) \tag{3.66}$$

Also

$$e_{br\nu k1} = e'_{br\nu k} - e''_{br\nu(k+1)} \tag{3.67}$$

which from equations (3.37) to (3.40)

$$e_{br\nu k1} = G \sum_{n=1}^{Q_2} H_{kn1} \frac{di_{\nu n(n+1)}}{dt} \tag{3.68}$$

where

$$H_{kn1} = \sum_{u=1}^{\infty} \frac{1}{u^2} \sin \frac{u\alpha_d}{2} \cos u[(k-\frac{1}{2})\alpha_d - (n-1)\alpha_d] \tag{3.69}$$

If the equivalent impedance of the network of figure 3.6 is, as shown in the figure, $z_{b\nu eq}$ then the induced current corresponding to induced e.m.f. in the kth bar only is

$$i_k = e_{b\nu k} / z_{b\nu eq} \tag{3.70}$$

If we assume that this current flows out from the kth bar and returns through the remaining Q_2-1 bars in the manner illustrated in figure 3.7(a), then the current in any of the remaining Q_2-1 bars can be calculated as a fraction of i_k. This fraction can be computed as the ratio of impedances by treating the network, at each node numbered 1 to N' in figure 3.6, as a current divider. For example, the current in the (k+1)th bar, which because of symmetry is the same as that in the (k-1)th bar, is

$$i'_{b\nu k(k+1)} \cong i'_{b\nu k(k-1)} = f_{k(k+1)} i_k \tag{3.71}$$

where

$$f_{k(k+1)} = f_{k(k-1)} = f_1 = -\frac{1}{2}\left|\frac{z_{eq2N'} + 2z_{e\nu}}{z_{b\nu}}\right| \tag{3.72}$$

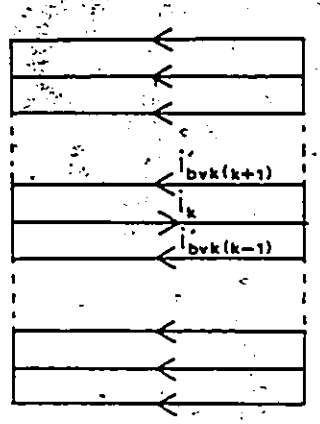

(a)

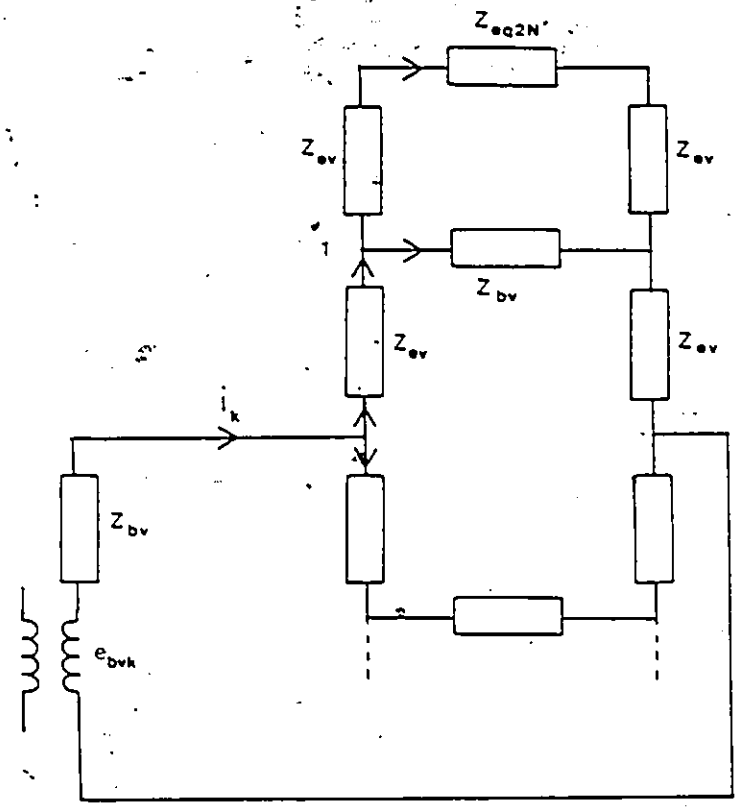

(b)

Figure 3.7: Network of Squirrel-cage Winding
(a) Illustration of the flow of current
(b) Calculation of current in the bars

where, as shown in figure 3.7(b), $z_{eq2N'}$ is the bars and end-ring impedances from 2 to N' lumped together as one. In a similar manner it can be shown that

$$i'_{b\nu k(k+2)} = i'_{b\nu k(k-2)} = f_{k(k+2)} i_k$$

where

$$f_{k(k+2)} = f_{k(k-2)} = f_2 = \left| \frac{z_{eq3N'} + 2z_{e\nu}}{z_{b\nu}} \right| f'_1 \qquad (3.73)$$

By following similar procedure as for equations (3.72) and (3.73) the factors f'_i can be computed for $i = 1$ to N'.

The distribution of the induced currents in a squirrel cage bars due to an induced e.m.f. in one bar alone can thus be written as

$$i'_{b\nu k} = f_k i_k \qquad (3.74)$$

where the vector of the bar currents

$$i'_{b\nu k} = [i'_{b\nu k1} \quad i'_{b\nu k2} \quad \cdots \quad i'_{b\nu kQ_2}]^T \qquad (3.75)$$

and the vector of the factors

$$f_k = [f_{k1} \quad f_{k2} \quad \cdots \quad f_{kQ_2}]^T \qquad (3.76)$$

for example, if Q_2 is odd and $k=1$

$$f_k = [1 \quad f_1 \quad f_2 \quad \cdots \quad f_{N'-1} \quad f_{N'} \quad f_{N'} \quad f_{N'-1} \cdots f_1]^T \qquad (3.77)$$

if Q_2 is even and $k = 1$

$$f_k = [1 \quad f_1 \quad f_2 \quad \cdots \quad f_{N'-1} \quad 2f_{N'} \quad f_{N'-1} \quad \cdots \quad f_1]^T$$

Since impedances vary only with ν but not with k the factors f_i (i = 1 to N') are therefore constant for all k but vary only with the order of the inducing field, ν.

If equations (3.70) and (3.74) are solved for all k from 1 to Q_2 then the net induced current in a bar due to all the induced e.m.f.s in all bars acting simultaneously is the sum of all the currents in that bar due to the individual e.m.f. acting one at a time. Hence,

$$i_{b\nu} = \sum_{k=1}^{Q_2} i'_{b\nu k}$$

$$= \sum_{k=1}^{Q_2} f_k i_k$$

$$= f i_k$$

$$= \frac{1}{z_{b\nu eq}} f e_{b\nu} \qquad (3.79)$$

where the net bar current vector is

$$i_{b\nu} = [i_{b\nu 1} \quad i_{b\nu 2} \quad \cdots \quad i_{b\nu Q_2}] \qquad (3.80)$$

and f is a symmetric $Q_2 \times Q_2$ matrix given by

$$f = \begin{bmatrix} 1 & f_1 & f_2 & \cdots & f_1 \\ f_1 & 1 & f_1 & \cdots & f_2 \\ f_2 & f_1 & 1 & \cdots & f_3 \\ - & - & - & - & - \\ f_1 & f_2 & f_3 & \cdots & 1 \end{bmatrix} \qquad (3.81)$$

The bar voltage vector

$$e_{b\nu} = [e_{b\nu 1} \quad e_{b\nu 2} \quad \cdots \quad e_{b\nu Q_2}] \tag{3.82}$$

Equation (3.79) can be written in the form of equation (3.54)

$$e_{b\nu} = z_{b\nu eq} f^{-1} i_{b\nu} \tag{3.83}$$

But from equation (3.64) we can write

$$e_{b\nu} = e_{bs\nu 1} + e_{br\nu 1} \tag{3.84}$$

Substituting (3.84) in (3.83) and by applying equation (3.68) it can be shown that equation (3.83) can be written thus

$$e_{bs\nu 1} = z_{b\nu eq} f^{-1} i_{b\nu} - GH_1 \frac{d}{dt} i_\nu \tag{3.85}$$

H_1 is like in equation (3.52) except the elements are computed by equation (3.69) instead of (3.29). $i_{b\nu}$ may be substituted for i_ν by applying equation (3.59).

3.4 Solution of the Machine Equation

Equation (3.54) (or (3.55) or (3.85)) is a linear periodic coefficient differential equation. Since there is no direct method of solving such equation we have to resort to a method of guess for the solution.

Let us assume that the mesh currents solution which satisfy equation (3.54) is of the form

$$i_{\nu k(k+1)} = I_{m\nu} \cos(s_\nu \omega_s t - \frac{\nu p}{2} \vartheta_k - \beta_\nu - \vartheta_{pf}) \tag{3.86}$$

and that they satisfy

$$\sum_{m=1}^{Q_2} i_{\nu m(m+1)} = 0 \tag{3.87}$$

The kth equation of the set of equations (3.54) is

$$e_{bs\nu k} = e_{\nu k(k+1)} - e_{br\nu k} \tag{3.88}$$

From equation (3.44)

$$\begin{aligned} e_{\nu k(k+1)} &= -z_{e\nu} i_{\nu 1} - z_{e\nu} i_{\nu 2} \cdots -(z_{b\nu} + z_{e\nu}) i_{\nu(k-1)k} \\ &\quad + (2z_{b\nu} + z_{e\nu}) i_{\nu k(k+1)} - (z_{b\nu} + z_{e\nu}) i_{\nu(k+1)(k+2)} \cdots \\ &\quad - z_{e\nu} i_{\nu Q_2 1} \\ &= -(z_{b\nu} + z_{e\nu}) i_{\nu(k-1)k} + (2z_{b\nu} + z_{e\nu}) i_{\nu k(k+1)} \\ &\quad - (z_{b\nu} + z_{e\nu}) i_{\nu(k+1)(k+2)} - z_{e\nu} \sum_{\substack{m=1 \\ m \neq k, k-1, k+1}}^{Q_2} i_{\nu m(m+1)} \end{aligned} \tag{3.89}$$

From equation (3.87) we can write

$$\sum_{\substack{m=1 \\ m \neq k, k-1, k+1}}^{Q_2} i_{\nu m(m+1)} = -i_{\nu(k-1)k} - i_{\nu k(k+1)} - i_{\nu(k+1)(k+2)} \tag{3.90}$$

Substituting equation (3.90) into (3.89) we have

$$\begin{aligned} e_{\nu k(k+1)} &= -(z_{b\nu} + z_{e\nu}) i_{\nu(k-1)k} + (2z_{b\nu} + z_{e\nu}) i_{\nu k(k+1)} \\ &\quad - (z_{b\nu} + z_{e\nu}) i_{\nu(k+1)(k+2)} + z_{e\nu} i_{\nu(k-1)k} + z_{e\nu} i_{\nu k(k+1)} \\ &\quad + z_{e\nu} i_{\nu(k+1)(k+2)} \end{aligned}$$

$$e_{\nu k(k+1)} = -z_{b\nu} i_{\nu(k-1)k} + 2(z_{b\nu} + z_{e\nu}) i_{\nu k(k+1)} - z_{b\nu} i_{\nu(k+1)(k+2)}$$

$$= z_{b\nu}(2i_{\nu k(k+1)} - i_{\nu(k-1)k} - i_{\nu(k+1)(k+2)}) + 2z_{e\nu} i_{\nu k(k+1)} \tag{3.91}$$

If from (3.86) we write

$$i_{\nu(k-1)k} = I_{m\nu}\cos(\Omega - \frac{\nu p}{2}(k-2)\alpha_d)$$

$$i_{\nu k(k+1)} = I_{m\nu}\cos(\Omega - \frac{\nu p}{2}(k-2)\alpha_d)$$

$$i_{\nu(k+1)(k+2)} = I_{m\nu}\cos(\Omega - \frac{\nu p}{2}k\alpha_d)$$

where

$$\Omega = s_\nu \omega_s t - \beta_\nu - \delta_{pf}$$

If we define

$$\Omega' = \Omega - \frac{\nu p}{2}(k-1)\alpha_d$$

then

$$2i_{\nu k(k+1)} - i_{\nu(k-1)k} - i_{\nu(k+1)(k+2)} = I_{m\nu}(2\cos\Omega' -$$

$$\cos\Omega'\cos\frac{\nu p}{2}\alpha_d + \sin\Omega'\sin\frac{\nu p}{2}\alpha_d - \cos\Omega'\cos\frac{\nu p}{2}\alpha_d$$

$$- \sin\Omega'\sin\frac{\nu p}{2}\alpha_d)$$

$$= I_{m\nu}(2\cos\Omega' - 2\cos\Omega'\cos\frac{\nu p}{2}\alpha_d)$$

$$= 2I_{m\nu}\cos\Omega' \left(1-\cos\frac{\nu p}{2}\alpha_d\right)$$

$$= 2i_{\nu k(k+1)}\left(1-\cos\frac{\nu p}{2}\alpha_d\right)$$

$$= 2i_{\nu k(k+1)}\left(1 - 1 + 2\sin^2\frac{\nu p}{2}\alpha_d\right)$$

$$= 4i_{\nu k(k+1)}\sin^2\frac{\nu p}{2}\alpha_d \tag{3.92}$$

Substituting (3.92) into (3.91) we have

$$e_{\nu k(k+1)} = \left(2z_{e\nu} + 4z_{b\nu}\sin^2\frac{\nu p}{2}\alpha_d\right)i_{\nu k(k+1)} \tag{3.93}$$

The second term of equation (3.88) is, from equation (3.27)

$$e_{br\nu k} = G\sum_{n=1}^{Q_2} H_{kn}\frac{di_{\nu n(n+1)}}{dt}$$

Substituting for H_{kn} from equation (3.29) we have

$$e_{br\nu k} = G\sum_{n=1}^{Q_2}\frac{di_{\nu n(n+1)}}{dt}\sum_{u=1}^{\infty}\frac{1}{u^2}\sin^2\frac{u\alpha_d}{2}\cos u(\vartheta_k - (n-1)\alpha_d)$$

$$= \sum_{n=1}^{Q_2} e_{kn}$$

$$= e_{kk} + \sum_{\substack{n=1\\ n\neq k}}^{Q_2} e_{nk} \tag{3.94}$$

The first term of the right-hand side of equation (3.94) is the e.m.f. induced in the kth mesh due to the kth mesh current, hence self-induced e.m.f., while the second term is the sum of the induced e.m.f.s in the kth mesh due to currents in the other meshes, hence the sum of the mutual induced e.m.f.s. A corrollary of this, however, is that the kth mesh current will cause self e.m.f. to be induced in the kth mesh and mutual e.m.f.s to be induced in the other meshes. Therefore for k=1, say,

$$e_{11} = G\frac{di_{\nu 12}}{dt} \sum_{u=1}^{\infty} \frac{1}{u^2} \sin^2 \frac{u\alpha_d}{2} \cos u(0-0)$$

and

$$e_{1n}\Big|_{n\neq 1} = G\frac{di_{\nu 12}}{dt} \sum_{u=1}^{\infty} \frac{1}{u^2} \sin^2 \frac{u\alpha_d}{2} \cos u(0-(n-1)\alpha_d)$$

The total e.m.f. induced in the rotor winding by the mesh current in the 1st mesh is

$$e_{11} + \sum_{n=2}^{Q_2} e_{1n} = G\frac{di_{\nu 12}}{dt} \sum_{n=1}^{Q_2} \sum_{u=1}^{\infty} \frac{1}{u^2} \sin^2 \frac{u\alpha_d}{2} \cos u(n-1)\alpha_d \tag{3.95}$$

$$= G\frac{di_{\nu 12}}{dt} \sum_{u=1}^{\infty} \frac{1}{u^2} \sin^2 \frac{u\alpha_d}{2} \sum_{n=1}^{Q_2} \cos u((n-1)\alpha_d)$$

$$= G\frac{di_{\nu 12}}{dt} \sum_{u=1}^{\infty} q(u) \sum_{l=0}^{Q_2-1} \cos ul\alpha_d \tag{3.96}$$

where

$$q(u) = \frac{1}{u^2} \sin^2 \frac{u\alpha_d}{2} \tag{3.97}$$

But

$$\sum_{i=0}^{Q_2-1} \cos ul\alpha_d = \cos(\frac{Q_2}{2} u\alpha_d) \sin(\frac{(Q_2-1)u\alpha_d}{2}) \operatorname{cosec} (\frac{u\alpha_d}{2}) + 1 \tag{3.98}$$

$$\text{Let } D(u) = \cos(\frac{Q_2}{2}u\alpha_d) \sin(\frac{(Q_2-1)}{2}u\alpha_d) \operatorname{cosec}(\frac{u\alpha_d}{2}) \tag{3.99}$$

Substituting (3.98) and (3.99) into (3.96) we have

$$e_{11} + \sum_{n=2}^{Q_2} e_{1n} = \sum_{u=1}^{\infty} [Gq(u) + Gq(u)D(u)] \frac{di_{\nu 12}}{dt}$$

$$= (L + M) \frac{di_{\nu 12}}{dt} \tag{3.100}$$

where

$$L = \sum_{u=1}^{\infty} Gq(u) \tag{3.101}$$

and

$$M = \sum_{u=1}^{\infty} Gq(u)D(u) \tag{3.102}$$

It is apparent from the foregoing that the self component,

$$e_{11} = L \frac{di_{\nu 12}}{dt} \tag{3.103}$$

and the sum of the mutual components

$$\sum_{n=2}^{Q_2} e_{1n} = M \frac{di_{\nu 12}}{dt} \tag{3.104}$$

From the air gap field step distribution corresponding to a mesh current equation (3.8) or (3.9) it is apparent that the mutual voltage component, equation (3.104), is equally divided among the $Q_2 - 1$ meshes. This is because these meshes see the same magnitude of the air gap magnetic field, corresponding to the mesh current k=1. Hence, induced e.m.f. in any mesh n due to a current in the 1st mesh can be written thus

$$e_{1n}\Big|_{n\neq 1} = \frac{M}{Q_2-1}\,\frac{di_{\nu 12}}{dt} \tag{3.105}$$

From equations (3.97), (3.99), (3.101), and (3.102) we can conclude that neither L nor M is dependent on k or ν. Hence, L and M are constants and only need to be calculated once for a machine, and equations (3.103) to (3.105) are general for any k. Therefore, we can generalize thus

$$e_{kk} = L\frac{di_{\nu k(k+1)}}{dt} \tag{3.106}$$

$$\sum_{\substack{n=1\\ n\neq k}}^{Q_2} e_{kn} = M\frac{di_{\nu k(k+1)}}{dt} \tag{3.107}$$

$$\sum_{\substack{n=1\\ n\neq k}}^{Q_2} e_{nk} = \frac{M}{Q_2-1}\sum_{\substack{n=1\\ n\neq k}}^{Q_2}\frac{di_{\nu n(n+1)}}{dt} \tag{3.108}$$

From equation (3.87) equation (3.108) becomes

$$\sum_{\substack{n=1\\ n\neq k}}^{Q_2} e_{nk} = -\frac{M}{Q_2-1}\,\frac{di_{\nu k(k+1)}}{dt} \tag{3.109}$$

Therefore substituting equations (3.106) and (3.109) into (3.94) we obtain

$$e_{br\nu k} = (L - \frac{M}{Q_2-1}) \frac{di_{\nu k(k+1)}}{dt} \tag{3.110a}$$

$$= js_\nu \omega_s (L - \frac{M}{Q_2-1}) i_{\nu k(k+1)} \tag{3.110b}$$

If we substitute equations (3.93) and (3.110b) into (3.88) we have

$$e_{bs\nu k} = (2z_{e\nu} + \gamma z_{b\nu} - js_\nu \omega_s (L - \frac{M}{Q_2-1})) i_{\nu k(k+1)} \tag{3.111}$$

where $\gamma = 4 \sin^2 \frac{\nu p}{2} \alpha_d$

Substituting for $e_{bs\nu k}$ from equation (3.25) and solving for the current we found that

$$i_{\nu k(k+1)} = I_{m\nu} \sin(s_\nu \omega_s t - \frac{\nu p \vartheta_k}{2} - \beta_\nu - \rho) \tag{3.112}$$

where

$$I_{m\nu} = \frac{E_{m\nu}}{Z_\nu} \tag{3.113}$$

where

$$Z_\nu = 2z_{e\nu} + \gamma z_{b\nu} - js_\nu \omega_s (L - \frac{M}{Q_2-1}), \tag{3.114}$$

$$= R_\nu + jX_\nu$$

and

$$\rho = \tan^{-1}(\frac{X_\nu}{R_\nu}) \tag{3.115}$$

Equation (3.113) shows that $I_{m\nu}$ does not vary with k, hence for any νth harmonic it is constant and thus it should be calculated only once for an instant in time and space and the mesh currents, for all mesh from 1 to Q_2, can be deduced from equation (3.112) by simply substituting $\vartheta_k = (k-1)\alpha_d$.

3.5 Effects of Slot Openings

Slot openings, or regions of lower magnetic permeance, exist on either of the surfaces adjacent to the air gap, as a mechanical requirement for the installation of the windings, and due to strong saturation of the iron material caused by large linkage and slot leakage fields. Those due to the former are generally referred to as actual slot openings, while those associated with the latter are called fictitious openings. Fictitious openings are commonly found at the tooth tip of a semi-closed slot and the bridge of a closed slot.

The presence of slot openings introduces into the analysis, a variable permeance in space and time. It can otherwise be viewed to effect a variable air gap length, $\delta(\vartheta,t)$, assuming linearity of the magnetic circuit. As such, most of the flux path will be through the regions with higher magnetic permeance, minimum air gap length. Due to fringing, however, the transition from the region of minimum air gap length to the maximum is not quite instantaneous. In fact, the expression depicting this variation is not simple [85, 86]. If the effects of the slot openings are accounted for by a slot permeance factor distribution $\xi(\vartheta, t)$, then the air gap flux density distribution

is modified thus:

$$B_g(\vartheta,t) = \xi(\vartheta,t)\, B_g'(\vartheta,t) \tag{3.116}$$

where $B_g'(\vartheta,t)$ is a distribution obtained by assuming a smooth air gap.

With the knowledge of the effective slot opening the basis for obtaining $\xi(\vartheta,t)$ was provided by Freeman [85], whose work was in turn based on the classical work of Carter [86]. For the case where the ratio of the tooth width to the air gap length is greater than 3.3 the following are the relevant equations: the permeance factor at any instant is

$$\xi = \frac{(1-y)}{[(a-y)(b-y)]^{1/2}} \tag{3.117}$$

where y is the independent variable, a = 1/b, and b is determined by the equation

$$\frac{b-1}{b} = \frac{w_o}{\delta} \tag{3.118}$$

$$\vartheta = \frac{\delta}{\pi r}\left[-\ln\left|\frac{1+c}{1-c}\right| + \ln\left|\frac{b+c}{b-c}\right| + 2\,\frac{w_o}{\delta}\tan^{-1}\left(\frac{c}{\sqrt{b}}\right)\right] - 0.5\, w_o/r \tag{3.119}$$

where

$$c^2 = \frac{b-y}{a-y} \tag{3.120}$$

3.6 Effects of Saturation

Saturation is a non-linear phenomenon and its intensity and location in a machine vary with time, current, and speed. Hence, its

effects on the behaviours of a machine vary as well, and are difficult to account for. Saturation in induction machines may be studied in relation to their effects by considering saturation in three regions: the core, teeth bodies, and teeth tips.

3.6.1 Effects of Saturation of the Core

The flux in the cores is the space integral of the flux in the air gap. That is, the air gap flux density is proportional to the space derivative of the core flux. Hence, if the core is saturated but the teeth are not, only the magnitude, not the shape of the air gap flux density waveform, is affected by saturation. The action of a saturated core in the case where both the core and teeth are saturated is such that it opposes the effect of the saturated teeth [87, 88], depending on the relative degrees of saturation of both regions. In all practical machines, however, the teeth are more saturated than the core. Hence, no appreciable error will be introduced if it is assumed that the core is unsaturated.

3.6.2 Effects of Saturation of the Teeth Body

The saturation of stator and rotor teeth causes the air gap flux density wave to be flattened at the peak regions. Since in all practical machines the teeth are usually saturated, these effects should be accounted for in an analysis. An air gap mmf distribution obtained by neglecting saturation may be modified to account for saturation according to equation 3.13. For an angular position the saturation factor used is obtained from the curve of saturation factor versus mmf,

which is derived from the air gap magnetization characteristic (i.e. curve of air gap flux density against total mmf of a closed magnetic circuit) of the machine. If the modified mmf distribution is resolved into Fourier components the magnitude of a harmonic component will comprise that of a saturation harmonic together with the other space harmonics. But since the saturation harmonic rotates at a different speed to the other space harmonics it would be incorrect to apply the Fourier components of this modified waveform to the preceeding theory of squirrel cage induction machines in sections 3.3 and 3.4 without further separating them into their respective components; saturation and other space harmonics.

If the distribution obtained by assuming the absence of saturation is resolved into Fourier series, a harmonic component of this does not include saturation and it rotates at one speed defined by equation (3.14). The flux density produced by the fundamental mmf of the latter distribution in a practical machine is by far the largest component present in the teeth and cores. This fundamental mmf wave is therefore responsible for producing the saturation harmonics which have the greatest practical significance and which need to be considered in any analysis. Hence, it is only this fundamental wave which needs to be modified for saturation by the procedure above. Other components of the Fourier series represent other space harmonic waves, caused by the arrangement of windings and the coreplate slotting, and do not have significant effects on the saturation of the iron materials. Hence, they may be employed directly in the preceding theory. The above

argument is principally based on the fact that: (i) the magnitude of the fundamental is by far greater than that of any of the harmonics; (ii) unlike the fundamental, the saturation factor corresponding to the peak value of any of the harmonics is unity; and (iii) the waveforms of the fundamental and the harmonics are all not in phase.

After the fundamental component has been modified for saturation, it should be resolved into Fourier series. The fundamental can be employed in the preceding theory directly, while the harmonics depicting saturation are employed in the theory with the following corrections:

(i) Since the saturation harmonics waves rotate at the same synchronous speed and in the same direction as the fundamental wave the slip of any saturation harmonic $s_\nu = s$.

(ii) Since the number of poles of the νth saturation harmonic waveform is νp then its frequency is νf, and hence, the frequency of the current it induces in the rotor is νfs.

3.5.2.1 Saturation Factor Versus MMF Curve

The curve of saturation factor versus total mmf of the magnetic circuit path is obtained by taking values of air gap flux density, B_g, and computing the corresponding values of total mmf, F_t, along half of a closed magnetic circuit path and the mmf in an air gap, F_g. From these the corresponding values of saturation factor are computed as

$$k_s = F_t / F_g \qquad (3.121)$$

If $B_g(\theta)$ is the flux density in the air gap at angle θ, the mmf

across the gap at this point is given by

$$F_g(\vartheta) = \frac{B_g(\vartheta)\delta'}{\mu_o} \tag{3.122}$$

where

$$\delta' = k_c\delta$$

The Carter's factor can be roughly estimated from the following expressions [89];

$$k_c = k_1 \quad k_2 \tag{3.123}$$

where

$$k_1 = \frac{\lambda_1(5\delta + w_{10})}{\lambda_1(5\delta + w_{10}) - w_{10}^2}$$

and

$$k_2 = \frac{\lambda_2(5\delta + w_{20})}{\lambda_2(5\delta + w_{20}) - w_{20}^2}$$

At no load there is negligible rotor current and rotor leakage flux, so the flux in the rotor iron is simply the mutual flux. The flux per rotor tooth pitch is

$$\varphi_{rt}(\vartheta) = \frac{B_g(\vartheta)\tau_p l'}{Q_2} \tag{3.124}$$

This flux exists principally in the tooth iron, but where the flux density is high the mmf may be sufficient to set up appreciable flux in the slots, radial ventilation ducts and the space occupied by the

coreplate insulation. Estimation of the flux density in the teeth using the tooth area only is therefore erroneous. The relationship between the apparent flux density B_t' and the actual flux density B_t is

$$B_t' = B_t + \mu_o H \frac{A_a}{A_i} \tag{3.125}$$

Since B_t, H, and A_i vary over the length of tapered teeth, the mmf over the rotor tooth length is obtained by sub-dividing the tooth into a number of thin laminae and summing their mmfs. To calculate the mmf across a particular lamination, the corresponding value of flux density must be found using (3.52) and A_i. Treating this as B_t' the corresponding value of H is obtained from a curve which relates B_t' to H according to (3.124) and for the particular B-H curve of the iron material, A_a, and A_i. The mmf is therefore obtained as

$$F_{rtl} = H_{rtl}\, h_{rtl} \tag{3.126}$$

Unlike the rotor, the stator iron carries some leakage flux in addition to the mutual flux. End-winding leakage flux is not carried by the stator iron, so flux per stator tooth pitch is

$$\varphi_{st}(\vartheta) = \frac{B_g(\vartheta)\tau_p l'}{Q_1} \cdot \frac{[x_m + (x_{ls}-x_{es})]}{x_m} \tag{3.127}$$

The mmf of a stator tooth is obtained by division into laminae, as described for the rotor teeth.

3.6.3 Effects of Saturation of the Teeth Tips

Saturation not only distorts the air gap field waveform by flattening the peak regions but also by creating more ripples or augmenting the existing ones. These ripples, as mentioned in section 3.5, are due to fictitious openings due to the saturation of the teeth tips of semi-closed slots or the bridges of closed slots. Levi [90] suggested accounting for this saturation of the tips by introducing an effective width of the slot opening.

$$w_{oeff} = \mu_o \frac{1}{1} \left(\frac{\sqrt{2} N_{sc} I_c}{B_i} \right) \tag{3.128}$$

where B_i is the value which satisfies simultaneously Ampere's law

$$H_i (w_1 - w_o) + \frac{B_i}{\mu_o} w_o = \sqrt{2} N_{sc} I_c \tag{3.129}$$

and the B-H characteristic of the iron laminations. In the case of closed rotor slots, $w_0 = 0$, and $w_1 = 2d/3$ where d is a characteristic width such as the diameter of a round bar.

Alternatively, if at a particular instant we know the total fluxes, ϕ, flowing through each tooth stem, the fictitious opening for each tooth tip may be determined as demonstrated below first for an example of a semi-closed slot and then for a closed slot.

Semi-Closed Slot

For any distance x from the edge of the tooth tip, figure 3.7,

$$\frac{1}{2}\varphi = \varphi_t(x) + \varphi_r(x)$$

$$= \varphi_t(x) + l'\int_x^d B_r(x)dx$$

Therefore

$$\varphi_t(x) = \frac{1}{2}\varphi - l'\int_x^d B_r(x)dx$$

But

$$B_r(x) = B_{ro}$$

Therefore

$$\varphi_t(x) = \frac{1}{2}\varphi - l'B_{ro}(d-x)$$

$$B_t(x) = \frac{\varphi_t(x)}{h(x)l'}$$

where

$$h(x) = h_1 + \frac{x}{a}(h_2 - h_1)$$

If the saturated value of the flux density in the tooth is B_{sat} then the width of the fictitious opening, x, can be determined from

$$B_t(x) = B_{sat}$$

i.e.

$$\frac{1}{2}\varphi - l'B_{ro}(d-x) = B_{sat}l'(h_1 + \frac{x}{a}(h_2 - h_1))$$

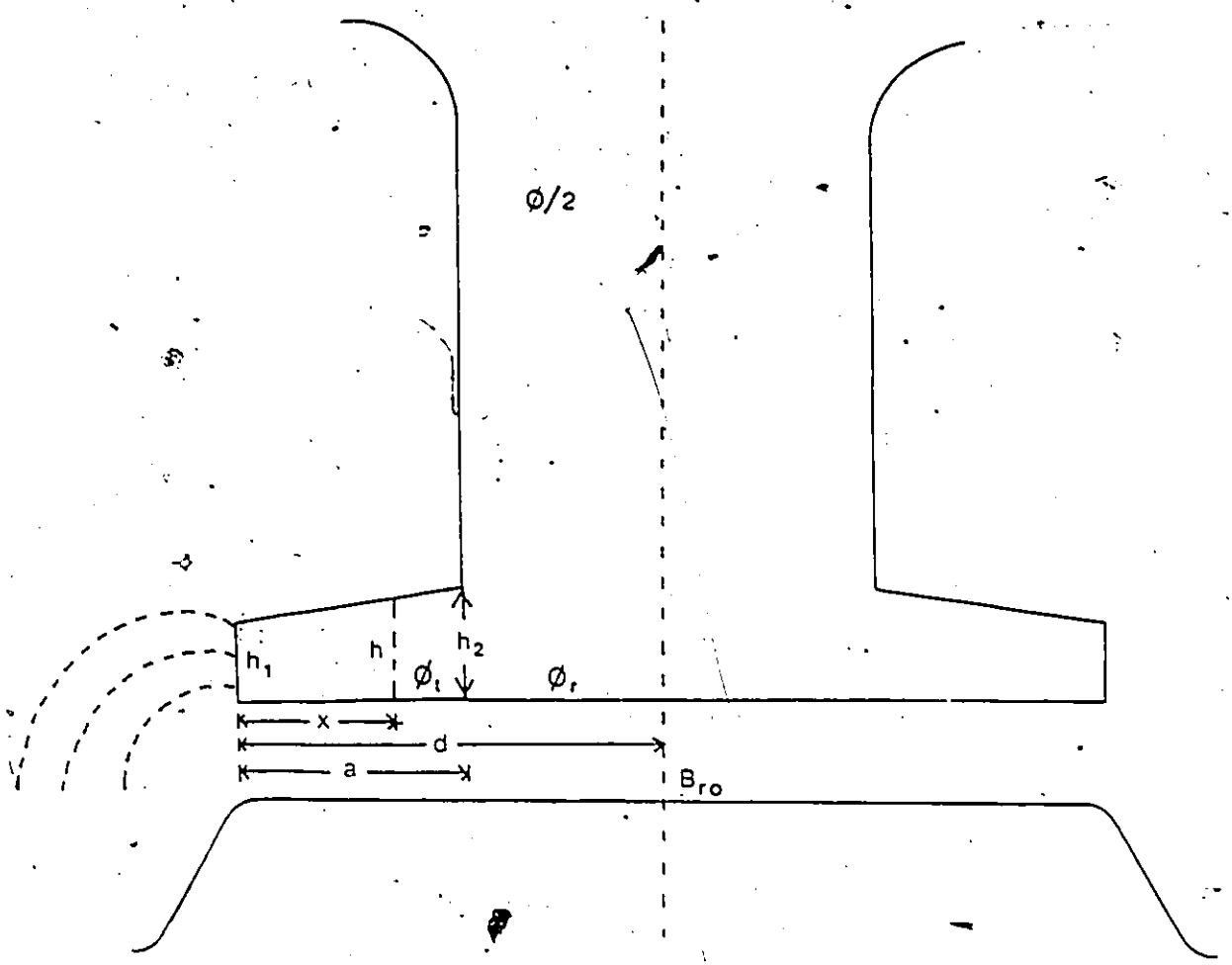

Figure 3.8: Calculation of Fictitious Opening of a Semi-Closed Slot.

which gives

$$x = \frac{a(0.5\varphi - l'dB_{ro} - B_{sat}l'h_1)}{l'((h_2-h_1)B_{sat} - aB_{ro})}; \quad x \geq 0 \qquad (3.130)$$

If x is negative implies no saturation at the tooth tips, hence no fictitious opening.

Closed Slot

For any distance x from the center of the bridge, figure 3.8, it can be shown that

$$\varphi_t(x) = \frac{\varphi}{2} - l'B_{ro}(d-x)$$

$$B_t(x) = \frac{\varphi_t(x)}{h(x)l'}$$

where

$$h(x) = (a+h_o) - \sqrt{(a^2 - x^2)}$$

If the saturated value of the flux density in iron is B_{sat} then the width of the fictitious opening, x can be determined from

$$B_t(x) = B_{sat}$$

i.e.

$$0.5\varphi - l'B_{ro}(d-x) = B_{sat}l'((a+h_o) - \sqrt{(a^2-x^2)})$$

$$0.5\varphi - l'B_{ro}d - B_{sat}l'(a+h_o) = -B_{ro}l'x - \sqrt{(a^2-x^2)}\, B_{sat}l'$$

$$B_{ro}\frac{x}{a} + \sqrt{(1-(\frac{x}{a})^2)}\, B_{sat} = -\frac{1}{al'}(0.5\varphi - l'B_{ro}d - B_{sat}l'(a+h_o))$$

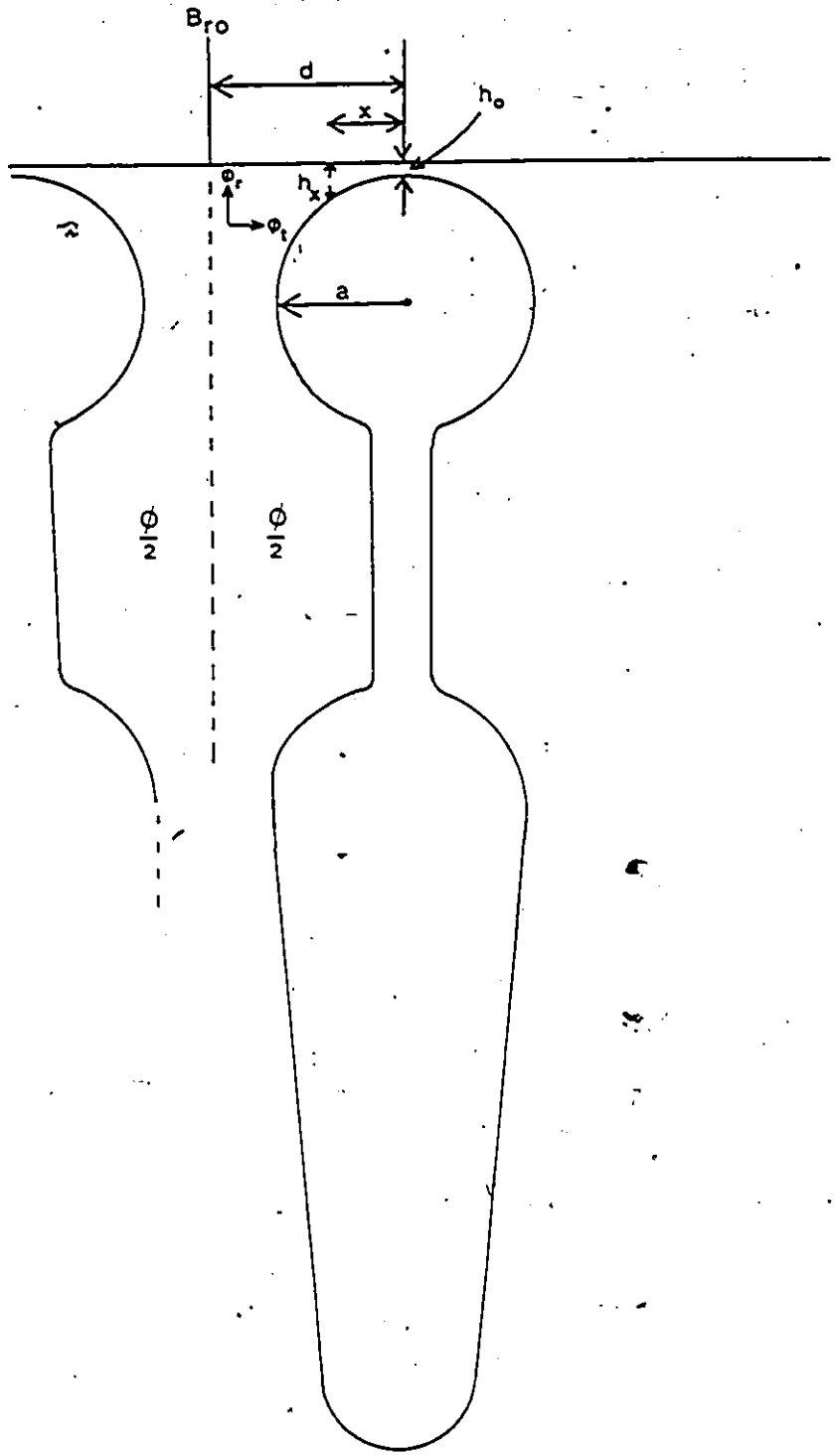

Figure 3.9: Calculation of Fictitious Opening of a Closed Rotor Slot

Let $\frac{x}{a} = \cos\gamma$, and

$$D = -\frac{1}{al'}\left(0.5\varphi - l'B_{ro}d - B_{sat}l'(a+h_o)\right)$$

then

$$B_{ro}\cos\gamma + B_{sat}\sin\gamma = D$$

Therefore

$$\cos(\gamma - \beta) = D/C$$

where

$$C = \sqrt{(B_{ro}^2 + B_{sat}^2)} \text{ and } \beta = \cos^{-1}(B_{ro}/C) \text{ or } \sin^{-1}(B_{sat}/C)$$

Therefore

$$\gamma = \cos^{-1}(D/C) + \cos^{-1}(B_{ro}/C)$$

and then

$$x = a\cos[\cos^{-1}(D/C) + \cos^{-1}(B_{ro}/C)];\ x \geq 0 \qquad (3.131)$$

A negative value of x implies no saturation and hence no fictitious opening.

3.7 The Machine Equations

Usually the known or given input parameters of an induction machine are the rms values of the supply voltage and current, and the power factor. For either a wye or delta connection of the stator three phase winding, the instantaneous values of the voltage and current can be defined. Any excited winding in a machine can be viewed in terms of self and mutual inductances. This is because an excitation, implicit or explicit, applied to a winding results in magnetic fields which link that winding and all other windings and materials in the device. If the

phase A of the stator winding is excited, for example, there will be a corresponding magnetic flux density distribution in the air gap and there will be some magnetic field in the slots carrying the conductors of the winding. Also there will be a magnetic field in the end regions. The field in the air gap links the phase A winding and this corresponds to a self inductance. On the other hand it also links phases B and C of the stator windings, all the meshes of the rotor's squirrel cage winding (figure 3.5), and the iron materials of the device: all these can be said to correspond to mutual inductances. The field in the slots corresponds to a self leakage inductance. The fields in the end region link the end windings of the other phases, and the iron materials of the end regions; hence they can be said to correspond to mutual leakage inductances.

If we introduce arbitrary equivalent currents to represent the hysteresis and eddy current phenomena due to the 'mutual' interactions of the fields created by winding of phase A and the iron materials, then an almost complete equation of the machine can be formulated as follow:

$$v_a(t) = i_a(t)r_{sa} + L_{sa}\frac{di_a(t)}{dt} + L_{sla}\frac{di_a(t)}{dt} + (M_{ab} + M_{labe})\frac{di_b(t)}{dt}$$

$$+ (M_{ac} + M_{lace})\frac{di_c(t)}{dt} + M_{laee}\frac{di_{laee}}{dt}$$

$$+ \sum_j (M_{a(h+e)j}\frac{di_{a(h+e)j}}{dt}) + \sum_{\nu=1}^{\infty}\sum_{m=1}^{Q_2} (M_{am\nu}\frac{di_{am\nu}}{dt}) \qquad (3.132)$$

where j refers to those harmonics and fundamental components which induce currents in the rotor squirrel cage winding. Equation (3.132) can be repeated for phases B and C respectively. By using the same thinking as above, the rotor equation for mesh m and any harmonic = 1 to ∞ in terms of the mesh currents can be written as

$$0 = (r_\nu + L_{1\nu}\frac{d}{dt})(2i_{am\nu} - i_{a(m-1)\nu} - i_{a(m+1)\nu}) +$$

$$2(r_{e\nu} + L_{e\nu}\frac{d}{dt})i_{am\nu} + \sum_{m=1}^{Q_2}[-(r_{e\nu} + L_{e\nu}\frac{d}{dt})i_{am\nu}] + M_{1mee\nu}\frac{di_{1mee\nu}}{dt}$$

$$+ \sum_{jj}(M_{(h+e)m\nu jj}\frac{di_{(h+e)m\nu jj}}{dt}) + L_{m\nu}\frac{d}{dt}(i_{am\nu} - i_{a(m+1)\nu})$$

$$+ \sum_{\substack{k=1\\k\neq m}}^{Q_2}[M_{mk\nu}\frac{d}{dt}(i_{ak\nu} - i_{a(k+1)\nu})] + M_{am\nu}\frac{di_a(t)}{dt} + M_{bm\nu}\frac{di_b(t)}{dt}$$

$$+ M_{cm\nu}\frac{di_c(t)}{dt} \qquad (3.133)$$

where jj refers to rotor fundamental and harmomics components which contribute significantly to core loss or torque of the machine.

Equations (3.132) and (3.133) represents a set of equations to be solved for the unknown currents, i_a, i_b, i_c, $i_{am\nu}$; m = 1 to Q_2, ν = 1 to ∞, for known balanced sinusoidal voltages v_a, v_b, v_c and for constant rotor speed; transient phenomenon are not considered. These equations are unsolvable directly as written, for the following reasons: (i) Equation (3.132) has infinitely many terms, and equation (3.133) is

just one of an infinite set of Q_2 equations.

(ii) Means of determining parameters like M_{laee}, $M_{a(h+e)j}$ etc. do not yet exist.

(iii) These equations are linear periodic coefficient differential equations.

Reason (i) can be removed by limiting the last term of equation (3.132) to j, and (3.133) to j sets of Q_2 equations; where j is as defined previously. Reason (ii) can also be removed by lumping the sixth term in equation (3.132) into the 4th and 5th, and seventh term into 8th; equation (3.134). This implies that existing techniques for evaluating the end mutual leakage inductances between two phases will be modified to account for eddy current loss in the end region. Also, the existing techniques for evaluating mutual inductances between any stator phase and a rotor winding mesh should be modified by a factor to account for the eddy current and hysteresis losses in the core. Terms four and five in (3.133) should be similarly lumped and accounted for. The equations of the machine will then be as follow:

$$v_a(t) = i_a(t)r_{sa} + L_{sa}\frac{di_a(t)}{dt} + L_{sla}\frac{di_a(t)}{dt} + (M_{ab} + M'_{labe})\frac{di_b(t)}{dt}$$

$$+ (M_{ac} + M'_{lace})\frac{di_c(t)}{dt} + \sum_{\nu=j}\sum_{m=1}^{Q_2}(M'_{am\nu}\frac{di_{am\nu}}{dt}) \qquad (3.134)$$

where the primes signify modifications as discussed above.

$$0 = (r_\nu + L_{1\nu}\frac{d}{dt})(2i_{am\nu} - i_{a(m-1)\nu} - i_{a(m+1)\nu})$$

$$+ 2(r_{e\nu} + L'_{e\nu}\frac{d}{dt})i_{am\nu} + \sum_{m=1}^{Q_2}[-(r_{e\nu} + L'_{e\nu}\frac{d}{dt})i_{am\nu}]$$

$$+ L_{m\nu}\frac{d}{dt}(i_{am\nu} - i_{a(m+1)\nu}) + \sum_{\substack{k=1\\k\neq m}}^{Q_2}[M_{mk\nu}\frac{d}{dt}(i_{ak\nu} - i_{a(k+1)\nu})]$$

$$+ M'_{am\nu}\frac{di_a(t)}{dt} + M'_{bm\nu}\frac{di_b(t)}{dt} + M'_{cm\nu}\frac{di_c(t)}{dt} \qquad (3.135)$$

However, reason (iii) can not be readily removed. But a closer observation of equation (3.135) shows that this is similar to (3.44). Hence, the solution method described in section 3.4 which is based on some knowledge of i_a, i_b and i_c can be employed to solve (3.135). This means either that equation (3.134) is implicitly satisfied by the solution, or that the necessary and sufficient condition for a satisfactory solution is for the resulting solution of (3.135) to satisfy equation (3.134).

CHAPTER 4

WAVEFORMS AND HARMONICS: THEIR INFLUENCE ON STRAY LOAD LOSS

The model of squirrel cage induction machines, developed in the last chapter, involves developing the waveforms of magnetic fields in the active region. Since these waveforms are influenced by the phenomena causing stray load loss in the machine they could provide some insight to the problem of understanding of this loss. In this chapter, an attempt is made to accomplish this by generating the waveforms of the magnetic fields in a practical machine. The waveforms are analyzed with the objective of studying how harmonics contribute to stray load loss in induction machines. Note that although the method is generally applicable, a specific machine geometry is chosen for study.

4.1 Magnetic Field of Stator

The stator winding of a practical example of a squirrel cage induction machine, table 4.1, is, as shown in figure 4.1, a balanced, 3-phase, full-pitch concentric winding. If a smooth air gap and the absence of saturation are assumed, the air gap flux density distribution for each phase and for all the phases together may be obtained using equation (3.12). These waveforms are as shown, for full-load, in figure 4.2 for four instants; t=0, t/24, t/12 and t/8, where T is the period (1/f). Any of these waveforms can be analyzed using a fast Fourier

Table 4.1: Typical details of a practical squirrel-cage induction machine.

Stator	
Rated Voltage	575 V
Number of Phases	3
Number of Poles	4
Number of Stator slots	36
Air-gap width	.5334 mm
Stator slot pitch	14.698 mm
Stator slot opening	3.3274 mm
Stator winding pitch	1 (full-pitch)
Stator winding type	concentric
Rated output	14.92 kw (20 Hp)
Line frequency	60 Hz
Number of turns per coil	17
Axial length	0.1778 m
Stacking factor	0.96
Balanced operation	yes

Rotor	
Number of rotor slots	28
Type of slot	double cage
Skew	0.
Rotor slot pitch	18.778 mm
Rotor slot opening	0. (closed)

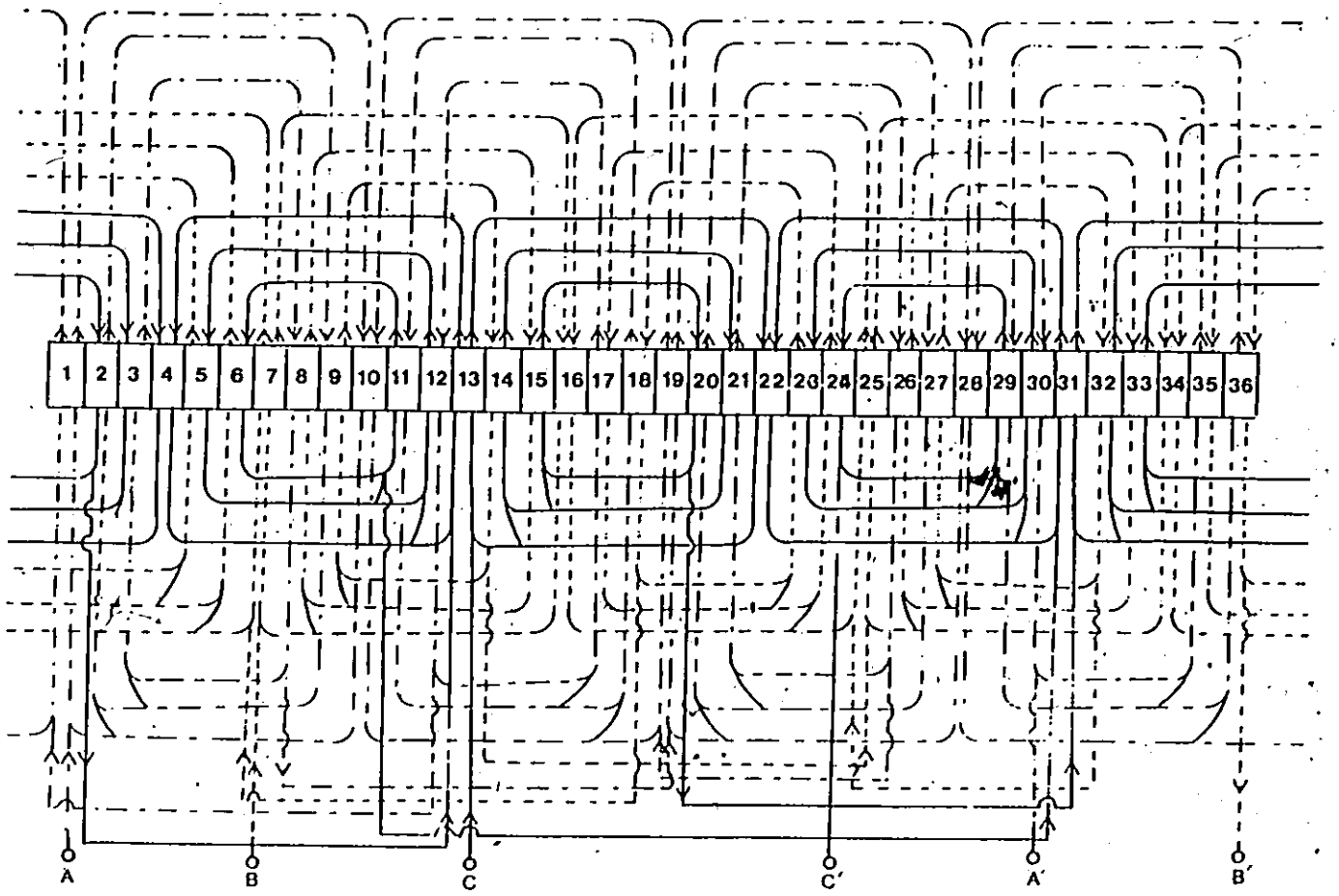

Figure 4.1: Layout of the Stator's full-pitch concentric winding.

transform algorithm, appendix A. Hence, with the aid of the algorithm the three phase field waveform of figure 4.2(a) was analyzed into a Fourier series. The amplitudes of the harmonics are plotted against the order of the harmonics, as the spectrum of the waveform, in figure 4.3. If each of the waveforms in figure 4.2(a) is analyzed for its significant harmonics, say those with amplitude greater than or equal to 0.1 Tesla, when the machine runs at no-load and full-load, the results will be as tabulated in table 4.2.

The observed harmonics are called winding distribution harmonics because they are created by the configuration of the winding. The geometric characteristics of a winding affecting the order and magnitude of these harmonics are: the concentration of conductors in slots and the arrangement of these conductors, and the number of phases and their arrangement. The harmonics due to the concentration of conductors in slots are called slot mmf harmonics while those associated with the phase arrangement of a winding are called phase belt harmonics. The orders of the latter harmonics, as in most standard works [17, 38, 91], are given by the expression

$$n = 2m_1k \pm 1 \quad ; k = 1, 2, 3 \tag{4.1}$$

and for the former

$$n = \frac{2Qk}{p} \pm 1 \tag{4.2}$$

where Q is the number of active slots (i.e. the number of slots in which there are current carrying conductors). Both slot mmf harmonics and

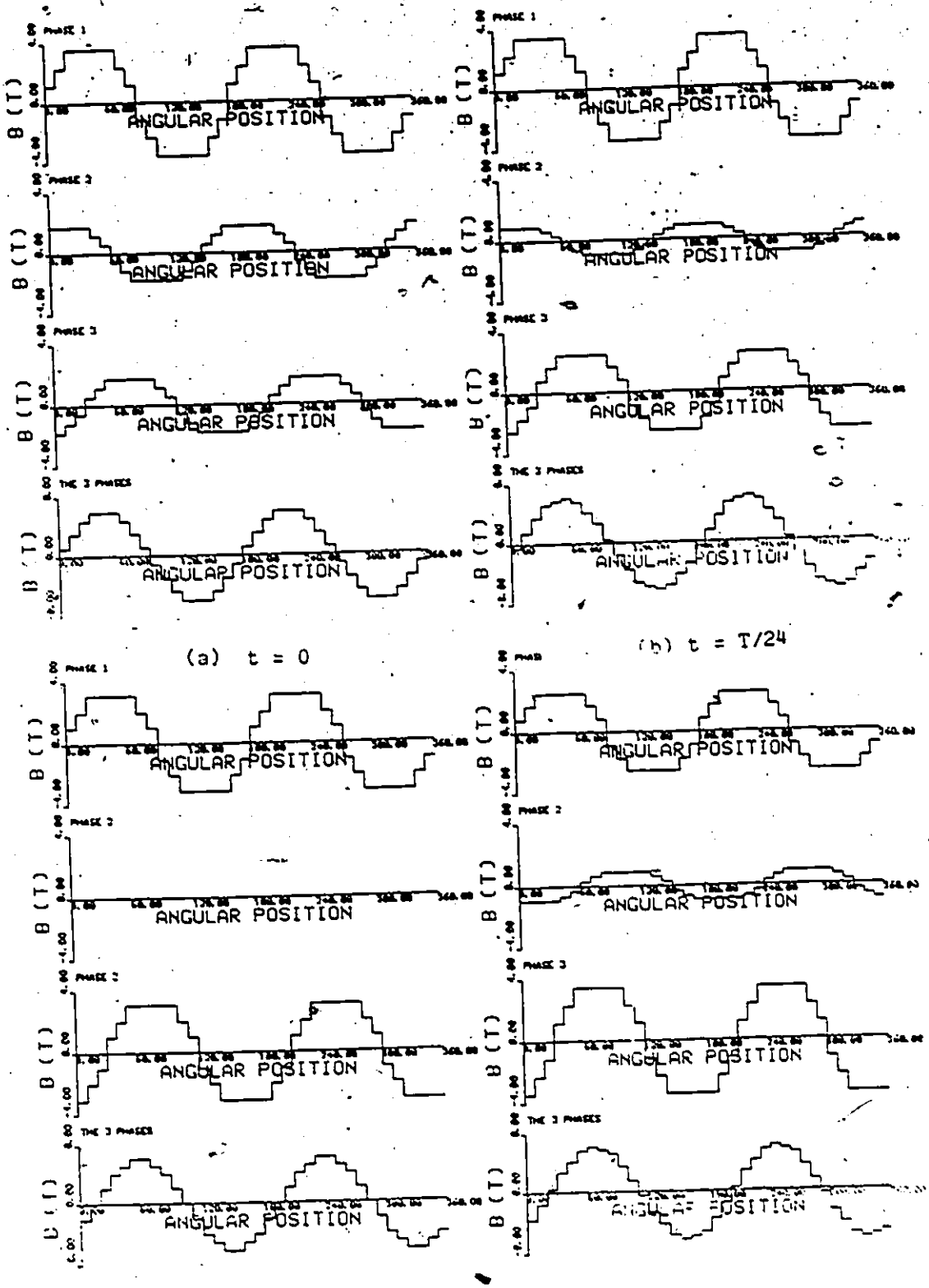

Figure 4.2: Step Distribution of the Stator's Air-Gap Flux Density Distribution.

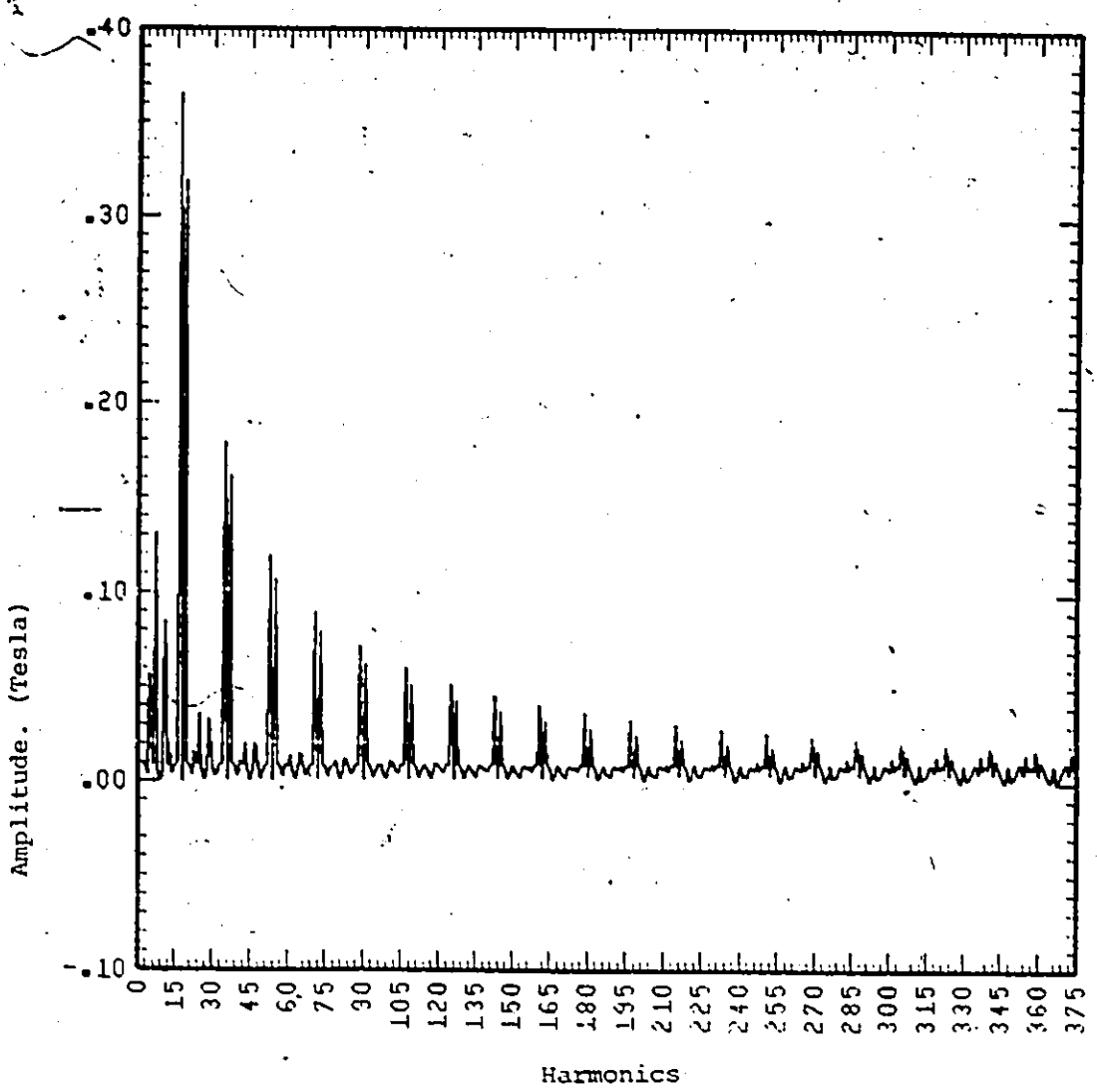

Figure 4.3: Spectrum of Three Phase Field Waveform of Figure 4.2(a).

Table 4.2:- Significant Harmonics of Stator Air Gap Waveforms (Amplitude > 0.1 Tesla)

Phase	Wave-Form	F/N	Harmonics
PHASE 1	a	F	1, 3, 9, 15, 17, 19, 35, 37
		N	1, 3
	b	F	1, 3, 9, 15, 17, 19, 35, 37, 53, 55, 71, 73
		N	1, 3, 17, 35
	c	F	1, 3, 9, 17, 19, 35, 37, 55
		N	1, 3
	d	F	1, 3, 9, 15, 17, 19, 35, 37, 53, 55, 73
		N	1, 3, 17, 35
	e	F	1, 3, 5, 7, 9, 15, 17, 19
		N	1, 3
	f	F	1, 3, 5
		N	1
	g	F	1, 3, 5, 7, 9, 13, 15, 17, 19, 35, 37, 53, 55
		N	1, 3, 17, 35
PHASE 2	a	F	1, 3, 17, 19
		N	1
	b	F	1, 3, 17, 19, 35, 37, 53, 55
		N	1, 17
	c	F	1, 3, 17, 19
		N	1
	d	F	1, 3, 17, 19, 35, 37, 53, 55
		N	1, 17
	e	F	1, 3
		N	1
	f	F	1, 3
		N	1
	g	F	1, 3, 17, 19, 35, 37, 53
		N	1
PHASE 3	a	F	1, 3, 17, 19
		N	1
	b	F	1, 3, 17, 19, 35, 37, 53, 55
		N	1, 17
	c	F	1, 3, 17, 19
		N	1
	d	F	1, 3, 17, 19, 35, 37, 53, 55
		N	1, 17
	e	F	1, 3
		N	1
	f	F	1, 3
		N	1
	g	F	1, 3, 17, 19, 35, 37, 53
		N	1
THREE PHASES	a	F	1, 7, 17, 19, 35, 37, 53, 55
		N	1, 17
	b	F	1, 7, 17, 19, 35, 37, 53, 55, 71, 73
		N	1, 17, 19, 35, 37, 53
	c	F	1, 7, 17, 19, 35, 37, 53, 55
		N	1, 17
	d	F	1, 7, 17, 19, 35, 37, 53, 55, 71, 73
		N	1, 17, 19, 35, 37, 53
	e	F	1, 3, 5, 7, 17, 19
		N	1
	f	F	1, 3, 5
		N	1
	g	F	1, 3, 5, 7, 13, 15, 17, 19, 35, 37, 53, 55
		N	1, 17, 19, 35, 37

Nomenclature

F - Full-load
N - No-load
a - Step distribution
b - Step distribution with stator slot ripple distribution super imposed
c - Step distribution with rotor slot ripple superimposed
d - Step distribution with both stator and rotor slots ripples superimposed
e - Step distribution with saturation
f - Fundamental of step distribution with satura·
g - Step distribution with saturation and stator ·tor slots ripples superimposed

phase belt harmonics together constitute winding distribution harmonics.

As expected [10, 17, 91], table 4.2 shows that the triplen harmonics are present in each of the phases, but because the machine is balanced they are absent in the resultant waveform of the three phases. The observed significant harmonics for the full-load case as compared with the no-load indicate that the magnitude of these harmonics increase with current.

4.1.1 Stator Fields with Effect of Slot Openings

For the stator and rotor punchings; figures 4.4 and 4.5 respectively, the effective slot openings were calculated using equations (3.128) and (3.129) for different values of stator currents. For the rotor, $\sqrt{2}\, N_{sc}\, I_c\, Q_1/Q_2$ was used in place of $\sqrt{2}\, N_{sc}\, I_c$. The variations of these openings with current are as shown in figure 4.6.

With the knowledge of the effective slot openings the permeance factor distributions were obtained for the stator and rotor as discussed in chapter 3, section 3.5. These distributions, for an instant in time and space, are as shown in figures 4.7(a) and (b). Each distribution was analyzed into a Fourier series using the algorithm of appendix A, and the corresponding harmonic spectra, for both distributions, are as plotted in figure 4.7(c).

To account for the effects of the slot openings these permeance factor distributions may be superimposed on the field waveforms according to equation (3.116). If the stator permeance factor distribution is superimposed on the three phase field waveform of figure

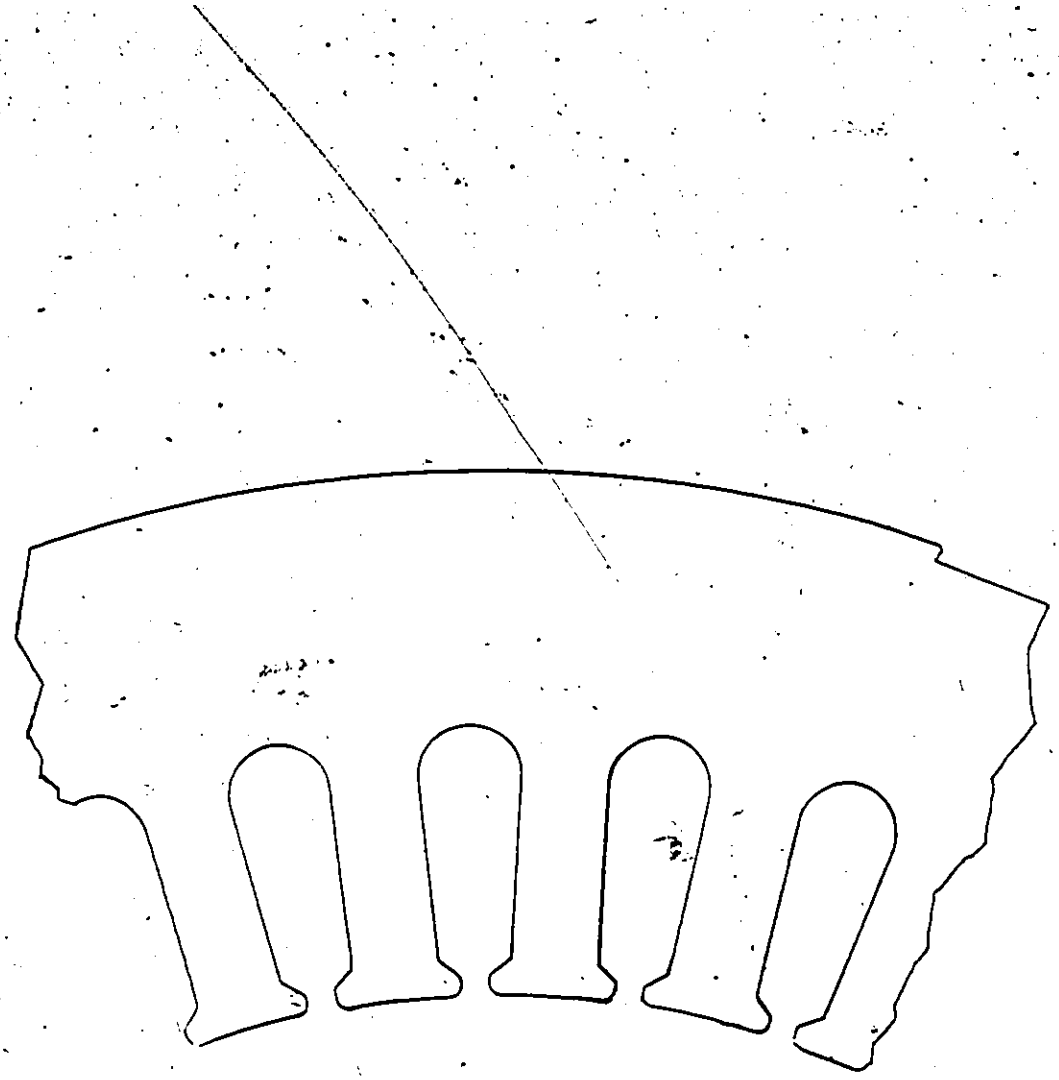

Figure 4.4: Stator Punching

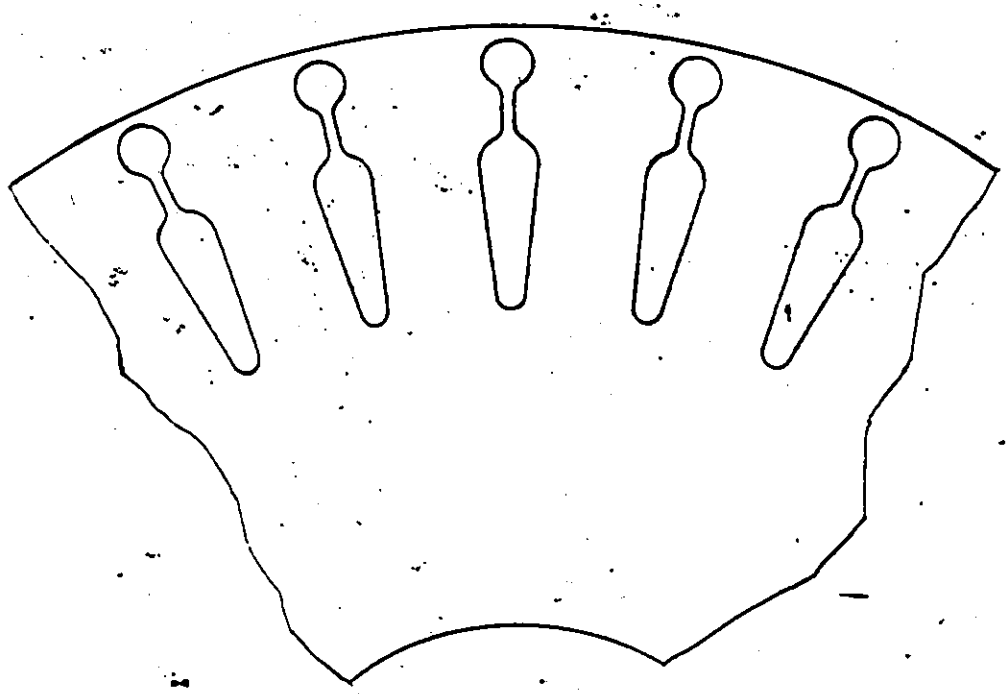

Figure 4.5: The Rotor Punching

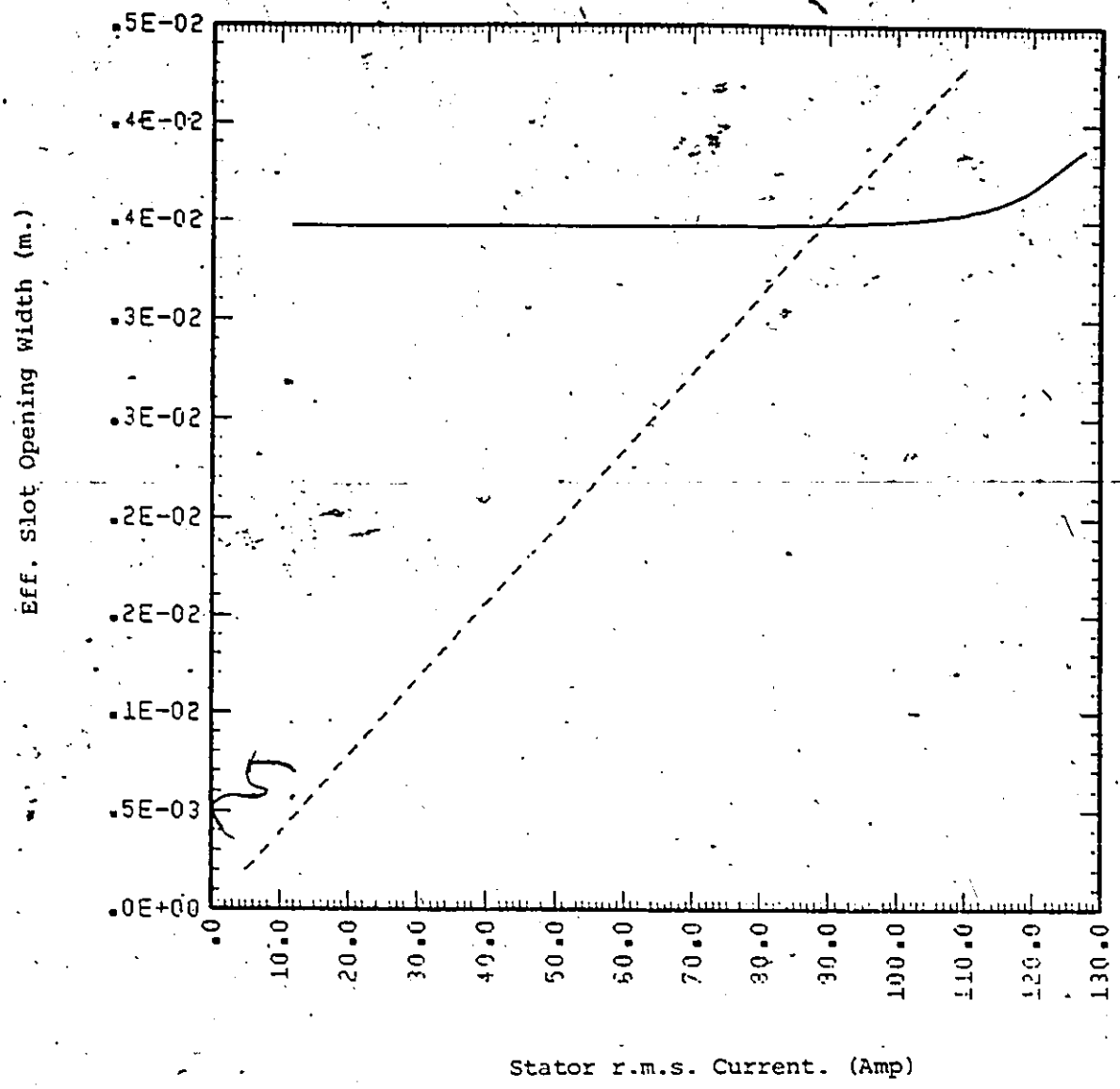

_____ = Stator Effective Slot Opening Width

- - - - - - - - - - - - - = Rotor Effective Slot Opening Width

Figure 4.6: Stator Current vs. Effective Slot Openings

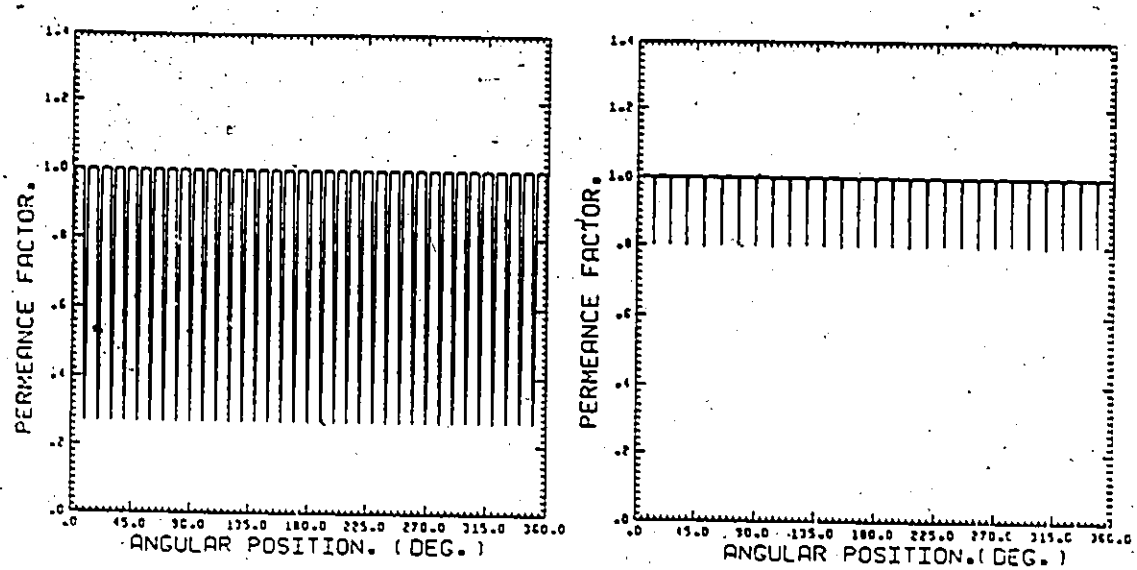

(a) (b)

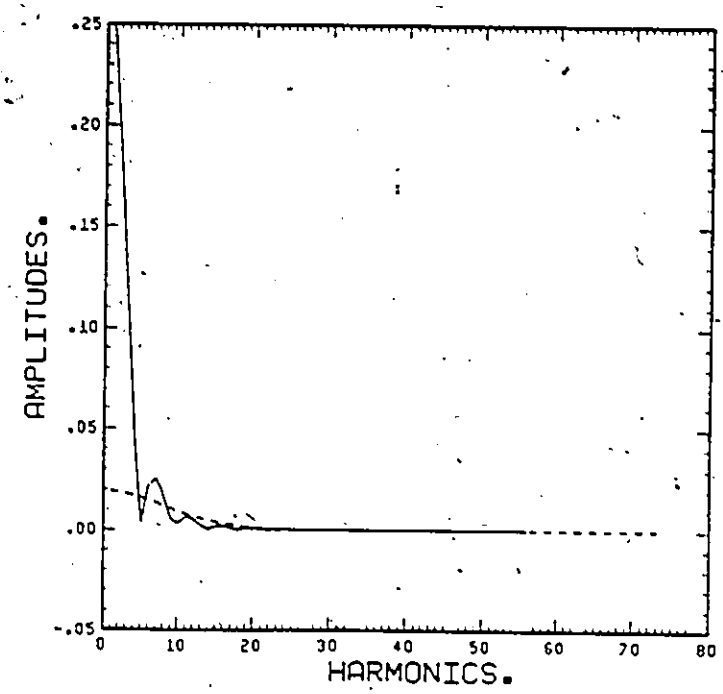

(c)

_____ Stator ---------- Rotor

Figure 4.4: Slots permeance factor distributions and spectral.
(a) Stator
(b) Rotor
(c) The Spectral

4.2(a) and the resulting waveform is analyzed into its harmonics, with the help of the algorithm in appendix A, the resulting waveform and its harmonic spectrum will be as shown in figure 4.8(a). Figures 4.8(b) and (c) show similar diagrams for the case when only the rotor permeance factor distribution and both stator and rotor permeance factor distribution are respectively superimposed on the field waveform. If the effects of slot openings are accounted for in each of the waveforms in figure 4.2(a) by superimposing the stator, the rotor, and then both the stator and rotor permeance factor distributions, and the resulting waveform in each case is analyzed, the observed significant harmonics are as presented in table 4.2 for the no-load and full-load conditions.

To further study the effect of the non-smooth air gap, the stator slots ripple distribution of figure 4.7(a) was superimposed on each sinusoidal waveform of the 1st, 7th, 17th, 19th, 35th, and 37th harmonics. The observed relative significant harmonics in each case, their phase angle, and their magnitude as a percentage of the magnitude of the original sinusoidal wave are as presented in table 4.3. The action of the slot permeance ripple on the fundamental component is such that it reduces its magnitude by a factor equal to $1-k_c$; where the Carter's factor, k_c, is half of the magnitude of the 0th harmonic of the ripple. It also introduces harmonics of orders

$$n = \frac{2Qk}{P} \pm 1 \quad ; k = 1, 2, 3, \ldots \tag{4.3}$$

The magnitude of any of these harmonics is a fraction of the original

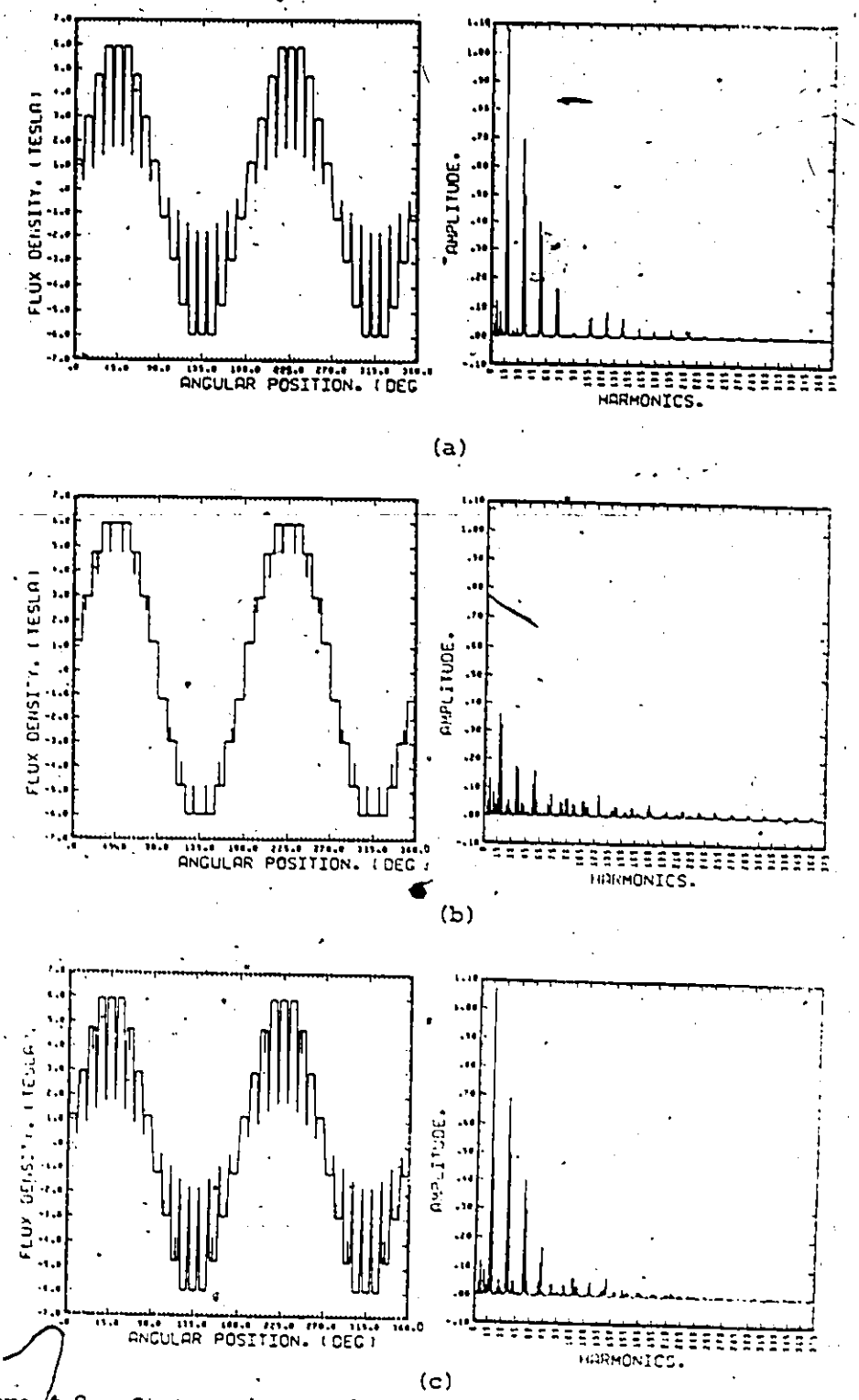

Figure 4.8: Stator air gap flux density with slot ripples.
(a) Stator slot ripple
(b) Rotor slot ripple
(c) Stator and rotor slot ripples

magnitude of the fundamental component. This fraction, for any k, is half of the magnitude of the kth harmonic of the ripple. In general, the effect of the slot permeance ripple on the νth harmonic sinusoidal component is the same as that of the fundamental: it reduces the magnitude of that harmonic to k_c of the original magnitude and introduces harmonics of orders

$$n_\nu = \frac{2Qk}{p} \pm \nu \quad ; k = 1, 2, 3, \ldots \tag{4.4}$$

each of which has a magnitude which is related to the original magnitude of the sinusoidal waveform by half the magnitude of the corresponding kth harmonic of the ripple. For example, for $\nu = 17$, n_ν corresponding to k = 0, 1, 2, 3, and 4, according to (4.4), are ± 17, 1 and 35, 19 and 53, 37 and 71, and 55 and 89 respectively. The third column of table 4.4, which shows the magnitudes and the percent half amplitudes of the first five harmonics of the ripple of figure 4.7(a), compare very well with those given by these n_ν as shown in the tenth column of table 4.3.

A study of the phases in table 4.3 shows that a harmonic component generated from an interaction of the ripple on a sinusoidal component of the field of one order does not have the same phase as that generated from that of another order. This implies that the resultant magnitude of a harmonic component is the vector sum of its components when the permeance ripple is superimposed on each sinusoidal component of the field. Since there is linearity in this case the resultant magnitude corresponds to that obtained when the permeance ripple is

Table 4.3: Effects of Non-Smooth Air-Gap on Stator Air-Gap Fields

Harmonics	(*)		(**)		1		7		17		19		35		37	
	% Mag.	Phase (rad.)	% Mag.	Phase (rad.)	% Mag.	Phase (rad.)	% Mag.	Phase (rad.)	% Mag.	Phase (rad.)	% Mag.	Phase (rad.)	% Mag.	Phase (rad.)	% Mag.	Phase (rad.)
1	100.0	1.569	86.62	1.567	86.51	1.567	--	--	12.46	-1.54	12.45	1.533	9.72	-1.505	9.72	1.498
7	2.15	1.557	1.98	1.559	--	--	86.52	1.547	0.02	1.515	0.02	1.512	--	--	--	--
11	1.37	1.550	1.43	1.553	--	--	12.40	1.567	0.05	1.522	0.04	1.522	--	--	0.01	1.432
17	5.69	1.538	17.59	1.544	12.42	1.546	0.03	1.530	86.52	1.512	9.91	-1.562	12.42	1.478	6.13	-1.526
19	5.25	1.534	7.77	1.543	12.48	1.540	0.03	1.525	9.53	-1.57	86.48	1.505	6.19	-1.534	12.44	1.471
25	0.6	1.523	0.34	1.527	--	--	12.45	1.519	0.07	1.506	0.09	1.499	0.06	1.443	0.06	1.441
29	0.52	1.515	0.46	1.523	--	--	9.72	1.540	0.06	1.494	0.06	1.487	0.11	1.451	0.09	1.447
35	2.87	1.504	11.34	1.516	9.68	1.519	0.02	1.511	12.46	1.484	6.04	1.555	86.47	1.450	3.07	1.571
37	2.69	1.500	8.12	1.515	9.76	1.512	0.02	1.503	6.16	1.546	12.51	1.478	2.32	-1.538	86.44	1.443
43	0.35	1.488	0.05	1.471	--	--	9.71	1.491	0.03	1.497	0.02	1.497	0.13	1.449	0.16	1.442
47	0.32	1.481	0.17	1.489	--	--	6.15	1.512	0.04	1.477	0.03	1.472	0.11	1.443	0.12	1.438
53	1.90	1.469	6.55	1.488	6.09	1.491	0.02	1.496	9.72	1.457	2.62	1.528	12.50	1.423	0.06	-1.209
55	1.81	1.465	5.68	1.488	6.17	1.485	0.02	1.485	2.75	1.518	9.75	1.450	0.22	1.535	12.50	1.415
61	0.24	1.453	0.04	1.522	--	--	6.13	1.464	0.01	1.504	--	--	0.04	1.440	0.03	1.445
65	0.23	1.447	0.03	1.418	--	--	2.72	1.484	0.02	1.466	0.02	1.474	0.05	1.427	0.05	1.429
71	1.42	1.435	2.69	1.458	2.68	1.464	--	--	6.13	1.430	0.14	1.526	9.74	1.395	1.19	1.520
73	1.36	1.431	2.69	1.463	2.73	1.457	--	--	0.25	1.477	6.14	1.422	1.02	1.534	9.72	1.388
79	0.19	1.419	0.04	1.489	--	--	2.70	1.436	--	--	--	--	--	--	--	--
89	1.13	1.401	0.13	1.349	0.20	1.436	--	--	2.71	1.402	1.10	1.470	6.14	1.368	1.36	1.498
91	1.08	1.396	0.26	1.475	0.20	1.430	--	--	1.05	1.466	2.69	1.395	1.23	1.505	6.11	1.360

* - The step distribution
** - The step distribution with stator slot ripple distribution superimposed on it.

Table 4.4: Magnitudes of Some Harmonics of Stator Slot Ripple

Harmonic	Amplitude	$\frac{1}{2}$ * Amplitude * 100%
0th	1.730195	86.51
1st	0.2492887	12.46
2nd	0.1944880	9.72
3rd	0.1226162	6.13
4th	0.0539279	2.70

superimposed on the step distribution in figure 4.2.

In rows b, c, and d in table 4.2 more significant harmonics are noticed at full-load than at no-load. One reason for this is the fact that a slot permeance ripple distribution acts so as to influence the amplitudes of the winding distribution harmonics, which in turn are functions of load. Another reason, as explained in chapter 3, is that fictitious slot openings are functions of currents, and hence load.

4.1.2 Stator Fields with Effects of Saturation

A typical B-H magnetization curve of an iron material is as shown in figure 4.9. Using this curve and equation (3.125) a typical curve of the apparent flux density against the magnetic intensity is as shown in the figure. By implementing the procedure described in section 3.6.2.1 the curve of saturation factor against mmf, figure 4.10, can be obtained. Hence, saturation may be accounted for by determining the corresponding saturation factor for an mmf at an angular position, and then using this factor and the mmf to determine the corresponding air gap flux density according to equation (3.13). If saturation is accounted for this way the three phase field waveform of figure 4.2(a) will become as shown, together with its harmonic spectrum, in figure 4.11(a). If, however, as discussed in section 3.6.2, saturation is accounted for only in the fundamental component, the resulting waveform and spectrum is as shown in figure 4.11(b). If the modified fundamental component is now replaced back into its original waveform the resulting waveform and its spectrum will be as shown in figure 4.12(a).

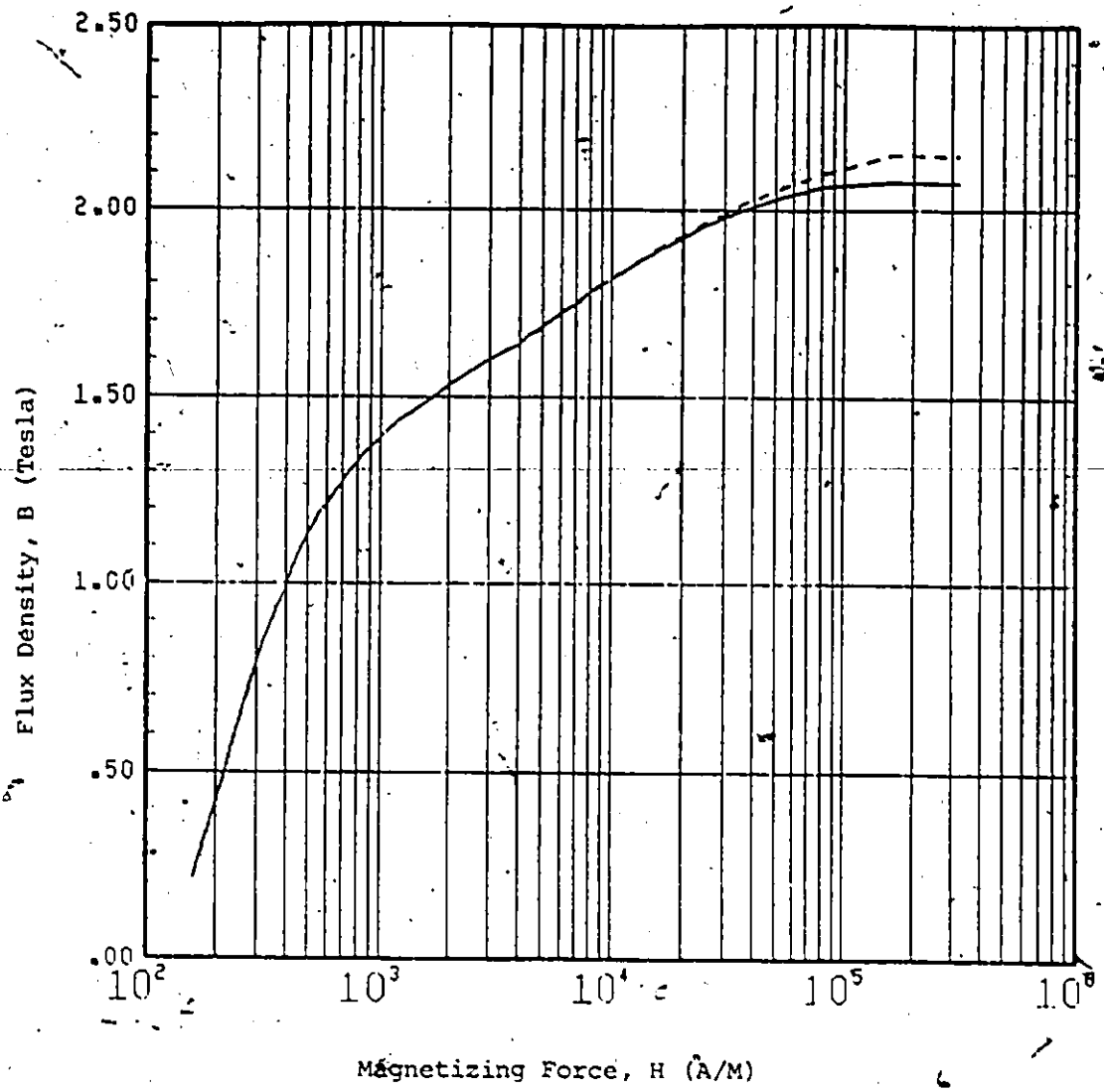

_____ = B-H Curve

---------- = Apparent B-H Curve

Figure 4.9:. B-H Magnetization Curves

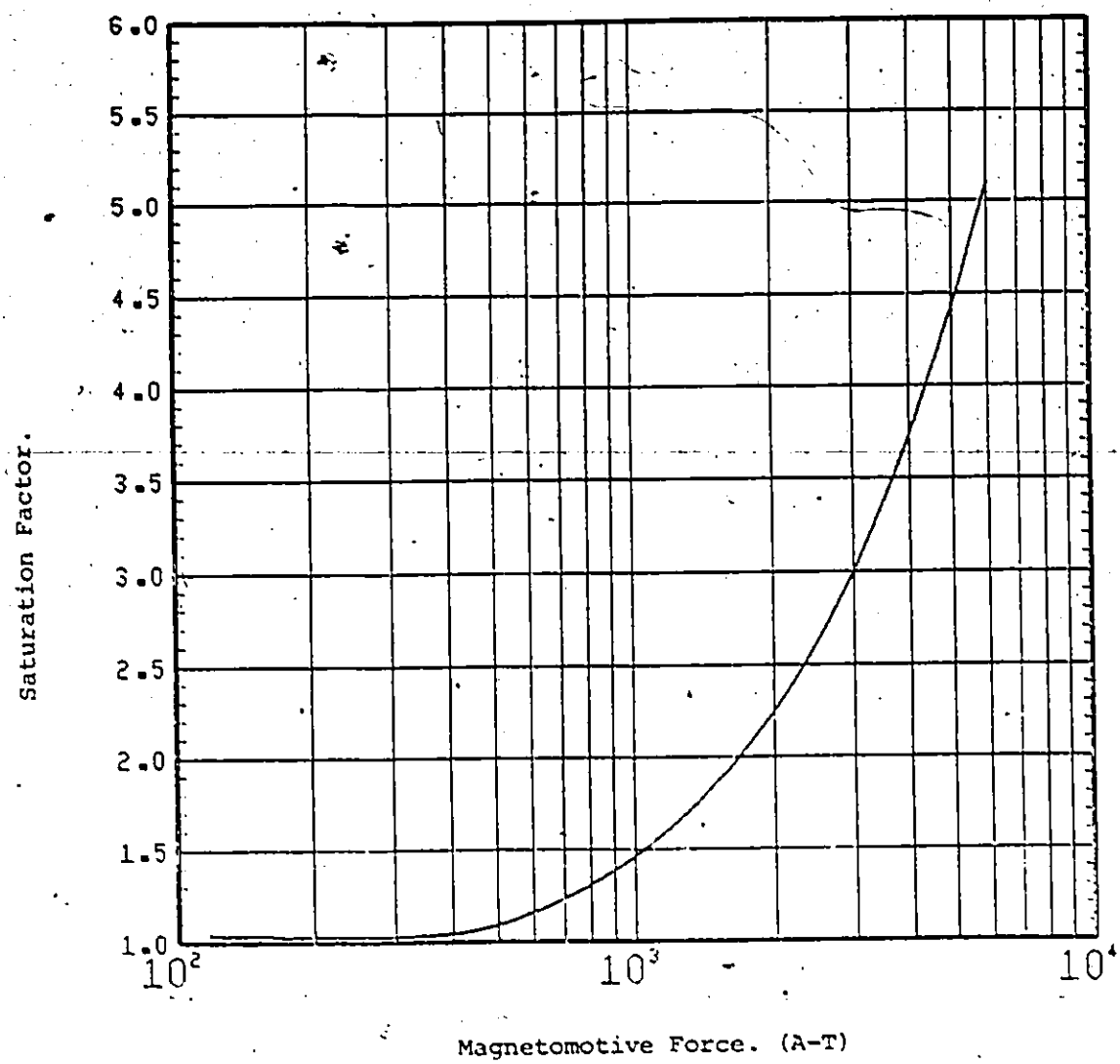

Figure 4.10: Saturation Factor Versus MMF.

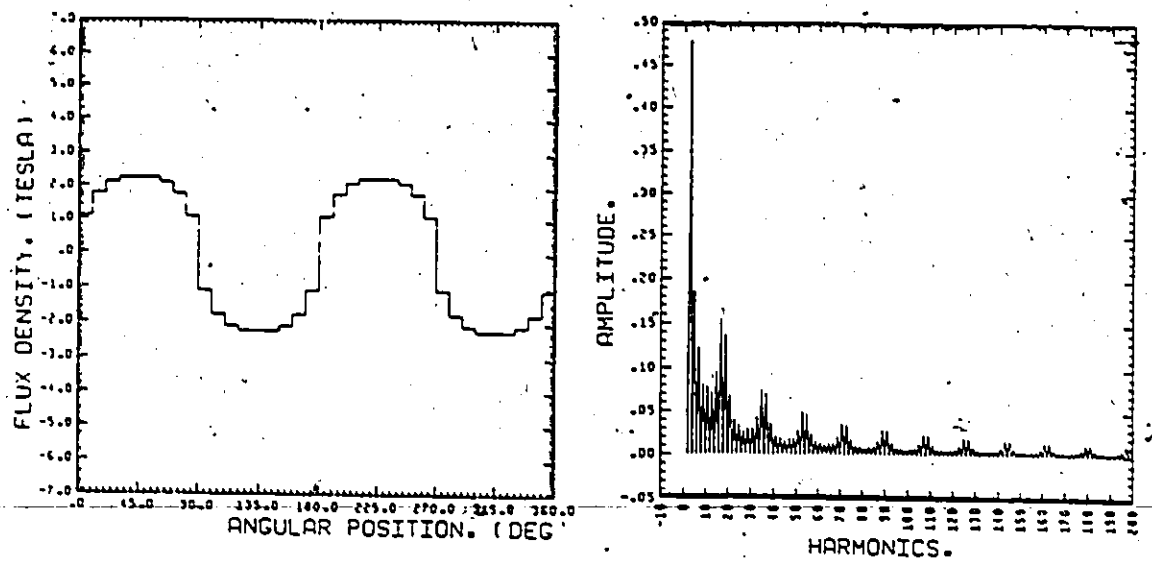

(a)

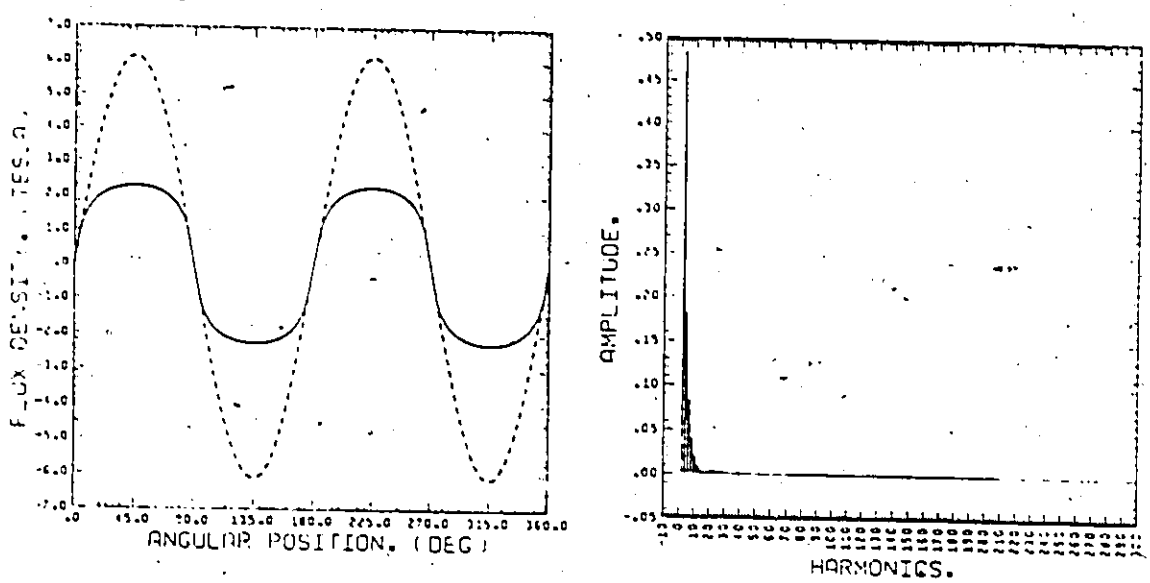

(b)

Figure 4.11: Stator air-gap flux density waveforms with saturation, and their spectral
(a) The step distribution with saturation
(b) The saturated fundamental of the step distribution

Accounting for saturation in each of the waveforms in figure 4.2(a), and analyzing the resulting waveforms for the no-load and full-load case, gives the observed significant harmonics as summarized in rows e and f in table 4.2. Table 4.5 show the percentage magnitudes of the fundamental and some selected harmonics of each of the waveforms in figures 4.11 and 4.12.

The effect of saturation on the fundamental waveform of the step distribution is that it reduces its magnitude and introduces, in order of decreasing magnitude, 3rd, 5th, 7th etc. harmonics. For the case study at full load the 3rd and 5th saturation harmonics are the most significant. At the no-load current, however, none are significant.

Due to the non-linear nature of saturation, its effect on the stator three phase field step waveform is not straightforward. The magnitudes of the fundamental and the third harmonic components of the four waveforms in figures 4.11 and 4.12 compare very well; see table 4.5. This implies that the third harmonic is principally a saturation harmonic, and that the effect of saturation on the step waveform yields the same fundamental component as that of a saturated fundamental component waveform. However, the magnitude of any winding distribution harmonic in figure 4.12(a) does not compare with that in 4.11(a), nor does the vectorial sum of that in figure 4.11(b) and the unsaturated steps waveform .

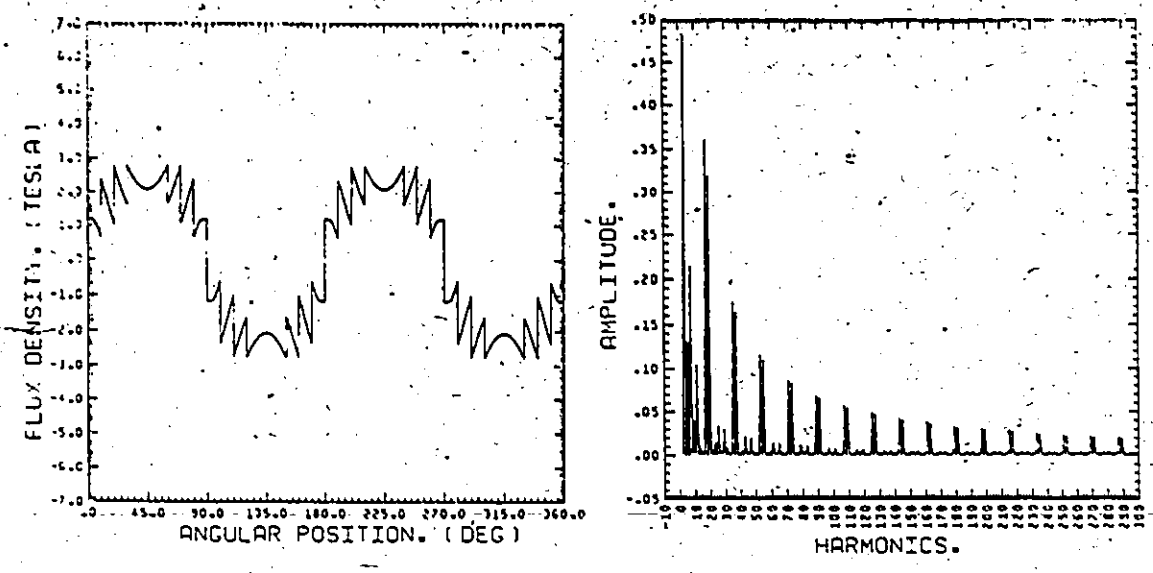

(a)

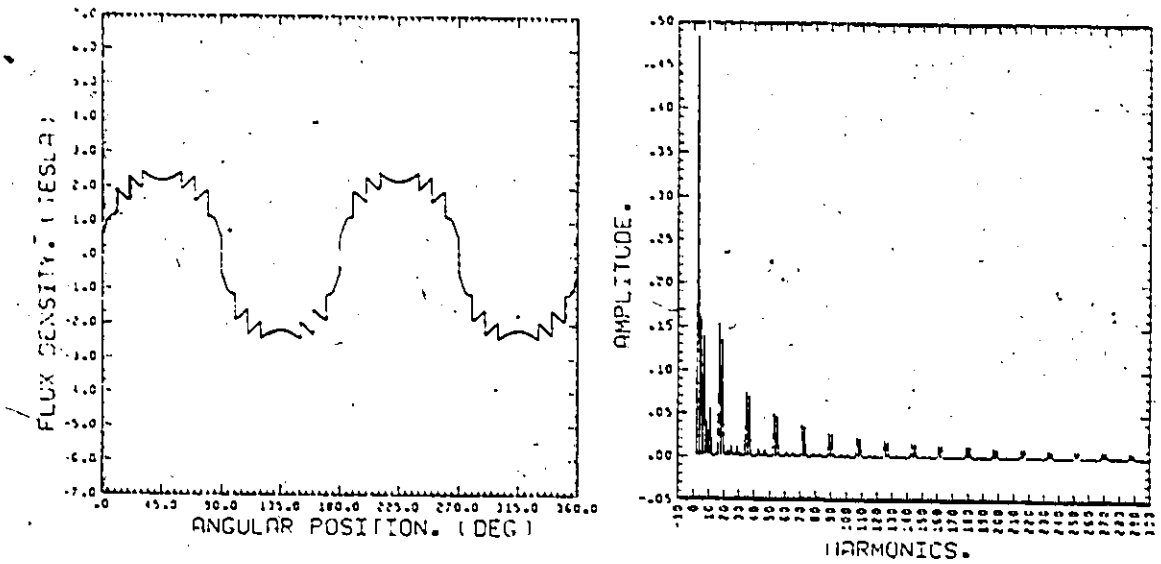

(b)

Figure 4.12: A study of how saturation influences the air gap field waveforms

equal that in 4.11(a). The reason for these discrepancies is not due to inaccurate evaluation of the magnitudes of the saturation harmonic components, but is due to the fact that saturation reduces the magnitudes of these space harmonics in the same order as the fundamental. However, unlike the fundamental, they do not produce any saturation harmonics. The physical interpretation of saturation is increased reluctance in the iron due to the property limitation of this material. Thus this reduction is brought about by the fact that all mmfs, fundamental and harmonics, in the same magnetic circuit path see the same reluctance.

The waveform of figure 4.12(b), therefore, is obtained by separating the mmf step waveform into two categories: the fundamental and the harmonics. The corresponding flux density waveform of the fundamental was obtained with saturation accounted for using the mmf-saturation factor curve. The corresponding flux density waveform of the other component, which is obtained without accounting for saturation, is multiplied by a reduction factor, equation (4.5). Finally, the resulting flux density waveforms for the two components are added together. As shown in table 4.5, the magnitudes of the fundamental and any harmonic in figure 4.12(b) compare with their counterparts in figure 4.11(a). Hence, if we define

$$\beta = \frac{\text{Magnitude of fundamental of saturated fundamental waveform}}{\text{Magnitude of unsaturated fundamental component waveform}} \qquad (4.5)$$

then a saturated air gap flux density distribution may be separated into its components as follows:

Table 4.5: Effects of Saturation on Stator Air Gap Field

Harmonics	(*)		Fig. 4.11(a)		Fig. 4.11(b)		Fig. 4.12(a)		Fig. 4.12(b)	
	% Mag.	Phase	% Mag.	Phase	% Mag.	Phase	% Mag.	Phase	% Mag.	Phase
1	100.0	1.569	42.71	1.569	42.78	1.567	42.80	-1.571	42.79	1.569
3	--	--	7.80	1.565	7.88	1.560	7.88	1.560	7.88	1.560
5	0.84	1.561	3.03	1.561	2.97	1.554	2.14	1.550	2.61	1.552
7	2.15	1.557	2.02	1.557	1.36	1.547	3.52	1.553	2.28	1.551
9	--	--	1.33	1.554	0.67	1.540	0.68	1.540	0.67	1.540
11	1.37	1.550	1.29	1.550	0.33	1.533	1.71	1.546	0.92	1.544
13	0.32	1.545	1.17	1.546	0.14	1.525	0.17	1.562	--	--
15	--	--	1.57	1.542	0.04	1.517	0.06	1.530	0.05	1.524
17	5.89	1.538	2.52	1.538	0.01	1.519	5.88	1.538	2.51	1.538
19	5.25	1.534	2.25	1.534	0.04	1.508	5.21	1.535	2.21	1.535
21	--	--	1.11	1.530	0.06	1.500	0.07	1.511	0.06	1.506
27	--	--	0.44	1.519	0.04	1.480	0.04	1.478	0.04	1.479
29	0.52	1.515	0.49	1.515	0.03	1.474	0.49	1.518	0.19	1.522
35	2.87	1.505	1.22	1.504	--	--	2.86	1.504	1.22	1.504
37	2.69	1.500	1.15	1.500	--	--	2.69	1.500	1.15	1.500

(*) - The step distribution without the effect of saturation (figure 4.24a))

$$B(\vartheta,t) = \frac{\mu_o F_1(\vartheta,t)}{\delta k_s(\vartheta,t)} + \beta \frac{\mu_o}{\delta} \sum_{n=2}^{\infty} F_n(\vartheta,t) \qquad (4.6)$$

The first term of equation (4.6) gives the fundamental component and the saturation harmonics while the second term represents the other space harmonics.

4.1.3 Stator Fields with Effects of Both Stator and Rotor Slot Openings and Saturation

The stator air gap field which accounts for both the effects of saturation and non-smooth air gap can be obtained by accounting for saturation on the step waveform obtained in section 4.1 and then superimposing the stator and rotor slots ripples (i.e. permeance factor distributions) on the resulting waveform. A waveform obtained in this way, for the three phase flux density distribution of figure 4.2(a), is shown, together with its spectrum, in figure 4.13(a).

An approximate form of this waveform, figure 4.13(b), is obtained by developing the corresponding saturated flux density waveform of a step mmf waveform according to the right-hand-side of equation (4.6). This flux density waveform is then multiplied by the stator and rotor slot permeance factor distributions. The magnitudes and phases of the fundamentals and harmonics of both waveforms in figure 4.13 are compared in table 4.6. The fact that they compare well implies that equation 4.6 is an adequate approximate means of separating saturation harmonics from the other space harmonics.

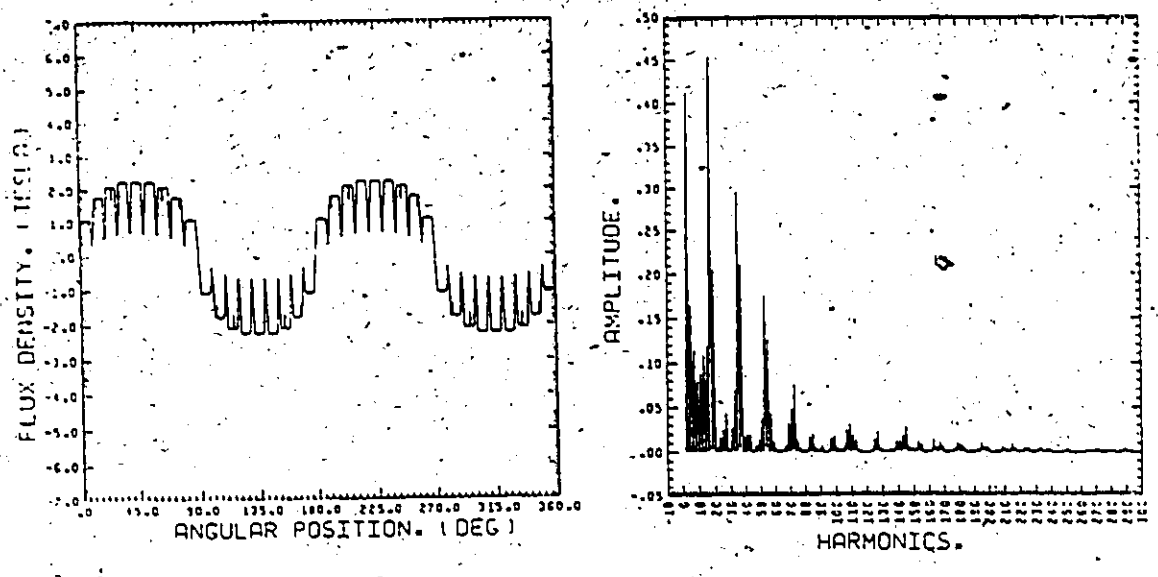

(a)

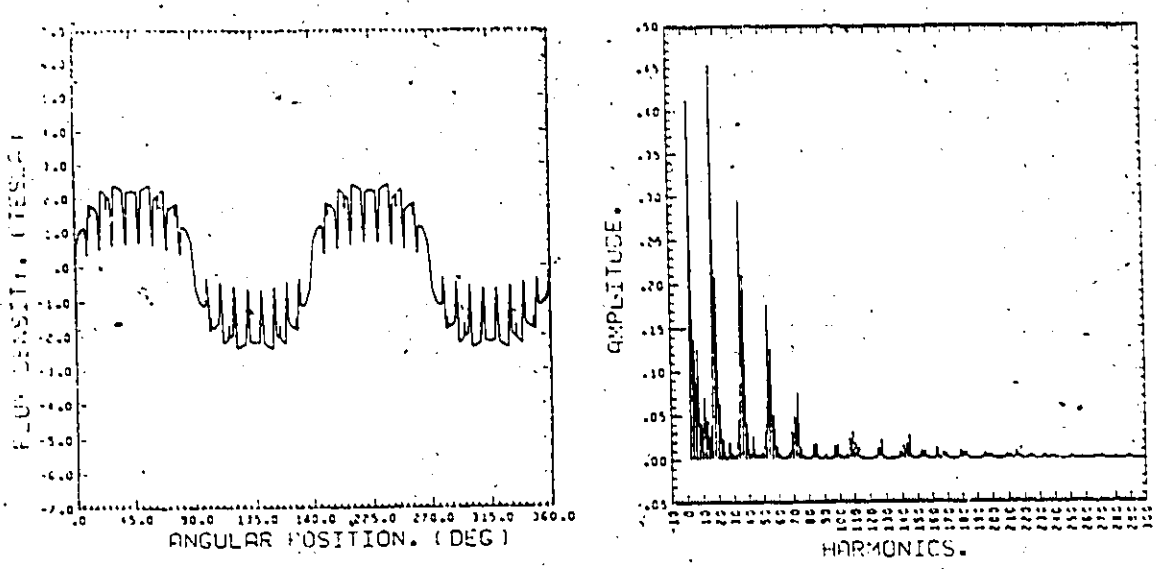

(b)

Figure 4.13: Stator air-gap flux density waveforms with saturation and stator and rotor slot ripples

Table 4.6 also summarizes the effects of the slot openings and saturation on the stator air gap magnetic field. The slot openings, including those due to saturation (fictitious slot openings), reduce the magnitude of the fundamental and augment the magnitude and change the phase of the harmonic components. The percentages of reduction and augmentation are constant with load for actual slot openings but vary with load for fictitious slot openings. Except for the fictitious slot openings, saturation does not affect the phases. It does, however, reduce the magnitude of the fundamental of the field waveform and create saturation harmonics. The percentage of reduction and the magnitudes of the saturation harmonics increase non-linearly with current, and hence with load. However, saturation reduces the magnitudes of the harmonic components in the field waveform. An additional effect of this is that the net effect of augmentation by the slot openings is limited.

4.2 Magnetic Fields of the Rotor

4.2.1 The Rotor Impedances

The rotor impedances consist of the rotor bar impedance, equations (3.22), and the end-ring impedance, equation (3.23). The real part of $z_{b\nu}$ is the resistance of the bar with the skin effect and the effect of heat appropriately accounted for, while the imaginary part is the reactance of the slot leakage inductance with skin effect accounted for. The bar impedance may either be determined analytically [10, 92, 93] or by a numerical method [94]. The former is employed in this work.

Table 4.6: Stator Fields and Effects of Both Stator and Rotor Slot Ripples and Saturation

Harmonics	(*)		(**)		(***)		Fig. 4.13(a)		Fig. 4.13(b)	
	% Mag.	Phase (rad.)	% Mag.	Phase (rad.)	% Mag.	Phase (rad.)	% Mag.	Phase (rad.)	% Mag.	Phase (rad.)
1	100.0	1.569	85.69	1.569	42.71	1.569	36.60	1.569	36.67	1.569
3	--	--	--	--	7.80	1.565	6.72	1.566	6.73	1.560
5	0.84	1.561	0.76	1.562	3.03	1.561	2.68	1.563	2.25	1.553
7	2.15	1.557	1.97	1.559	2.02	1.557	1.86	1.559	2.07	1.553
9	--	--	--	--	1.33	1.554	1.30	1.556	0.69	1.545
11	1.37	1.550	1.48	1.553	1.29	1.550	1.43	1.553	1.16	1.550
13	0.32	1.545	0.55	1.553	1.17	1.546	1.77	1.550	0.73	1.552
15	--	--	0.90	1.547	1.57	1.542	1.92	1.547	0.62	1.555
17	5.89	1.538	17.52	1.544	2.52	1.538	7.41	1.544	7.41	1.544
19	5.25	1.534	7.78	1.543	2.25	1.534	3.34	1.543	3.39	1.543
21	--	--	--	--	1.11	1.530	0.05	1.496	1.03	1.531
27	--	--	0.91	1.530	0.44	1.519	0.70	1.528	0.34	1.542
29	0.52	1.515	0.45	1.529	0.49	1.515	0.04	1.497	0.13	1.500
35	2.87	1.504	11.32	1.516	1.22	1.504	4.82	1.516	4.83	1.516
37	2.69	1.500	8.10	1.515	1.15	1.500	3.45	1.515	3.45	1.515
41	0.11	1.499	0.88	1.509	0.37	1.492	0.33	1.504	0.11	1.530
43	0.35	1.488	0.83	1.506	0.33	1.488	0.33	1.508	0.45	1.504
53	1.90	1.469	6.59	1.488	0.81	1.469	2.86	1.488	2.88	1.488
55	1.81	1.465	4.85	1.489	0.77	1.465	2.08	1.488	2.08	1.489
57	--	--	0.82	1.483	0.41	1.461	0.71	1.486	0.83	1.480

* - The step distribution (figure 4.2(a)
** - The step distribution with both stator and rotor ripples superimposed on it
*** - The step distribution with saturation only accounted for

For a double cage rotor slot, figure 4.14, the bar impedance $z_{b\nu}$ is given by the resultant impedance of the equivalent circuit of figure 4.15. This equivalent circuit was derived [93] by dividing the slot into regions, A, N, B, and O as shown in figure 4.14. The parameters in the circuit, as distinguishable by the respective subscripts, are, therefore, the resistances and the self leakage reactances of each region. The calculation of these parameters and the end leakage impedance are discussed in appendix B.

4.2.2 Magnetic Field of the Rotor

If the instantaneous induced, νth harmonic current in the nth mesh (or nth bar) is $i_{\nu n(n+1)}$ (or $i_{b\nu n}$) it can be shown, as in section 3.2, that the air gap mmf produced is equivalent to

$$F_{b\nu n}(\vartheta,t) = \frac{i_{\nu n(n+1)}(t)}{2}\begin{cases} (2\frac{\alpha_d}{\pi}) \; ; \; 0 \le \vartheta \le \frac{1}{2}\alpha_d \\ \frac{-\alpha_d}{\pi} \; ; \; \frac{1}{2}\alpha_d \le \vartheta \le (2\pi - \frac{1}{2}\alpha_d) \\ (2\frac{\alpha_d}{\pi}) \; ; \; (2\pi - \frac{1}{2}\alpha_d) \le \vartheta \le 2\pi \end{cases} \qquad (4.7(a))$$

for mesh currents, or

$$F_{b\nu n}(\vartheta,t) = \frac{i_{b\nu n}(t)}{2}\begin{cases} (1 - \frac{\vartheta-(n-1)\alpha_d}{\pi}) \; ; \; (n-1)\alpha_d \le \vartheta \le 2\pi \\ (\frac{(n-1)\alpha_d-\vartheta}{\pi} - 1) \; ; \; 0 \le \vartheta \le (n-1)\alpha_d \end{cases} \qquad (4.7(b))$$

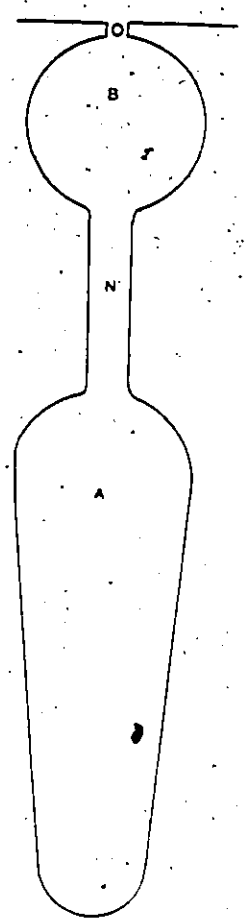

Figure 4.14: A typical shape of a double cage rotor slot

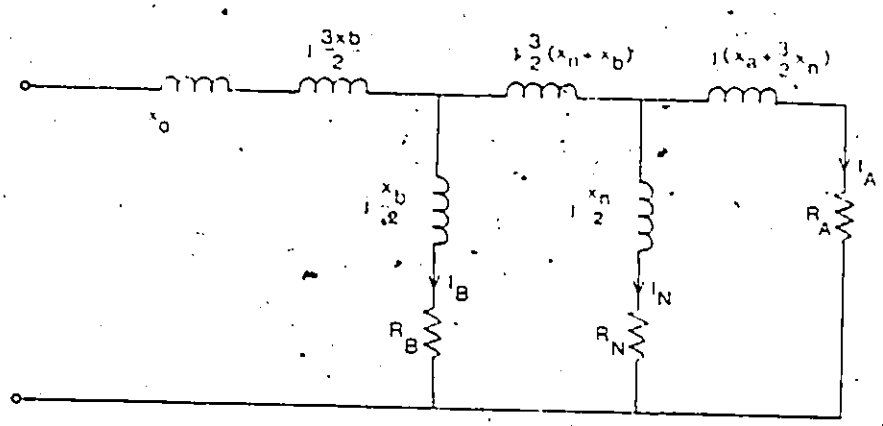

Figure 4.15: An equivalent circuit for the double cage of figure 4.14

for bar currents, where $\alpha_d = 2\pi/Q_2$. The total mmf for all bars and for all harmonics which induce currents in the rotor bars is

$$F_r(\vartheta,t) = \sum_{n=1}^{Q_2} \sum_{\nu=1}^{N} F_{b\nu n}(\vartheta,t) \qquad (4.8)$$

$F_r(\vartheta,t)$ can be treated in the same manner as the stator mmf in order to obtain the corresponding flux density distribution with saturation and both stator and rotor slot openings duly accounted for. A typical rotor air gap flux density waveform and its spectrum obtained this way, is as shown in figure 4.16. Table 4.7, which is similar to table 4.2, shows the significant harmonics of the rotor field waveforms.

Similar observations about all types of harmonics as were made for the stator are made for the rotor fields. Note, however, that the winding distribution harmonics are the combination of sets of that type of harmonic produced by each stator component that induces current in the rotor. This is because currents which flow in the rotor winding are induced by the stator fundamental acting together with some harmonics. If a νth stator harmonic induces current in the rotor winding the corresponding rotor winding distribution harmonics will be of the order

$$n = \frac{Q_2 k}{p} \pm \nu \quad ; \quad k = 0, 1, 2, 3, \ldots \qquad (4.9)$$

4.3 Overall Resultant Air-Gap Field

In the preceding sections the magnetic field waveform in the air gap has been taken to be due to either the excitation of the stator

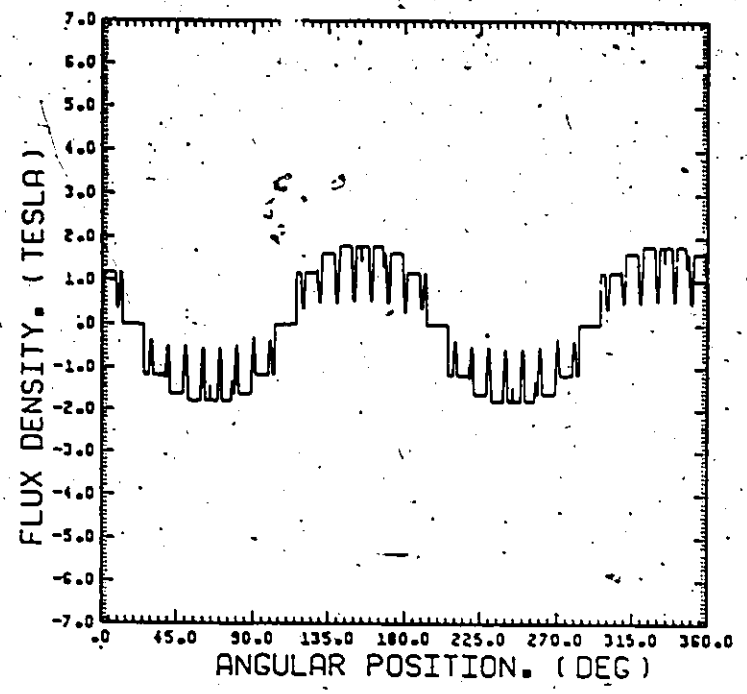

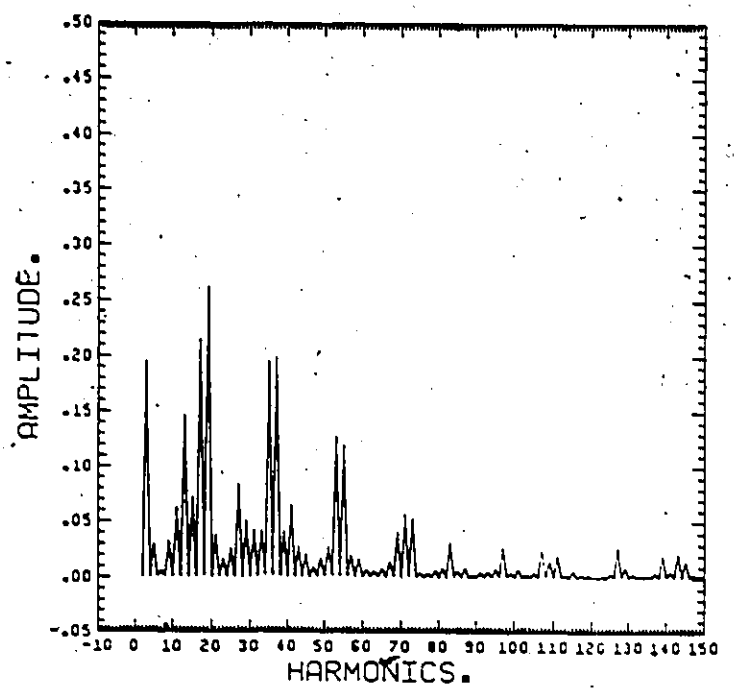

Figure 4.16: The waveform, and its spectrum, of the rotor air gap flux density with saturation and stator and rotor slot ripples.

Table 4.7: Significant Harmonics of Rotor Air Gap Waveforms (Amplitude > 0.1 Tesla)

Waveform	F/N	Harmonics
a	F	1, 13, 15, 27, 29
	N	1,
b	F	1, 13, 15, 17, 19, 27, 35, 37, 53, 55
	N	1, 17, 19
c	F	1, 13, 15, 27, 41
	N	1
d	F	1, 13, 15, 17, 19, 27, 35, 37, 53, 55
	N	1, 17, 19
e	F	1, 3, 13, 15
	N	1
f	F	1, 3
	N	1
g	F	1, 3, 13, 17, 19, 35, 27, 53, 55
	N	1, 17, 19

Note: Nomenclature is as in table 4.2.

winding only or to the rotor winding only. In most operations of the induction machines, however, both the stator and rotor windings have currents flowing in them simultaneously, hence the air gap field will be the resultant of that due to the rotor and the stator. Due to non-linearity, however, this resultant, for the magnetic flux density waveform, can not be merely taken as the sum of the resulting waveforms in sections 4.1.3 and 4.2.2 (i.e. figures 4.13(a) and 4.16). The approach taken, therefore, is to first solve the linear problem before solving the non-linear one. This implies that with the knowledge of the supply current the stator air gap mmf distribution is obtained, and then by neglecting saturation and considering everything else the corresponding flux density distribution is obtained. Then using this with the theory in chapter 3, the induced currents in the rotor windings are obtained and hence the rotor air gap mmf distribution can be obtained. The air gap mmf field distributions are then summed together. This resultant air gap mmf is then used to obtain the corresponding distribution of saturation factors, figure 4.17, from the curve of figure 4.10.

This saturation factors distribution is used to modify the linear stator air gap flux density distribution to obtain the non-linear one (figure 4.18(a)), one with saturation accounted for. This modified waveform is separated into the saturation and the other space harmonic components according to equation 4.6. These components are therefore employed to obtain the actual rotor current and then the rotor air gap magnetic flux density distribution with saturation accounted for, as in

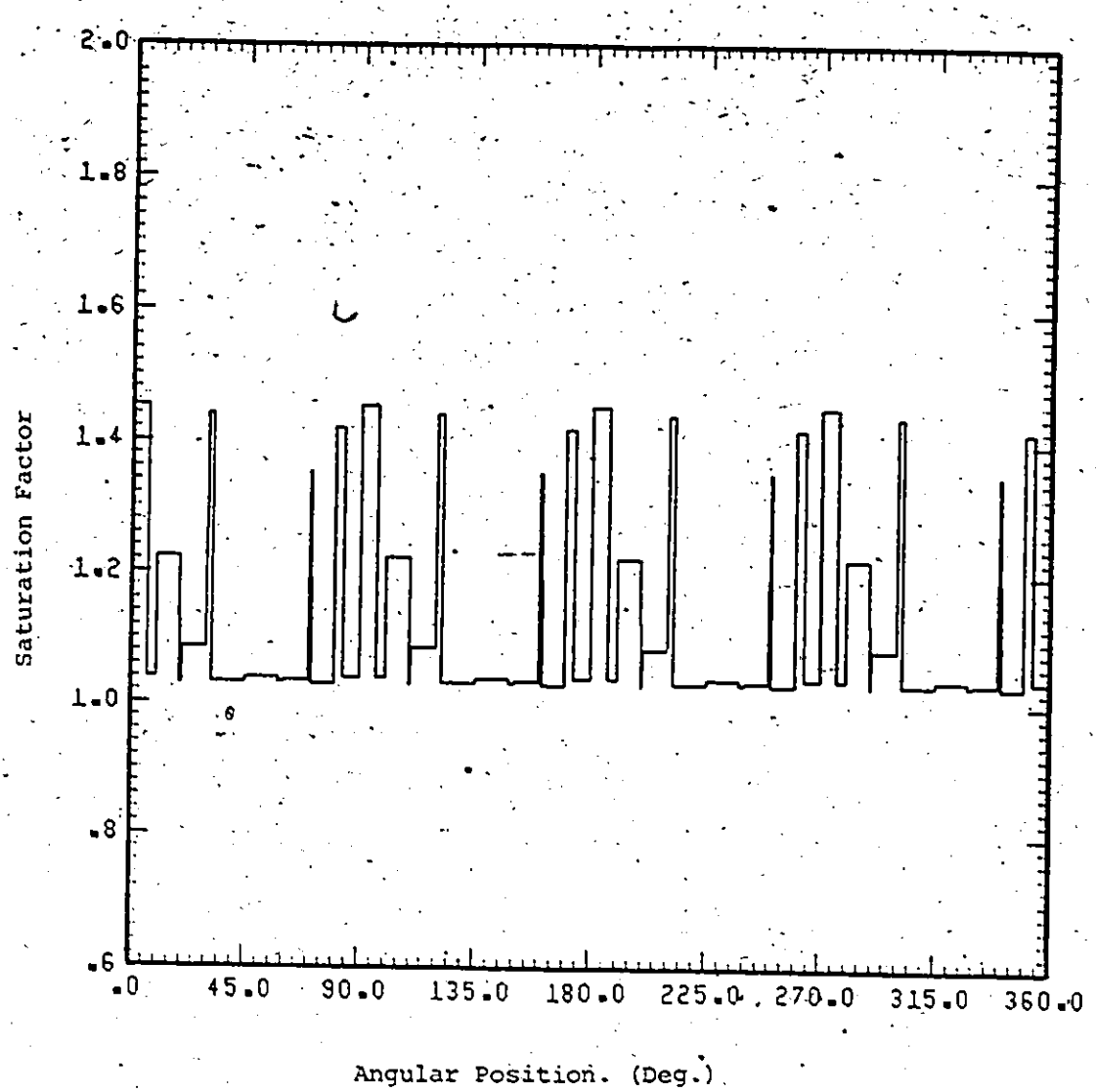

Figure 4.17: Saturation Factor Distribution

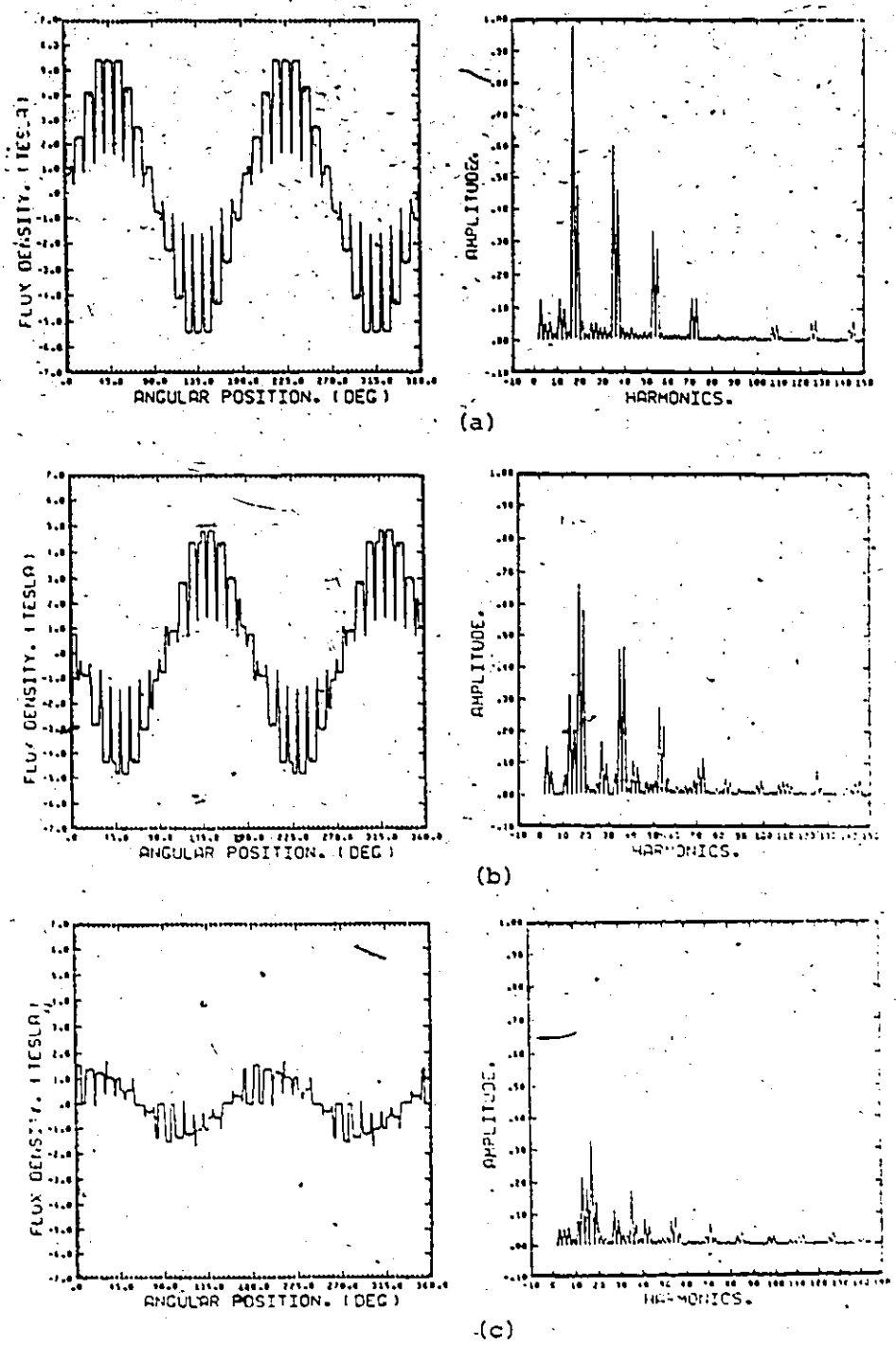

Figure 4.18: The stator, rotor, and the overall resultant gap flux density waveforms with their spectral.
(a) Stator
(b) Rotor
(c) The resultant

the stator, by using the same saturation factor distribution (figure 4.18(b)). The resultant air gap flux density waveform, figure 4.18(c) is obtained as the sum of figure 4.18(a) and 4.18(b). This corresponds to summing together the stator and rotor air gap mmf distributions and modifying the resulting waveform using the saturation factor distribution of figure 4.17.

4.4 Discussions: Harmonics and Stray Load Losses

The important harmonics in induction motors may be classified as shown in figure 4.19. For the practical case study in this work, the magnitudes of some 22 harmonics (which are selected to represent all types of harmonics in figure 4.19), each expressed as a percentage of the fundamental of the stator step distribution at full load, are compared for various waveforms as shown in tables 4.8(a), for the full-load case; table 4.8(b), for the locked rotor condition at locked-rotor current; table 4.8(c), for the locked rotor case at full-load supply current; and table 4.8(d), for the no-load case at no-load supply current.

If the supply to the motor is kept constant at the rated values the saturation harmonics are largest at no-load and decrease as slip increases. In other words, the magnitude of saturation harmonics tends to decrease as the motor is loaded. There are two reasons for this decrease: First, the machine becomes less saturated under load due to the decrease of the phasor difference between the applied voltage and primary impedance drops. Second, for squirrel-cage motors, the rotor

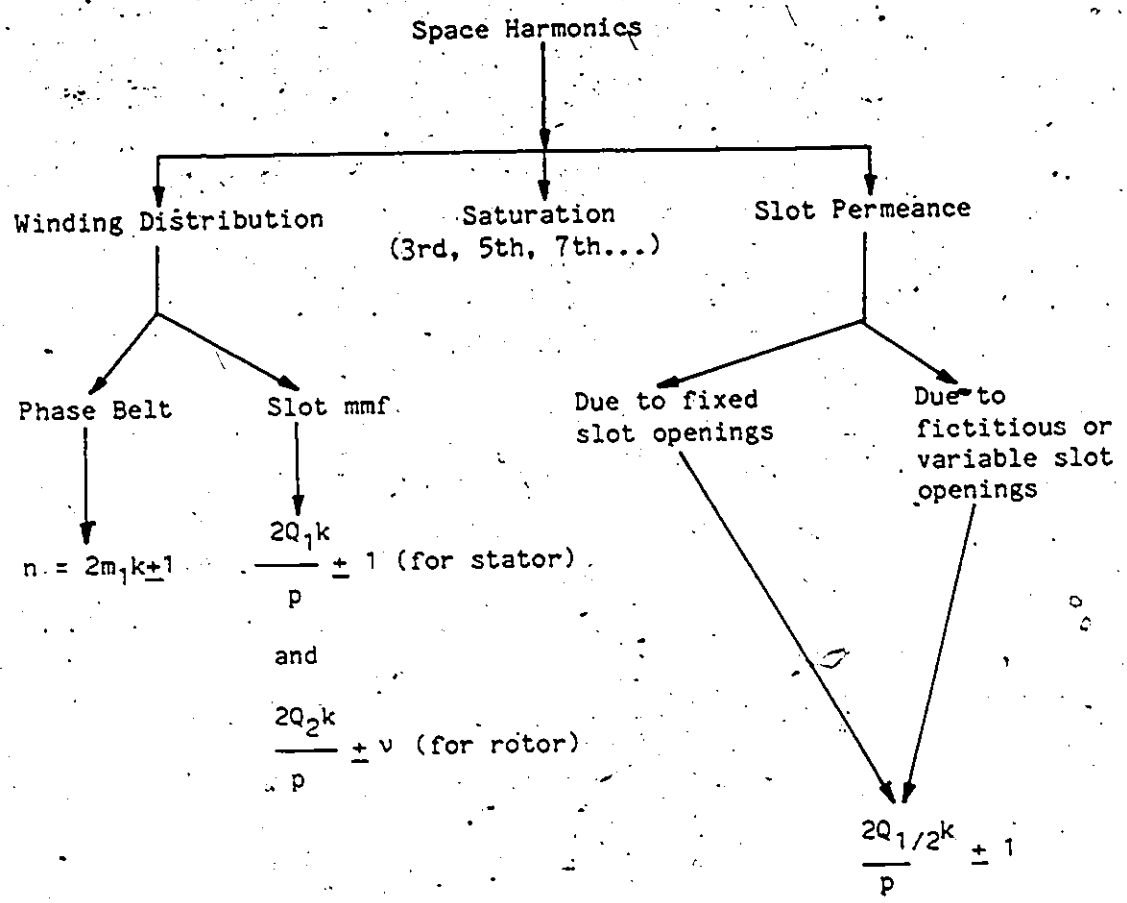

$k = 0, 1, 2, 3...$

Figure 4.19: Classification of Harmonics in Induction Motors

Legend for Tables 4.8(a), (b), (c) and (d)

(a) - stator step

(b) - stator with stator ripples

(c) - stator with rotor ripples

(d) - stator with stator and rotor ripples

(e) - stator with saturation

(f) - stator with both ripples and saturation

(g) - rotor step

(h) - rotor with stator and rotor ripples

(i) - rotor with saturation

(j) - rotor with both ripples and saturation

(k) - resultant step

(l) - resultant with stator and rotor ripples

(m) - resultant with saturation

(n) - resultant with both ripples and saturation.

Table 4.8(a): Full-load Case (I_1 = 26.7A, s = 0.0)

HARMONICS	STATOR						ROTOR				RESULTANT			
	(a)	(b)	(c)	(d)	(e)	(f)	(g)	(h)	(i)	(j)	(k)	(l)	(m)	(n)
1	100.0	86.62	99.79	86.42	93.89	81.36	94.87	82.02	82.58	71.42	24.77	21.47	20.07	17.47
3	--	--	--	--	2.60	2.17	--	0.67	4.20	3.88	--	0.90	1.61	1.23
5	0.84	0.75	0.85	0.75	0.71	0.90	--	1.10	1.47	2.34	0.83	0.29	1.22	1.12
7	2.15	1.98	2.15	1.98	0.94	0.99	--	0.16	1.15	0.76	2.16	1.46	1.53	1.01
9	--	--	--	--	0.89	0.43	--	0.76	0.59	1.06	--	0.22	0.36	0.44
11	1.37	1.43	1.38	1.44	2.59	2.22	--	0.27	1.45	1.66	1.39	2.00	0.92	1.33
13	0.32	0.37	0.11	0.17	2.24	1.68	7.29	5.96	8.94	7.71	7.00	6.11	4.89	4.28
15	--	--	0.19	0.18	0.64	0.51	6.33	5.81	6.96	6.30	6.33	5.36	4.18	3.41
17	5.89	17.59	5.89	17.58	6.12	16.91	--	11.70	2.92	10.01	5.88	6.67	4.17	5.04
19	5.25	7.77	5.25	7.78	3.90	8.19	--	11.63	2.92	11.06	5.24	4.79	3.60	3.43
21	--	--	--	--	1.34	1.10	--	0.52	0.66	1.25	--	0.74	0.20	0.58
27	--	--	0.20	0.20	1.21	0.98	3.50	3.00	3.91	3.59	3.52	3.26	2.43	2.26
29	0.52	0.46	0.31	0.26	1.19	0.73	3.28	2.77	3.04	2.71	2.76	2.29	1.91	1.58
35	2.87	11.34	2.87	11.33	2.70	10.42	--	9.12	1.50	8.26	2.884	3.22	2.09	2.69
37	2.69	8.12	2.69	8.11	2.12	7.98	--	8.98	1.54	7.91	2.70	2.44	1.86	4.74
41	0.11	0.01	0.09	0.20	0.99	0.53	2.30	1.46	2.42	2.15	2.22	2.45	1.44	1.66
43	0.35	0.05	0.15	0.14	0.77	0.75	2.22	2.20	2.28	2.03	2.53	1.81	1.76	1.23
53	1.90	6.55	1.90	6.56	1.41	5.77	--	5.71	0.85	4.50	1.88	1.59	1.38	1.30
55	1.81	5.68	1.99	5.49	1.89	4.99	1.71	7.24	1.30	6.13	0.40	2.33	0.31	1.78
57	--	--	0.21	0.17	0.27	0.44	1.67	1.57	1.55	1.65	1.67	1.26	1.21	0.86
71	1.42	2.69	1.23	2.51	1.19	2.27	1.34	3.83	1.98	3.25	2.71	1.61	1.94	1.18
73	1.36	2.69	1.35	2.70	1.47	2.27	--	2.27	0.68	1.97	1.34	0.54	0.95	0.47

Table 4.8(b): Locked-Rotor Case At Locked-Rotor Current
(I_1 = 133.97A, s = 1.0)

HARMONICS	STATOR						ROTOR				RESULTANT			
	(a)	(b)	(c)	(d)	(e)	(f)	(g)	(h)	(i)	(j)	(k)	(l)	(m)	(n)
1	501.76	433.73	500.71	432.72	427.86	374.23	628.59	542.42	385.44	336.07	127.41	108.34	110.98	96.53
3	--	--	0.11	0.14	29.17	24.03	--	4.39	103.61	91.58	--	6.16	13.91	13.92
5	4.23	3.76	4.26	3.77	11.41	15.23	--	7.49	59.37	59.34	4.15	0.84	4.84	7.26
7	10.79	9.91	10.79	9.91	22.40	16.84	--	0.64	11.56	9.16	10.86	6.39	9.81	6.68
9	--	--	--	--	9.62	7.96	--	5.25	15.96	17.02	--	0.71	5.39	4.61
11	6.88	7.16	6.91	7.22	12.49	8.43	--	1.58	17.12	12.63	7.01	11.03	0.85	1.92
13	1.59	1.87	0.55	0.86	38.87	31.16	48.26	39.24	65.63	60.44	46.83	40.78	28.98	24.99
15	--	0.12	0.97	0.89	10.73	3.23	41.28	38.53	10.28	16.15	41.90	35.59	13.89	14.01
17	29.57	88.92	29.54	88.86	39.50	85.90	--	78.39	10.60	53.96	29.45	9.18	3.47	10.64
19	26.35	39.81	26.32	39.82	1.99	51.80	--	77.80	9.00	53.12	26.27	40.61	12.71	24.91
21	--	--	--	--	9.69	12.69	--	3.36	2.54	11.35	0.15	5.02	1.84	1.56
27	--	--	1.02	1.99	19.75	16.13	23.19	19.65	16.12	15.29	23.35	22.06	14.88	13.06
29	2.62	2.28	1.57	1.28	3.84	6.78	21.75	18.40	4.05	6.30	18.97	15.37	6.09	4.08
35	14.39	57.13	14.38	57.11	10.91	44.59	--	60.76	12.57	46.01	14.46	5.09	3.97	8.06
37	13.50	41.18	13.51	41.17	0.56	41.94	--	59.69	2.80	31.57	13.58	22.11	6.55	15.26
41	0.54	--	1.45	1.03	12.35	8.90	15.24	9.24	1.91	4.56	14.85	16.16	9.17	8.43
43	1.75	0.24	0.73	0.73	4.56	0.30	14.69	14.61	1.52	2.63	16.26	12.07	7.24	4.48
53	9.52	32.69	9.53	32.73	1.75	20.34	--	37.57	3.59	23.05	9.39	4.72	3.98	4.59
55	9.06	28.49	10.00	27.57	7.78	19.33	11.34	48.87	8.33	29.42	2.43	1.12	2.07	2.45
57	--	--	1.06	0.86	4.26	2.66	11.09	10.50	1.60	8.05	11.00	7.91	4.94	3.99
71	7.11	13.03	6.17	12.14	4.79	8.67	8.92	25.55	5.93	13.88	15.85	4.33	5.35	0.62
73	6.80	13.16	6.76	13.23	9.11	5.33	--	14.31	3.44	10.23	6.68	4.50	0.77	1.77

-.8(c): Locked-Rotor Case at Full-Load Current
(I_1 = 26.7A, s = 1.0)

HARMONICS	STATOR						ROTOR				RESULTANT			
	(a)	(b)	(c)	(d)	(e)	(f)	(g)	(h)	(i)	(j)	(k)	(l)	(m)	(n)
1	100.0	86.62	99.79	86.42	95.51	82.71	95.07	82.21	89.46	77.52	5.23	4.74	4.96	4.48
3	--	--	--	--	0.22	0.10	--	0.65	0.98	0.35	--	0.92	0.28	1.03
5	0.84	0.75	0.85	0.75	0.54	0.61	--	1.12	1.10	2.15	0.83	0.01	0.58	0.17
7	2.15	1.98	2.15	1.98	1.28	1.21	--	0.40	0.55	0.58	2.16	1.45	1.91	1.31
9	--	--	--	--	--	0.12	--	0.79	0.54	1.22	--	0.10	--	0.11
11	1.37	1.43	1.38	1.44	1.36	1.37	--	1.23	0.47	0.38	1.39	2.01	1.37	1.90
13	0.32	0.37	0.11	0.17	1.05	0.67	7.30	5.95	7.94	6.57	7.01	6.14	6.39	5.62
15	--	--	0.19	0.18	0.59	0.23	6.35	5.84	5.26	5.86	6.34	5.35	5.79	4.93
17	5.89	17.59	5.83	17.58	6.16	17.15	--	11.71	0.64	11.36	5.86	5.64	5.34	5.17
19	5.25	7.77	5.25	7.78	4.43	7.85	--	11.63	0.57	11.22	5.24	4.25	4.74	3.91
21	--	--	--	--	0.28	0.33	--	0.50	0.15	0.43	--	0.76	0.01	0.73
27	--	--	0.20	0.20	0.39	0.48	3.51	2.98	3.45	2.96	3.53	3.30	3.16	2.97
29	0.52	0.46	0.31	0.26	0.22	--	3.29	2.79	2.94	2.56	2.74	2.26	2.44	2.04
35	2.87	11.34	2.87	11.33	2.83	10.77	--	9.12	0.28	8.69	2.88	2.02	2.57	1.84
37	2.69	8.12	2.69	8.11	2.27	7.92	--	8.96	0.21	8.29	2.70	1.39	2.45	1.23
41	0.11	--	0.09	0.20	0.34	--	2.31	1.40	2.04	1.30	2.22	2.50	2.03	2.25
43	0.35	--	0.15	0.14	0.29	0.11	2.22	2.22	2.00	2.00	2.54	1.79	2.26	1.62
53	1.90	6.55	1.90	6.56	1.76	6.01	--	5.70	0.17	5.43	1.88	0.59	1.65	0.52
55	1.81	5.68	1.99	5.49	1.73	5.15	1.71	7.41	1.76	6.99	--	1.33	0.01	1.22
57	--	--	0.21	0.17	--	0.15	1.68	1.60	1.39	1.46	1.67	1.24	1.44	1.11
71	1.42	2.69	1.23	2.51	1.44	2.40	1.35	3.94	1.29	3.66	2.74	1.25	2.44	1.12
73	1.36	2.69	1.35	2.70	1.42	2.42	--	2.24	0.24	2.22	1.34	0.01	1.22	0.01

Table 4.8(d): No-Load Case (I_1 = 7.21A, s = 0.0005)

HARMONICS	STATOR						ROTOR				RESULTANT			
	(a)	(b)	(c)	(d)	(e)	(f)	(g)	(h)	(i)	(j)	(k)	(l)	(m)	(n)
1	27.00	23.39	26.99	23.38	23.63	20.46	1.92	1.66	1.68	1.45	26.92	23.30	23.54	20.38
3	--	--	--	--	1.16	1.01	--	--	0.01	0.01	--	--	1.16	1.01
5	0.23	0.20	0.23	0.20	0.20	0.18	--	--	--	--	0.23	0.20	0.20	0.18
7	0.58	0.53	0.58	0.53	0.34	0.31	--	--	--	--	0.58	0.53	0.34	0.31
9	--	--	--	--	0.12	0.12	--	--	--	--	--	--	0.12	0.12
11	0.37	0.39	0.37	0.39	0.22	0.23	--	--	--	--	0.37	0.39	0.23	0.23
13	0.01	0.10	--	0.01	0.01	0.01	0.15	0.13	0.14	0.12	0.16	0.15	0.12	0.11
15	--	--	--	--	0.23	0.33	0.13	0.11	0.11	0.01	0.13	0.12	0.26	0.37
17	1.59	4.75	1.59	4.75	1.39	4.16	--	0.24	--	0.20	1.59	4.74	1.39	4.14
19	1.42	2.10	1.42	2.10	1.24	1.84	--	0.24	--	0.22	1.42	2.09	1.24	1.83
21	--	--	--	--	0.16	--	--	--	--	--	--	--	0.16	--
27	--	--	--	--	--	--	0.14	0.01	0.01	--	0.01	0.01	0.01	--
29	0.14	0.12	0.13	0.11	0.01	0.01	0.01	0.01	0.01	--	0.15	0.12	0.01	0.01
35	0.77	3.06	0.77	3.06	0.68	2.68	--	0.19	--	0.16	0.77	3.05	0.68	2.67
37	0.73	2.19	0.73	2.19	0.64	1.92	--	0.19	--	0.17	0.73	2.18	0.64	1.91
41	--	--	--	--	--	--	--	--	--	--	--	--	--	--
43	0.01	--	0.01	--	--	--	--	--	--	--	0.11	--	--	--
53	0.51	1.77	0.51	1.77	0.45	1.55	--	0.12	--	0.11	0.51	1.76	0.45	1.54
55	0.49	1.53	0.50	1.52	0.43	1.33	--	0.01	--	0.01	0.49	1.52	0.42	1.33
57	--	--	--	--	--	0.01	--	--	--	--	--	--	0.01	0.01
71	0.38	0.72	0.37	0.71	0.33	0.62	--	--	--	--	0.39	0.72	0.34	0.62
73	0.37	0.73	0.37	0.73	0.32	0.64	--	0.01	--	--	0.37	0.72	0.32	0.63

currents tend to damp out the saturation harmonics. If however, the motor is operated at a fixed supply voltage (rated) and the supply current is allowed to vary with slip from the no-load to the locked rotor the saturation harmonics are virtually the same at no-load up to the rated or full-load but gradually increases as the supply currents increase with increasing slip toward the locked-rotor condition. Therefore saturation harmonics contribute to stray load loss in induction motors. Their contributions, which are in the form of surface and additional conductor losses due to induced circulating currents, increase with the magnitude of these harmonics which in turn depend on the excitation and phase relation between stator and rotor fields.

At no-load the magnitudes of the winding distribution harmonics are about 30% of their counterparts at full-load. This is because the no-load supply current is about 30% of that a full-load. Hence, these harmonics vary with current. Since as the load increases the supply current also increases, then the magnitudes of these harmonics increases with load. They therefore contribute to stray load loss. Since the stator winding distribution harmonics fluxes travel with respect to the rotor, they produce rotor surface losses and tooth pulsation losses. Some of them induce currents in the rotor windings and hence contribute to the rotor conductor losses. The winding distribution harmonics are also responsible for the dips in the torque versus speed characteristic. A similar case to that for the stator winding distribution harmonics applies to the rotor winding distribution harmonics. They produce surface and tooth pulsation losses in the stator.

The slot permeance harmonics are discussed in section 4.1.1. The main influences of the slot openings (actual and fictitious) are that they decrease the magnitude of the fundamental component of the air gap field and augment the magnitudes of some of the space harmonics. The increase of the magnitudes of the slot permeance harmonics with load are caused, on one hand, by the fact that the slot ripples are always superimposed on the air-gap field distribution, which is obtained by assuming a smooth air-gap, and on the other, by the fictitious slot opening width which increases with load. The reason for this increase is obvious, even though the amount of increment is quite small. The reason for increase due to slot permeance harmonics is more because of the phase difference between the two superimposed distributions. Since the slot mmf and permeance harmonic fields have the same numbers of poles and same frequencies in the rotor, the total loss they produce is more than the sum of their losses determined independently, unless it happens that they are displaced 90 degrees in time or space. The relative magnitudes of the slot permeance harmonics fields are less at load than at no-load. The reason for this is mainly the rotor reaction which is significant at load slips and negligible at no-load slip. The slot permeance harmonics cause losses in the stator and rotor in the same manner as the winding distribution harmonics.

CHAPTER 5

PREDICTION AND MEASUREMENT OF TORQUE

As shown in the last two chapters, the magnetic field in an air gap, which is made up of two components, a stator and a rotor air gap field, can be resolved into a series of harmonics. These are produced by concentrating the winding into slots, by a non-uniformity of the air gap caused by slotting, and by saturation. The fundamental and some of the harmonics act on the rotor to produce currents which are responsible for the rotor component of this air gap field. The conventional notion of the electromagnetic torque is that it results from the interaction between the rotor winding conductors carrying the current induced by the fundamental component of the air gap field, and the fundamental component of the air gap rotating field. This notion, when extended to include harmonics as in the chain equivalent circuit of figure 3.2, views electromagnetic torque as resulting from the interactions between the currents in the rotor winding and those components of the rotating air gap magnetic field which induces these currents in the rotor. In this work, however, the electromagnetic torque is viewed as the torque equivalent of the overall air gap power. This, when analyzed in more detail as is done in chapter 6, includes useful and non-useful components of power which are assumed to cross the air gap from the stator to the rotor. We also consider a component of

non-useful powers, those which cause additional iron loss, as a result of reflection across the air gap from the rotor to the stator.

This chapter commences with a derivation of the expressions for the instantaneous and time-average electromagnetic torques of induction machines. These together with the theory presented in chapter 2 and the ideas of chapter 3 are then developed into an algorithm which is used to predict and study the torque-speed and torque-time characteristics of a practical machine. Parasitic torques in this machine are also studied using this algorithm. The remainder of the chapter is devoted to a presentation of a dynamometer test that was performed in order to obtain a practical torque-speed characteristic for comparison with the predicted, and a general discussion of the results.

5.1 Derivation of an Expression for Electromagnetic Torque

The electromagnetic torque results from the interaction of currents in the rotor winding conductors and the rotating magnetic field in the air-gap. The latter $B(\vartheta, t)$, includes the fundamental and all harmonics to infinity. If the instantaneous current carried in a rotor conductor is i_{rc} then the elementary force produced by this current interacting with the air gap rotating field is

$$f = B(\vartheta,t)\, i_{rc} l \tag{5.1}$$

The torque produced by this current-carrying conductor is therefore

$$\tau = fr = f\frac{D}{2} = B(\vartheta,t) i_{rc} l \frac{D}{2} \tag{5.2}$$

From equation (4.7) the relationship between the instantaneous current carried in a rotor bar and the air gap flux density distribution due to that current can be generally written as

$$B_{r\nu n}(\vartheta,t) = \frac{\mu_o i'_{b\nu n}(t)}{\delta} m(\vartheta) \tag{5.3}$$

where

$$m(\vartheta) = \frac{1}{2k_c k_s(\vartheta,t)} \begin{cases} \left(1 - \dfrac{\vartheta - (n-1)\alpha_d}{\pi}\right) ; & (n-1)\alpha_d \leq \vartheta \leq 2\pi \\ \left(\dfrac{(n-1)\alpha_d - \vartheta}{\pi} - 1\right) ; & 0 \leq \vartheta \leq (n-1)\alpha_d \end{cases} \tag{5.4}$$

if $i'_{b\nu n}$ is a bar current, or

$$m(\vartheta) = \frac{1}{2k_c k_s(\vartheta,t)} \begin{cases} \left(2 - \dfrac{\alpha_d}{\pi}\right) ; & 0 \leq \vartheta \leq \dfrac{1}{2}\alpha_d \\ \dfrac{-\alpha_d}{\pi} ; & \dfrac{1}{2}\alpha_d \leq \vartheta \leq \left(2\pi - \dfrac{1}{2}\alpha_d\right) \\ \left(2 - \dfrac{\alpha_d}{\pi}\right) ; & 2\pi - \dfrac{1}{2}\alpha_d \leq \vartheta \leq 2\pi \end{cases} \tag{5.5}$$

if $i'_{b\nu n}$ is a mesh current.

Equation (5.3) can otherwise be written as

$$B_{r\nu n}(\vartheta,t) = \frac{\mu_o i_{b\nu n}(\vartheta,t)}{\delta} \tag{5.6}$$

where

$$i_{b\nu n}(\vartheta,t) = i'_{b\nu n}(t)\, m(\vartheta) \tag{5.7}$$

The implication of equation (5.7) is that a current in a bar situated at an angular position is now replaced by an equivalent conceptual current which can be viewed as a layer of current sheet over the rotor surface distributed along the periphery in the manner implied by the right-hand side of the equation. The fact that these two currents are equivalent implies that they produce the same flux density waveform in the air gap.

From equation (5.2) the average instantaneous torque produced by this conceptual current can therefore be written thus

$$\tau_{\nu n}(t) = \frac{lD}{2}\int_0^{2\pi} B(\vartheta,t)\,\frac{\partial i_{b\nu n}(\vartheta,t)}{\partial\Delta}\,d\vartheta \qquad (5.8)$$

where Δ is an arbitrary geometric coordinate which determines the mutual position of the stator and rotor windings (i.e. Δ is a virtual displacement angle). Hence, $\tau_{\nu n}$ is a force tending to change the given coordinate.

If $i_{b\nu n}(\vartheta,t)$ is substituted from (5.6), we have the instantaneous electromagnetic torque produced by the νth harmonic current in the nth bar given by (5.8) as

$$\tau_{\nu n}(t) = \frac{lD}{2\mu_o}\int_0^{2\pi} B(\vartheta,t)\,\frac{\partial B_{r\nu n}(\vartheta,t)}{\partial\Delta}\,d\vartheta \qquad (5.9)$$

With a given angular rotor velocity the resultant or net electromagnetic torque is equal to the sum of torques due to currents in all bars and of all harmonics of the magnetic field. That is

$$\tau_{em}(t) = \frac{lD}{2\mu_o}\int_0^{2\pi} B(\vartheta,t)\,\frac{\partial B_r(\vartheta,t)}{\partial\Delta}\,d\vartheta \qquad (5.10)$$

where $B(\vartheta,t)$ is like figure 4.18(c) obtained in the manner discussed in section 4.3 and $B_r(\vartheta,t)$ is like figure 4.18(b). Integrating (5.10) over a time period T the time-average-electromagnetic torque is obtained as

$$\tau_{em} = \int_0^T \tau_{em}(t)\, dt \qquad (5.11)$$

$$= \frac{lD}{2\mu_o} \int_0^T \int_0^{2\pi} B(\vartheta,t) \frac{\partial B_r(\vartheta,t)}{\partial \Delta}\, d\vartheta dt$$

5.2 Torque-Time, and Torque-Speed Characteristics

The theory in chapter 3 together with the ideas in chapter 4 and the torque equations in the last section are developed into the following algorithm:

Step 1): Preliminary exercises include determining the following:

(1) Curves of the effective slot openings versus supply currents for the rotor and stator slots.

(2) Curve of saturation factor versus air-gap mmf.

(3) L and M as in equations (3.101) and (3.102).

Step 2): Using the effective slot opening of the stator and rotor to estimate Carter's factor by solving equation 3.123.

Step 3): Determine the rotor bar and end-ring segment impedances for (i) the fundamental component, (ii) the saturation harmonics, and (iii) the space harmonics.

Step 4): At a particular time instant and rotor position determine the ripple distribution for the stator and rotor; i.e. the distribution of the slot permeance factor against the

circumferential angular position.

Step 5): Establish the step distribution of the air gap mmf ($F_s(\vartheta,t)$) and the corresponding flux density distribution due to the excitation of the stator winding only.

Step 6): Multiply the flux density distribution in step 5) by the two ripple distributions in step 4) and resolve the resulting waveform into the fundamental and its harmonic components.

Step 7): For each sinusoidal component of the resulting flux density waveform in step 6) determine the magnitude or the maximum value of the induced current in the rotor winding. If this current is above a preset criterion determine the corresponding step air-gap mmf distribution due to its flow in the rotor winding. Then add together all step distributions of the air gap mmf due to currents in the rotor winding to get the resultant rotor step mmf distribution, $F_r(\vartheta,t)$.

Step 8): Add stator and rotor air gap step mmf distribution (i.e. $F_s(\vartheta,t) + F_r(\vartheta,t)$) and use this to establish the saturation factor distribution around the air gap periphery $k_s(\vartheta,t)$. Also determine the mean value of $k_s(\vartheta,t)$.

Step 9): By using $k_s(\vartheta,t)$ and the fundamental component of the stator step distribution of the air gap flux density distribution obtained in step 5) determine the stator saturation harmonic components.

Step 10): Establish β (see section 4.1.2) and use it to modify the other stator space harmonics obtained in step 6).

Step 11): Repeat step 7) for the stator saturation harmonics.

Step 12): Repeat step 7) for the saturated fundamental component and the other modified stator space harmonics.

Step 13): The final resultant rotor air gap step mmf distribution is the sum of that obtained in steps 11) and 12).

Step 14): $B_s(\vartheta,t)$ is obtained from the stator step distribution of the air gap mmf from step 5), $k_s(\vartheta,t)$, and the two ripple distributions. Similarly, $B_r(\vartheta,t)$ and $\frac{\partial B_r(\vartheta,t)}{\partial \Delta}$ are obtained from the rotor step distribution of the air gap mmf (step 13)), $k_s(\vartheta,t)$, and the two ripple distributions (step 4)).

Step 15): Obtain the instantaneous electromagnetic torque from $B_s(\vartheta,t)$, and $B_r(\vartheta,t)$, and $\frac{\partial B_r(\vartheta,t)}{\partial \Delta}$ by solving equation (5.10).

Step 16): To obtain $\tau_{em}(t)$ for another time instant (and hence another rotor position) repeat steps 14) to 15). The time average electromagnetic torque is obtained by solving equation (5.11).

The above algorithm was implemented for a practical induction motor (table 4.1). The variations of instantaneous electromagnetic torque with time, at the full-load condition of operation, are as shown in figure 5.1. The curves shown in the figure represents the following three cases:

Case A: - The air gap mmf waveforms used in step 14) above to obtain $B_s(\vartheta,t)$, $B_r(\vartheta,t)$, and $\frac{\partial B_r(\vartheta,t)}{\partial \Delta}$ are of the step distribution.

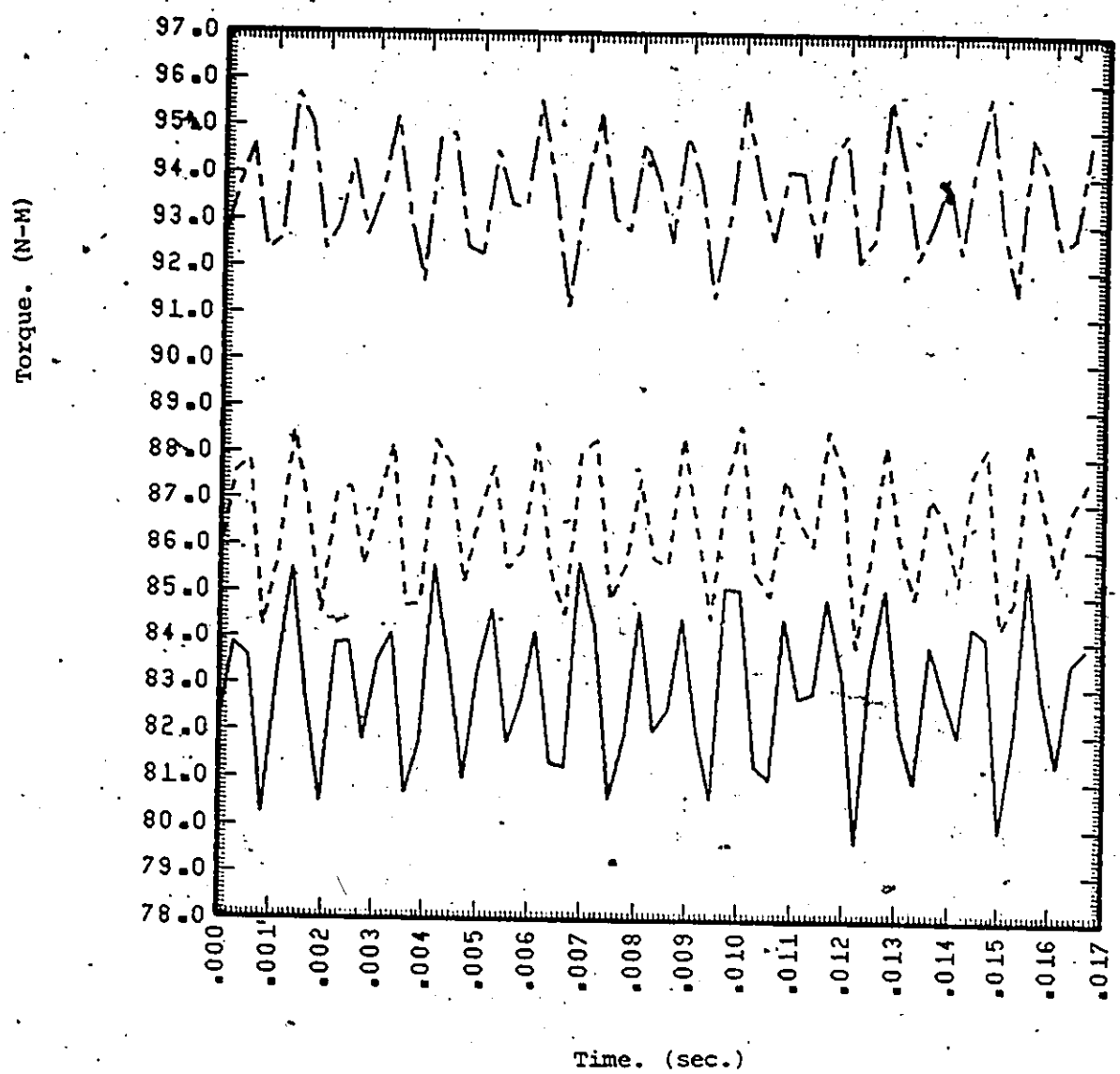

_____ Case A (stator and rotor fields are step distributions)

--------- Case B (stator field is fundamental, rotor is step distribution)

___._____. Case C (Stator and rotor fields are fundamental sinusoidal distributions)

Figure 5.1: Torque Versus Time

Case B: - The stator air gap mmf waveform used in obtaining $B_s(\vartheta,t)$ in step 14) is of the fundamental sinusoidal distribution, while that of the rotor, used in obtaining $B_r(\vartheta,t)$ and $\frac{\partial B_r(\vartheta,t)}{\partial \Delta}$ is of the step distribution. This case corresponds to phenomena characterized by the conventional model of induction machines.

Case C: - The air gap mmf waveforms for both the stator and rotor, which are employed in step 14) of the above algorithm for deriving $B_s(\vartheta,t)$, $B_r(\vartheta,t)$, and $\frac{\partial B_r(\vartheta,t)}{\partial \Delta}$ are taken to be of fundamental sinusoidal components.

Also using the above algorithm the torque versus speed characteristics of the practical machine are predicted for the case when saturation is neglected and when it is not, figure 5.2.

5.3 Effects of Harmonics

The criterion referred to in step 7) of the algorithm in section 5.2 may be in the form of the maximum value of the induced current in the bars or mesh of the squirrel-cage rotor winding. The essence of this criterion is to control or select the harmonics which induce currents in the rotor winding. Table 5.1 shows the harmonics number and rotor conductor loss for various criteria.

No significant change is observed in the time average torque and rotor conductor loss as the number of harmonics which induce currents in the rotor winding is increased. Also, except for slight increments in the magnitude of the difference between the maximum and the minimum

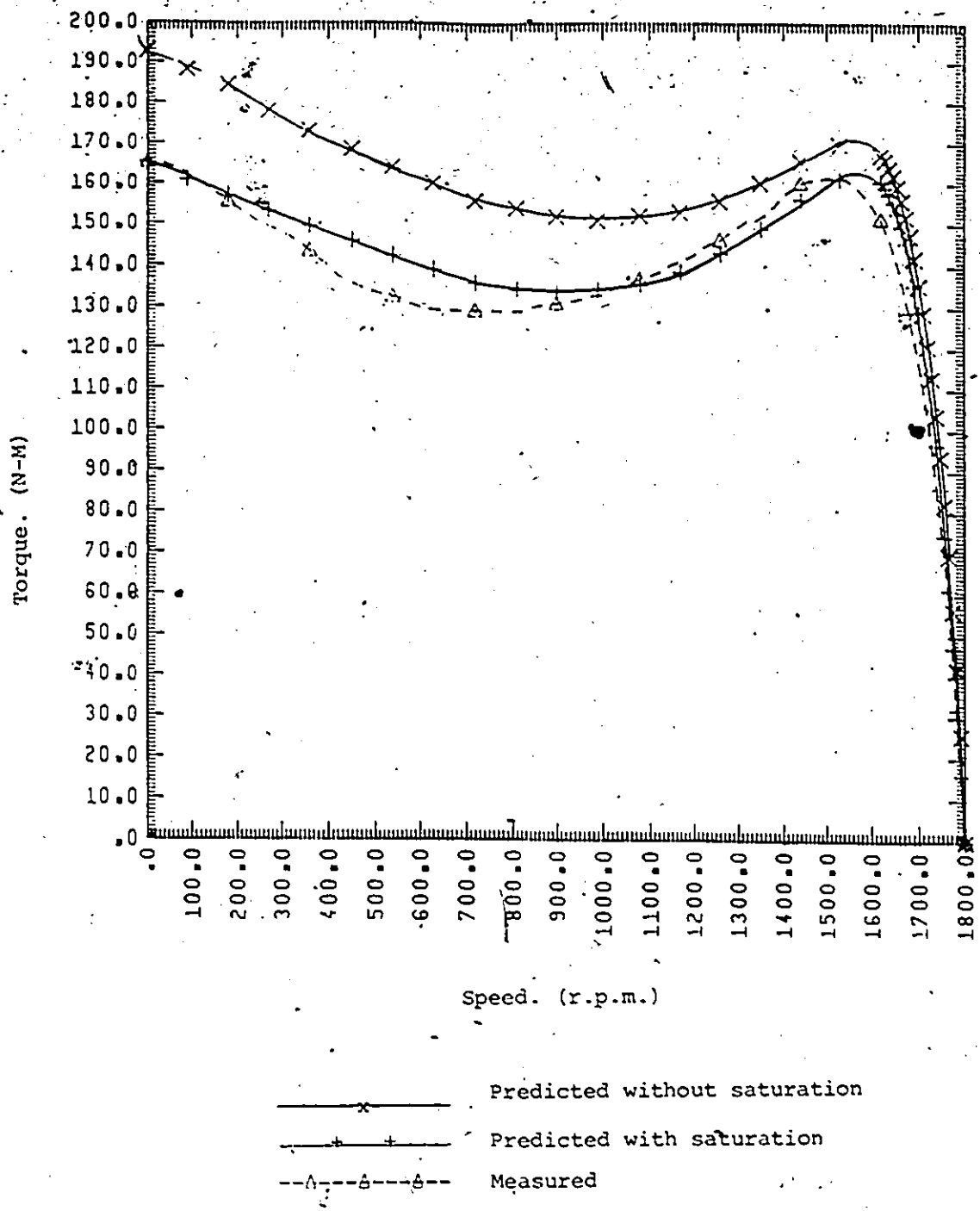

Figure 5.2: Torque - Speed Characteristics

Table 5.1: Effects of Harmonics

Criterion I_{rmax} (Amps.)	Observed Harmonics	Time Average Torque (N-m)	Time Average Rotor Cond. Loss (Watts)
*	----	81.49	435.0
**	1	93.57	475.99
***	1	86.48	476.99
200.0	1	82.93	476.99
50.0	3^, 1, 17	82.51	479.27
25.0	3^, 1, 17, 19, 35	82.47	480.30
15.0	3^, 5^, 1, 7, 17, 19, 35, 37	82.47	481.38
5.0	1, 3^, 5^, 7^, 9^, 11^, 13^, 15^, 17^, 19^, 5, 7, 11, 17, 19, 35, 37, 53	82.63	481.64

* - Measured
** - Stator mmf fundamental sinusoidal rotor mmf fundamental sinusidal
*** - Stator mmf fundamental sinusoidal, rotor mmf step
^ - Saturation harmonic

torque in the torque - time characteristics corresponding to these criteria, figure 5.3, no other significant differences are observed between the curves in the figure. The reason for this insignificant influence on the behaviours of the machine is partly due to the relatively low magnitude of the maximum induced current by each of these harmonics, (table 5.2), and hence very low corresponding rotor conductor loss. Also contributing to this lack of observable influence are the power factors of the impedances of these harmonics. Except for the first few saturation harmonics the secondary power factors of the harmonic components are generally low. This implies that the stator and rotor waveforms of a harmonic component are positioned so that they damp each other out and are hence unable to produce any significant torque.

However, the differences between the time-average torques of cases A, B, and C described in section 5.2 (see table 5.1) are quite significant. The torque corresponding to case C is greater than that corresponding to the situation represented by the conventional equivalent circuit (case B), which in turn is greater than that corresponding to the actual phenomenon in the machine (case A). The significant differences among these three cases lie in the absence of the slot mmf harmonics and their companion harmonics due to permeance ripple and saturation in the stator model of case B, and in both the rotor and stator models of case C.

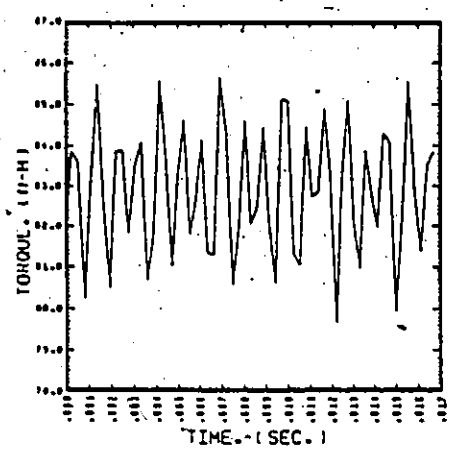

(a) (Max. rotor mesh curr.> 200.0A)

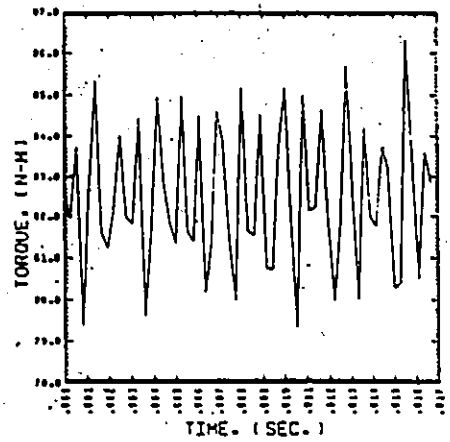

(b) (Max. rotor mesh curr.> 50.0A)

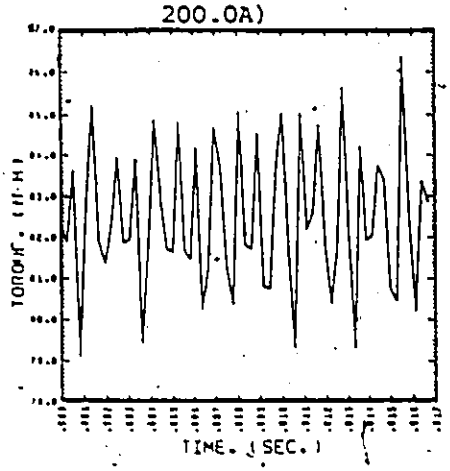

(c) (Max. rotor mesh curr> 25.0A)

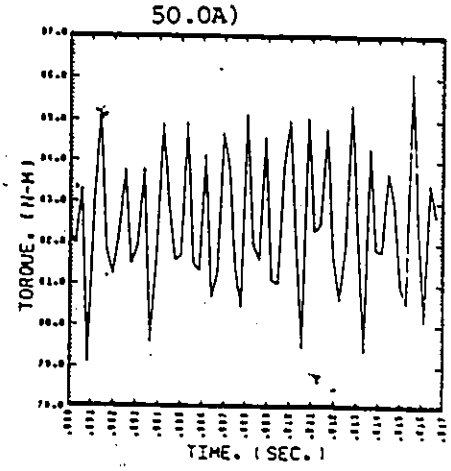

(d) Max. rotor mesh curr. > 15.0A)

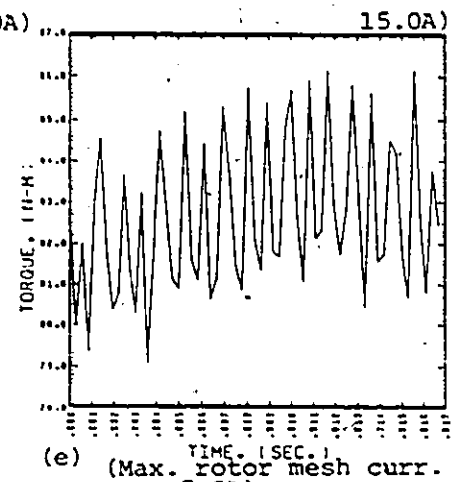

(e) (Max. rotor mesh curr. > 5.0A)

Figure 5.3: Torque vs. Time

Table 5.2: Typical Predicted Values of some parameters for some Harmonics

Harmonics	Typical Maximum Rotor Current (Amp)	Typical Secondary Power Factor	Typical Rotor Conducting Loss (Watt)	Typical Instantaneous Torque (N-m)
3^	65.58	0.82	0.89	-0.1981
5^	17.96	0.66	0.0852	-3.93×10^{-4}
7^	10.67	0.54	0.0053	1.32×10^{-2}
9^	9.27	0.47	0.0138	1.76×10^{-3}
11^	12.47	0.42	0.0104	-5.95×10^{-3}
13^	5.58	0.42	0.0003	8.74×10^{-4}
15^	6.05	0.40	0.0003	1.98×10^{-4}
17^	8.95	0.35	0.0042	5.07×10^{-5}
19^	6.27	0.34	0.0041	-2.1×10^{-3}
1	2334.52	0.98	475.91	87.73
5	10.83	0.15	0.17	-1.072×10^{-3}
7	21.27	0.15	1.1293	-8.43×10^{-3}
11	8.14	0.11	0.0289	-1.1×10^{-3}
17	66.39	0.095	1.59	5.34×10^{-2}
19	30.60	0.095	0.63	3.95×10^{-3}
35	25.12	0.074	0.0865	1.19×10^{-2}
37	16.61	0.074	0.142	2.05×10^{-3}
53	8.04	0.063	0.014	-1.54×10^{-3}

5.3.1 Analysis of the Torque Equation

One of the important advantages of the form of the torque expression in section 5.3.1, equations (5.10) and (5.11), is that it facilitates a detailed analysis of the roles of harmonics in the developed torque of induction machines. This fact can be demonstrated as in reference [17] if we express the stator air gap flux density distribution as

$$B_s(\vartheta,t) = \sum_{\nu}' B_{m\nu} \sin(\nu\vartheta \mp \omega_s t) \qquad (5.12)$$

An arbitrary magnetic flux density harmonic of the order ν travels with respect to the stator at an angular velocity $\omega_{s\nu} = \pm \omega_s/\nu$ [91]. If the rotor rotates at an angular velocity ω_r, the relative velocity of the same harmonic with respect to the rotor will be

$$\omega_{r\nu} = \pm \frac{\omega_s}{\nu} - \omega_r \qquad (5.13)$$

This harmonic induces in the rotor winding a voltage causing a current which produces a rotor flux density spectrum of harmonics determined by the properties of the rotor winding (armature reaction). In general, we may write for this spectrum referred to a coordinate system related to the rotor the expression

$$B_{r\nu}(\vartheta,t) = \sum_{u=1}^{\infty} B_{u\nu} \sin[u\vartheta' \mp (\pm \omega_s - \nu\omega_r)t - \vartheta_{upf}] \qquad (5.14)$$

If the spectrum is referred to the stator coordinate system, for which $\vartheta' = \vartheta - \omega_r t$, (5.14) will have the form

$$B_{r\nu}(\vartheta,t) = \sum_{u=1}^{\infty} B_{u\nu} \sin[u(\vartheta - \omega_r t) \mp (\pm \omega_s - \nu\omega_r)t - \vartheta_{upf}] \qquad (5.15)$$

The resultant flux density will be given by the sum of all the harmonics for all values of ν with saturation and ripple effect appropriately accounted for

$$B_r(\vartheta,t) = \sum_{\nu} \sum_{u} B_{u\nu} \sin[u(\vartheta - \omega_r t) \mp (\pm \omega_s - \nu\omega_r)t - \vartheta_{upf}] \qquad (5.16)$$

Substituting $B(\vartheta,t) = B_s(\vartheta,t) + B_r(\vartheta,t)$, and then equations (5.12) and (5.16) in (5.10) we have the general expression for the torque as

$$\tau_{em}(t) = \frac{\delta l D}{2\mu_o}\left\{ \int_0^{2\pi} \sum_{\nu} B_{m\nu} \sin(\nu\vartheta \mp \omega_s t) \sum_{\nu} \sum_{u} B'_{u\nu} \cos[u(\vartheta - \omega_r t) \mp (\pm\omega_s - \nu\omega_r)t - \vartheta_{upf}]d\vartheta + \int_0^{2\pi} \sum_{\nu} \sum_{u} B_{u\nu} \sin[u(\vartheta - \omega_r t) \mp (\pm\omega_s - \nu\omega_r)t - \vartheta_{upf}] \sum_{\nu} \sum_{u} B'_{u\nu} \cos[u(\vartheta - \omega_r t) \mp (\pm\omega_s - \nu\omega_r)t - \vartheta_{upf}]d\vartheta \right\} \qquad (5.17)$$

where $B'_{u\nu}$ implies a modified $B_{u\nu}$ due to the partial derivative.

The second term of equation (5.17) does not give any torque, because

$$\int_0^{2\pi} \sin\vartheta \cos\vartheta d\vartheta = 0$$

and the first term is, according to the relation

$$\int_0^{2\pi} \sin m\vartheta \cos(n\vartheta - \varphi)d\vartheta$$

for all $m \neq n$ also equal to zero. Only for $m = n$ has it the real value

$\pi \sin \varphi$.

Therefore, according to equation (5.17) a torque can arise only if for certain stator harmonics of the order $\nu = \sigma$ a harmonic of the order $u = \sigma$ can also be found in the spectrum of all rotor harmonics. This means, that a torque can be produced only by harmonics having an equal number of pole-pairs.

The torque of such a harmonic will then be

$$\tau_{em\sigma} = \frac{\delta l D}{2\mu_o}\int_0^{2\pi} B_{m\nu} \sin(\nu\vartheta \mp \omega_s t) \sum_{\nu=1}^{\infty} B'_{\sigma\nu} \cos[\sigma(\vartheta - \omega_r t)$$

$$\mp (\pm\omega_s - \nu\omega_r)t - \vartheta_{\sigma pf}]d\vartheta \qquad (5.18)$$

The resultant torque is obtained by a summation with respect to all values of σ, i.e. all harmonics for which rotor harmonics of the same order exist. Integrating equation (5.18) we then obtain

$$\tau_{em} = \sum_{\sigma} \tau_{em\sigma} \approx \sum_{\sigma} \sum_{\nu} \sin[\sigma\omega_r t \pm (\pm \omega_s - \nu\omega_r)t + \vartheta_{\sigma pf} \mp \omega_s t]$$

$$= \sum_{\sigma} \sum_{\nu} \sin\{[\sigma\omega_r \pm (\pm \omega_s - \nu\omega_r) \mp \omega_s]t - \vartheta_{\sigma pf}\} \qquad (5.19)$$

The resultant torque according to equation (5.19) is generally varying sinusoidally with time and its mean value is zero. A torque independent of time will be produced only if the term in the square bracket of the sine function is equal to zero, i.e.

$$\sigma\omega_r \pm (\pm \omega_s - \nu\omega_r) \mp \omega_s = 0 \qquad (5.20)$$

Equation (5.20) is satisfied in two entirely different cases.

Case 1: - Equation (5.20) is identically satisfied for all $_r$ by the condition

$$\sigma = \nu \qquad (5.21)$$

This means that a certain stator harmonic of the order generates in its spectrum of rotor harmonics of the armature reaction a fundamental harmonic of the same order .

Case 2: - Equation (5.20) may also be satisfied at a certain velocity $_r$ on the condition that

$$\sigma \neq \nu \qquad (5.22)$$

This means that although there exists a harmonic of the order in both the stator and rotor harmonic spectra, the rotor harmonic of the order σ has been generated by a stator harmonic of a different order ($\nu \neq \sigma$). For this case equation (5.20) may be written in the form

$$\omega_r \pm \frac{\pm\omega_s - \nu\omega_r}{\sigma} = \pm \frac{\omega_s}{\sigma} \qquad (5.23)$$

The left hand side of equation (5.23) determines the absolute velocity of the rotor harmonic of the order produced by the stator harmonic of the order $\nu \neq \sigma$ referred to the standing coordinate system connected with the stator. The right-hand side of the equation (5.23) then determines the absolute velocity of the stator harmonic of the order referred to the

same system. Equation (5.20) can thus be satisfied only if both the rotor and stator harmonics of the same order have equal velocities in the air gap, i.e. only at a certain angular rotor velocity ω_r. If the relevant rotor harmonic with the rotor standing ($\omega_r = 0$) has the same sense of rotation as the corresponding stator harmonic of the same order, the condition (5.23) is satisfied already with the rotor standing, i.e. when

$$\omega_r = 0 \tag{5.24}$$

If, however, for $\omega_r = 0$ its sense is opposite to that of the stator harmonic, condition (5.23) will be satisfied either at the rotor velocity

$$\omega_r = \pm \frac{2\omega_s}{\sigma - \nu} \tag{5.25}$$

or at the velocity

$$\omega_r = \pm \frac{2\omega_s}{\sigma + \nu} \tag{5.26}$$

The essential difference between the first and second case will be best recognized from the following consideration. Let us assume that the rotor rotates at an angular velocity $\omega_r = 2\omega_s/(\sigma + \nu)$. The condition (5.21) satisfies equation (5.20) for all values of ω_r, i.e. also for the considered velocity given by equation (5.16). Thus, equation (5.20) is satisfied for the condition (5.21) as well as for the condition (5.22). As the load torque is changed the rotor speed begins to change and after a certain time Δt its position with respect to the

system rotating at the original speed ω_r will be changed by an angle $\Delta\vartheta$. Consequently, the position of all the rotor mmf harmonics will change as well. If for instance, the original position of the rotor harmonic of the order σ in the spectrum of the νth harmonic is determined, according to (5.21), by the expression

$$\sin\,[\,\sigma\vartheta - (\omega_s - \nu\omega_r)t - \vartheta_{upf}] \tag{5.27}$$

it will then be given by the relation

$$\sin\,[\sigma(\,\vartheta - \Delta\vartheta\,) - (\omega_s - \nu\omega_r)(t - \Delta t) - \vartheta_{upf}] \tag{5.28}$$

where σ, $\Delta\vartheta$ and $(\omega_s - \nu\omega_r)\,\Delta t$ are the corresponding changes of phase .

To the space displacement $\Delta\vartheta$ corresponds in the field of the νth harmonic the time displacement $\nu\Delta\vartheta$; from this follows the value $\Delta t = (\nu\Delta\vartheta)/(\omega_s - \nu\omega_r)$. The foregoing expression may thus be written in the form

$$\sin\,[\sigma\vartheta - (\omega_s - \nu\omega_r)t - \Delta\vartheta(\sigma - \nu) - \vartheta_{upf}] \tag{5.29}$$

If $\sigma = \nu$, equation (5.29) will be identical with equation (5.27) so that the position of the rotor magnetomotive forces with respect to the original system has not changed. Therefore the motor will be changing its speed until its torque, because of a change of the phase angle φ, is balanced by the load torque, which is characteristic for the induction motor. Thus, if a certain stator mmf harmonic of the order σ produces in the spectrum of the rotor magnetomotive forces, a harmonic of the same order σ ($\nu = \sigma$), these harmonics form an asynchronous torque.

If $\sigma \neq \nu$, it follows from equation (5.29) that in a time t the position of the rotor magnetomotive forces has changed with respect to the original system by a phase angle $\Delta\vartheta(\sigma - \nu)$. Because, as follows from the consideration of equation (5.17), the torque is proportional to the sine of the phase angle between the two mmfs, the torque will be changed already by the change of the phase angle. Therefore, in this case ($\sigma \neq \nu$) small changes in load torque will cause only an angular displacement of the rotor with respect to the original system and the motor will preserve its original speed given by equation (5.26), which is characteristic for the synchronous motor. Thus, if the spectra of the stator and rotor magnetomotive force harmonics contain harmonics of the same order σ and if the rotor harmonic of this order is produced by a stator harmonic of another order ($\nu \neq \sigma$), then these harmonics form a synchronous torque.

5.4 The Measurement of Torque Speed Characteristics

The torque speed curve at full voltage was measured by means of an accelerometer using a d.c. tachometer [17,19], figure 5.4 and plate 5.1.

If an induction motor is running on no load, and the phase sequence of the supply is suddenly reversed, the machine decelerates from a speed of almost n_s in one direction to standstill, and then accelerates to a speed of almost n_s in the other direction. During the deceleration and acceleration there is an electromagnetic torque acting on the rotor, depending on the instantaneous slip of the rotor with

respect to the revolving magnetic field.

If the rotor inertia is J, and the instantaneous rotor speed is ω_r, the electromagnetic torque τ_{em} is given by

$$\tau_{em} = J\frac{d\omega_r}{dt} \pm \tau_{fw} \qquad (5.30)$$

where τ_{fw} is the friction and windage torque of the rotating parts, and the minus and plus signs correspond to the decelerating and accelerating periods, respectively. All that is needed, therefore, is to obtain a speed (ω_r) and an acceleration ($\dot{\omega}_r$) signal during the speed reversal. When these signals are fed into the x and y axes of a plotter, the resulting curve, apart from a small correction due to the friction and windage torques, is the torque-speed characteristic to a scale of J N.m/rad/s.

Although the friction torque may be a significant part of the total torque when the machine is operating at reduced voltage, it is totally negligible compared with the torque developed when the machine is operating on full-voltage.

If the speed signal is obtained from a d-c tachogenerator and differentiated electrically, the noise in the original signal must be filtered out before the differentiation process. Most of the noise is due to the commutator segments and hence its frequency is proportional to the rotor speed.

The torque speed characteristic measured by the accelerometer, after correcting for friction and windage, is shown in figure 5.2, together with those predicted.

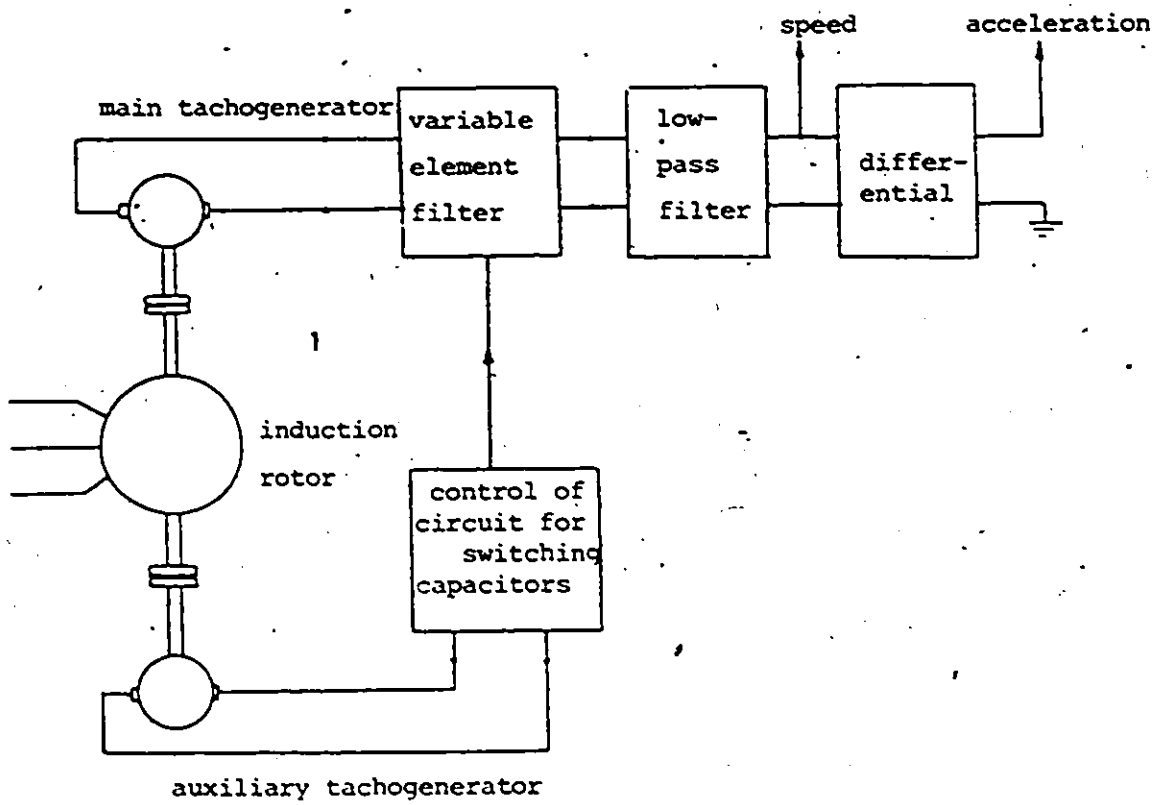

Figure 5.4: Block diagram of accelerometer connections

Plate 5.1: Set up for the measurement of torque-speed characteristic

5.4.1 Comparison of Predicted and Measured Torques

As shown in figure 5.2 the predicted torque speed curve compare reasonably well with the measured. As expected the torque predicted without saturation is larger than that measured at every slip. The difference became slightly more pronounced as slip and current increase. The predicted curve with saturation should have compared better with the measured than as shown in figure 5.2 had the measured currents been used, at every speed for which torque is calculated, for the prediction rather than estimated values. This problem was realized at the time of the measurement but due to unavailability of an a-c ammeter/plotter unit, the current-speed curve was unable to be measured.

One of the problems which was encountered when predicting the torque speed curve with saturation is that excessive deviations were observed between predicted instantaneous torques in one period of $T = 1/60$ at high slip and current. While some pronounced deviation is expected due to the production of synchronous torques (see section 5.3.1), especially at high slip and high current, the observed deviation was rather excessive. It was later discovered that the excessive deviation was brought about by the fact that at high currents the algorithm becomes quite sensitive to incorrect saturation factors; especially if they are higher than actual.

CHAPTER 6

PREDICTION TECHNIQUES FOR STRAY LOAD LOSS

In chapter 2 the state of the art of the calculation of stray load loss in induction machines was reviewed. Problems of prediction appear to have been well considered. An in-depth research, however, reveals that the empirical literature published on the achievements on this area is subject to very large discrepancies reported between calculated and measured results. This creates grave doubts on methods formulated to date. Indeed, most manufacturers, worldwide, prefer, at the design stage, to account for stray load loss through a nominal assignation method in conjunction with empirical expressions. Universally these techniques are based only on past experiences of the designers and have little rational analytic basis. In this chapter two new methods for predicting stray loss at the design, manufacturing, or utilization stages are proposed. Both of these methods are based on the new model presented in chapter 3 since they employ the algorithm of section 5.2 in chapter 5.

Before presenting these methods in sections (6.2.2 and 6.2.3 of this chapter the general concepts of losses in squirrel cage induction machines are discussed in section 6.1. Later in the chapter these proposed methods are applied to a practical machine and their results are compared with that measured using the input-output technique and

with predicted values at the design stage using the nominal assignation technique.

6.1 General Concept of Losses in Squirrel-Cage Induction Machine

A certain fraction of the power applied to an electric machine is lost, mainly as heat, while the rest is electromechanically converted for use as mechanical energy. Most of the loss occurs during the course of transportation and conversion of power, involving mainly the physical properties of the materials of transportation and the geometry of the device. A detailed description of losses in a machine can not be realized in isolation of the concept of power flow in the air gap. The reverse, however, is possible as evidenced by some published work on the latter [95, 96].

The flow of power supplied from the power system to a squirrel-cage induction machine can be considered as follows:

1) The input power first travels through the stator winding and hence part of it is expended as I^2R loss or stator copper loss.

2) The remainder, which is now viewed as electromagnetic power, can be resolved into two components: non-leakage, and leakage. The non-leakage components are transferred across the stator winding/air gap boundary either into the air gap or out of the air gap back to the power system. Power transferred into the air gap is either absorbed to account for mechanical power conversion or transferred across the rotor winding/air gap boundary. The loss component of this power is in the iron material. Since the field associated with this component of power interacts with

the iron materials during the course of transfer, it induces eddy currents in the core and causes hysteresis loss.

Part of the leakage component is used up in the stator windings by the 'skin effect' phenomenon. The remainder can further be split into two: end region, and non-end region leakage powers. The non-end leakage may penetrate the stator/air gap boundary into air gap.

Unlike the non-leakage component which is assumed to be one-dimensional in the air gap (radial), the non-end region leakage component has components in three dimensions. This notion about dimensions is one of the assumptions on which the theory, and hence the technique, developed in this work is based (see section 3.2). The notion originates from ignoring the significant properties of the tangential magnetic field which exists in the air gap, generally as an elementary function of both stator and rotor currents. The justification for this neglect lies in the fact that in practice the magnitude of the tangential field is generally small compared with that of the radial field and its emf - inducing properties may reasonably be absorbed within leakage inductance. Even though, as pointed out in [95] it is a significant factor in establishing torque and energy flows across winding surfaces.

The tangentially and axially directed components of the non-end region leakage power constitute circulations of power in the space surrounding the stator windings and are not directly involved in the transfer of power between the windings and the air gap. They modify the

distribution of non-leakage power over the air-gap space as it radiates from (or is absorbed by) the rotor. In summary, these tangential and axial leakage are non-useful stored leakage powers. Their loss component is also hysteresis and eddy current loss in the iron material; and they are partly responsible for noise and vibration in the machine. The radial component of the non-end winding leakage power in the air gap crosses the air gap to penetrate the surface on the other side. Since they do not penetrate well enough to cause power distribution in the rotor winding, and they do not contribute to the power conversion process, they essentially appear as additional iron loss on the surface and the tooth body of the rotor.

The end-leakage power is the power associated with the end-region magnetic fields. Part of this power is stored in the air spaces in the end regions while the rest is expended as heat, due to eddy current loss, in the materials, especially ferromagnetic, of the end regions.

3) The non-leakage power transferred across the rotor winding/air gap boundary set up electric power to flow in the squirrel cage winding. This power flows in the machine like that in the stator, i.e. (1) and (2) above.

The above arguments are supported by the machine equations presented in chapter 3, section 3.7. For example if equation (3.132) is

multiplied by $i_a(t)$ we have

$$i_a(t)v_a(t) = i_a^2(t)r_{sa} + i_a(t)L_{sa}\frac{di_a(t)}{dt} + i_a(t)L_{sla}\frac{di_a(t)}{dt} +$$

$$i_a(t)L_{slae}\frac{di_a(t)}{dt} + i_a(t)M_{ab}\frac{di_b(t)}{dt} + i_a(t)M_{labe}\frac{di_b(t)}{dt} +$$

$$i_a(t)M_{ac}\frac{di_c(t)}{dt} + i_a(t)M_{lace}\frac{di_c(t)}{dt} + i_a(t)M_{laee}\frac{di_{laee}}{dt} +$$

$$i_a(t)\sum_j (M_{a(h+e)j}\frac{di_{a(h+e)j}(t)}{dt}) + i_a(t)\sum_{\nu=1}^{\infty}\sum_{m=1}^{Q_2} M_{am\nu}\frac{di_{am\nu}(t)}{dt}. \tag{6.1}$$

The left hand side of equation (6.1) gives the instananeous power supply to the phase A of the machine from the power system. The first term of the right-hand side is the d.c. stator copper loss. The second, fifth and seventh terms represent the stored magnetic energy of the air gap field, which is delivered by, and returned to, the power system through each phase. The third term is the power associated with the slot leakage fluxes and is expended in the winding as the 'skin effect' loss. This term and the first add to give the a.c. stator copper loss for phase A winding. Terms four, six, and eight are the part of the end-leakage power magnetically stored in the end-region air space and which merely circulates around the windings at the end-region.

The ninth term of the right-hand side of equation (6.1) gives rise to the part of the end-leakage power, appearing as eddy-current

loss in the end-region materials. That part of the stored magnetic energy of the air gap field which appears as hysteresis and eddy current losses in the core originates in the tenth term. The last or the eleventh term of equation (6.1) gives rise to the sum of the power absorbed in the air gap for mechanical power conversion, the useful power transfer to the rotor, and the radial component of the non-end leakage power which is expended as additional iron loss on the surface and tooth-body of the rotor. Because the derivation of equations of the machines in chapter 3 is based on the assumption that there is only the radial component of magnetic field in the air gap, the radially and axially oriented components of the non-end leakage power are not represented in equation (6.1).

6.2 Method 1 for Predicting Stray Load Loss

6.2.1 A Criticism of the Conventional Method of Estimating Total Load Loss

No Load: The no load test is usually performed at the rated voltage and at the no-load supply current, which is about 1/3 the full-load or rated current. The interpretation commonly given to the result of this test is that since the slip is negligible, negligibly small current is induced in the rotor winding. Therefore, the no-load input power gives only the no-load stator conductor loss, the fundamental frequency core loss, and the friction and windage loss. Hence, normally deduced from such a test are the core, and friction and windage loss components of the apparent total loss, or total full-load loss determined using the

method of segregation. Also, partly deduced from the test is the magnetizing reactance of the machine.

The magnetizing reactance so deduced is basically that of the fundamental frequency and, hence, differs, though slightly, from that existing under the actual full-load performance. Also, since the core loss so determined from the no-load test does not include the additional losses in the iron surfaces and tooth body due to the harmonics, it will be slightly in error.

Locked Rotor: In the loss-segregation method of determining the total load loss of a squirrel-cage induction machine, the locked rotor test is performed in order to establish the rotor resistance, stator and rotor reactances parameters. These parameters are used in the equivalent circuit of the machine which in turn is used in determining the full-load performance. The locked rotor test is usually performed at the rated or full-load current and slip of unity. Under this condition of operation, compared to the full-load condition the displacement angle between the stator and rotor air gap field is increased. This will affect the magnitudes of the fundamental and harmonic components of the resultant air gap field. Also, the heating condition at this locked rotor condition is greater. Ultimately these may make the value of these parameters slightly different from those which exist under the actual full-load condition of operation.

Full-Load: The full-load loss performance is deduced from the conventional equivalent circuit for an induction machine. The usual

theory of this is based on the assumption that the radial component of the magnetic field in the air gap of the machine is sinusoidally distributed in space, and forms a single wave that rotates round the air gap at its synchronous speed. This condition would only exist, however, if the surfaces of stator and rotor were both smooth, the windings were sinusoidally distributed on them, and saturation is absent.

In the real machine, as already demonstrated in the previous chapters, the windings are placed in slots. Therefore the resulting mmf and flux density distributions are not sinusoidal, but contain, apart from the fundamental wave, a series of harmonics, which also rotate round the air gap at their own synchronous speeds. Since the magnitudes of the mmf harmonics are proportional to the currents in the windings, the losses produced by them are also dependent on the load currents.

6.2.2 The Proposed Method

The shortcomings of the conventional method for determining losses under no load and locked rotor are not as serious as those discussed under full-load. The shortcomings discussed under full load are principally responsible for stray load loss in induction machines. Hence, it will be used as the basis for developing a method of prediction in conjunction with the new model presented in this work. Let us consider two machines: one is the actual machine: the other is hypothetical. The hypothetical machine is exactly the same as the actual machine except that under the same loading conditions the stator air gap field excitation is a single and purely sinusoidal mmf waveform,

instead of the non sinusoidal waveform, e.g. figure 4.18(a), which exists in the air gap of the actual machine.

The hypothetical machine is equivalent to a machine described by the conventional model or the machine representing the method of segregation. Since this machine is identical to the actual machine in every other respect, then the difference between the air gap powers of the two machines is equal to stray full-load loss. This implies that if the electromagnetic torque computed using the algorithm of section 5.2 for the actual machine is τ_{ema} and that computed for the hypothetical is τ_{emh}, then the stray full-load loss is

$$P_{stray} = 2\pi n_s(\tau_{emh} - \tau_{ema}) \tag{6.2}$$

6.3 Method 2 for Predicting Stray Load Loss

6.3.1 Estimation of Rotor Conductor Loss

For any harmonic ν and for the circular ladder network of the squirrel cage winding, figure 3.5, we can define a vector of the mesh currents as

$$i_{mesh\nu} = [i_{\nu 12} \quad i_{\nu 23} \quad \cdots \quad i_{\nu Q_2 1}] \tag{6.3}$$

The corresponding vector of the bar currents can be obtained according to equations (3.26(a)) and (3.26(b)) using the transformation matrix **c**. If this vector is defined as

$$i_{bar} = [i_{b\nu 1} \quad i_{b\nu 2} \quad \cdots \quad i_{b\nu Q_2}]^T \tag{6.4}$$

If each element of the vector in equation (6.3) is squared we obtain a new vector

$$i_{meshv2} = [i^2_{v12} \quad i^2_{v23} \quad \cdots \quad i^2_{vQ_21}] \tag{6.5}$$

In a similar manner, for equation (6.4) we have

$$i_{barv2} = [i^2_{bv1} \quad i^2_{bv2} \quad \cdots \quad i^2_{bvQ_2}] \tag{6.6}$$

The average rotor conductor loss can then be shown to be

$$P_{rcloss} = \frac{2}{vp}(r_b^T \, i_{barv2} + r_{er}^T \, i_{meshv2}) \tag{6.7}$$

where r_b^T and r_{er}^T are Q_2 vectors defined as

$$r_b^T = [r_{bv} \quad r_{bv} \quad \cdots \quad r_{bv}]$$

and

$$r_{er}^T = [r_{erv} \quad r_{erv} \quad \cdots \quad r_{erv}]$$

where r_{bv} is the real component of the bar impedance (see equation (3.20)), and r_{erv} is the real component of an end ring segment impedance (see equation (3.21)).

It has been shown in chapter 3, section 3.4, that the resultant resistance of a single mesh is

$$r_{meshv} = 4r_{bv} \sin^2\frac{vp\pi}{2Q_2} + 2r_{erv} \tag{6.8}$$

Therefore, an alternative to equation (6.7) can be written thus

$$P_{rcloss} = \frac{2}{vp} r_{meshv} \sum_{m=1}^{Q_2} i^2_{vm(m+1)} \tag{6.9}$$

6.3.2 The Proposed Method

If the real power loss components in induction machines are classified as:

(i) Stator copper loss; P_{scu}

(ii) Stator iron loss; P_{sfe}

(iii) Stator stray loss; P_{ss}

(iv) Rotor conductor loss; P_{rcu}

(v) Rotor iron loss; P_{rfe}

(vi) Rotor stray loss; P_{rs}

(vii) Friction and windage; P_{f+w}

then the generalized real power flow in induction motors may be illustrated as shown in figure 6.1. The horizontal bars depict the useful power flow, while the verticals show the losses. If the motor runs unloaded at the no-load supply current and slip, the flow diagram will be as shown in figure 6.2. If the motor runs loaded at full-load current and slip, the flow diagram will be as in figure 6.3.

With reference to the standard definition of stray load loss as stated in section 2.11.1 the friction and windage, and the core losses component of the apparent load loss are deduced from a no-load test. Thus applying the interpretation generally given to the result of this test, as discussed in section 6.2.1, implies that in figure 6.2 the rotor conductor loss, P_{rcunl}, and the rotor iron loss, P_{rfenl}, are zero. Then we can write,

$$P_{(f+w)nl} = P_{emnl} \tag{6.10}$$

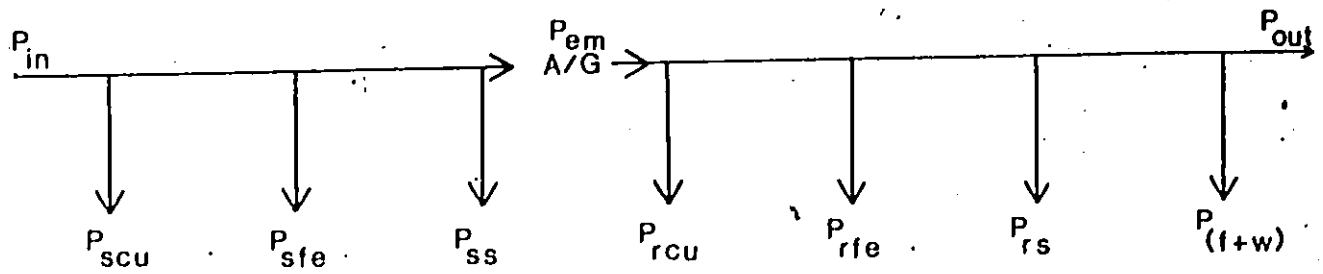

Figure 6.1: Generalized real power flow in induction motors

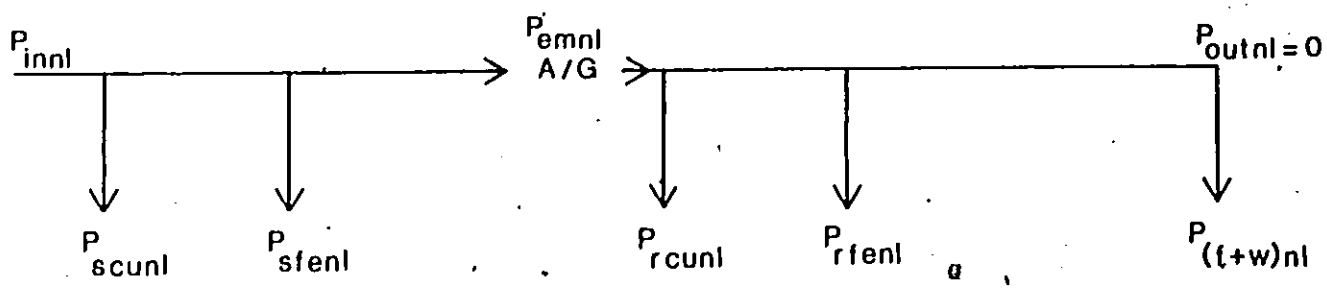

Figure 6.2: Real power flows at no-load.

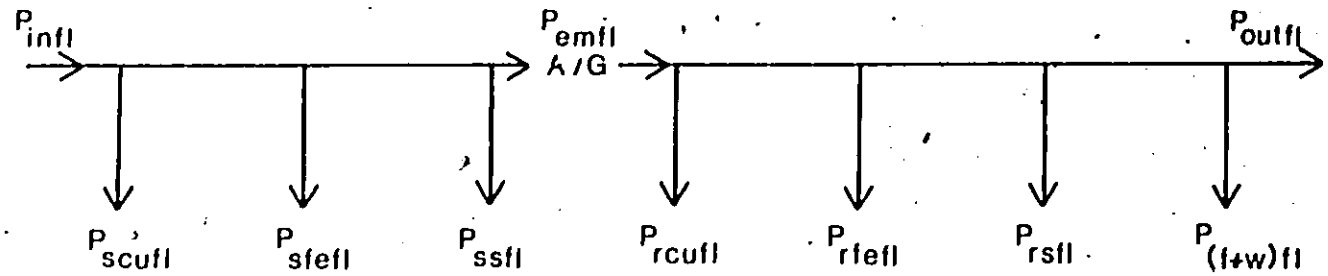

Figure 6.3: Actual real power flow at full-load.

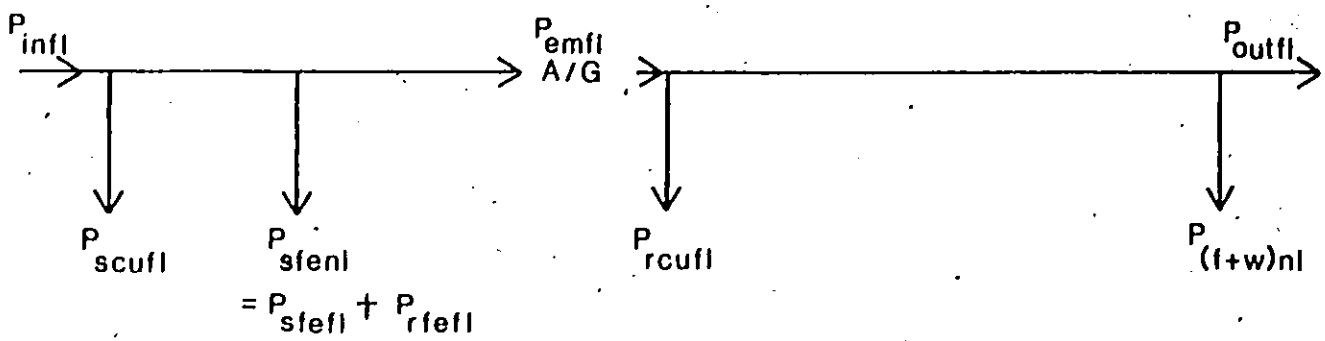

Figure 6.4: Apparent real power flow at full-load.

which means that the friction and windage loss measured at the no load is equal to the no load air gap power. We can also write,

$$P_{sfenl} = P_{innl} - P_{emnl} - P_{scunl} \tag{6.11}$$

By the standard definition in section 2.1.1 the full-load flow diagram corresponding to the apparent full-load losses is that shown in figure 6.4, as opposed to the one shown in figure 6.3 which illustrates the actual real power flow at the full-load condition of operation, and hence corresponds to the actual full-load losses. Since stray load loss is the difference between the actual full-load losses and the apparent full-load losses, then stray full-load power loss is the difference between figures 6.3 and 6.4. Thus, from the diagrams,

$$P_{ssfl} = P_{infl} - P_{emfl} - P_{scufl} - P_{sfenl} \tag{6.12}$$

and

$$P_{rsfl} = P_{emfl} - P_{outfl} - P_{rcufl} - P_{(f+w)nl} \tag{6.13}$$

The total stray full-load loss of the motor is then the sum of equations (6.12) and (6.13).

The developed algorithm, section 5.2, can be used to estimate P_{emnl}, and hence, $P_{(f+w)nl}$ and P_{sfenl} from the knowledge of the no-load current and slip. With the knowledge of the full-load supply current and slip P_{emfl} can be similarly deduced; and P_{rcufl} can be estimated using equation (6.7) and (6.9). The stator copper loss at full-load and no-load can be estimated from any standard expressions or numerical technique [10, 88, 89].

6.4 Measurement of Stray Load Loss

Stray load loss of the practical machine discussed in table 4.1 was measured by the input - output method (see section 2.2.1 (I)). Basically three tests were performed: no-load, d.c., and full-load tests. The no-load test was set up as shown in figure 6.5. The no-load core, and friction and windage losses were determined from this test as:

$$P_{nl} = P_1 + P_2 = P_{scunl} + P_{(f+w)} + P_{core} \tag{6.14}$$

where

$$P_{(f+w)} + P_{core} = P_{nl} - P_{scunl} \tag{6.15}$$

where

$$P_{scunl} = 3I^2_{nl}r'_1$$

where

$$I_{nl} = \frac{1}{3}(I_a + I_b + I_c)$$

The d.c. stator winding resistance was measured through a d.c. test. The set up of the test is as shown in figure 6.6. The rheostat was used to adjust the current to approximately the rated value. The winding temperature was measured in order for the test resistance to be corrected to that at full-load running test. The d.c. stator winding resistance was established from the test results as:

$$r_1 = \frac{V_{dc}}{2I_{dc}} \tag{6.16}$$

Finally, a full-load test was performed, figure 6.7. The

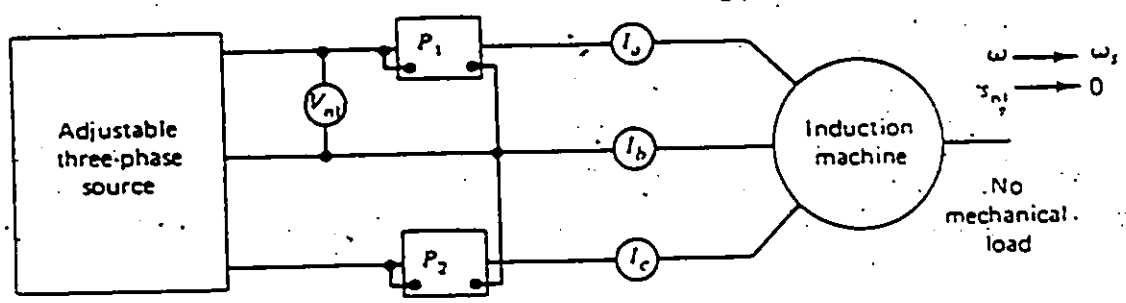

Figure 6.5: Set-up for No-Load Test

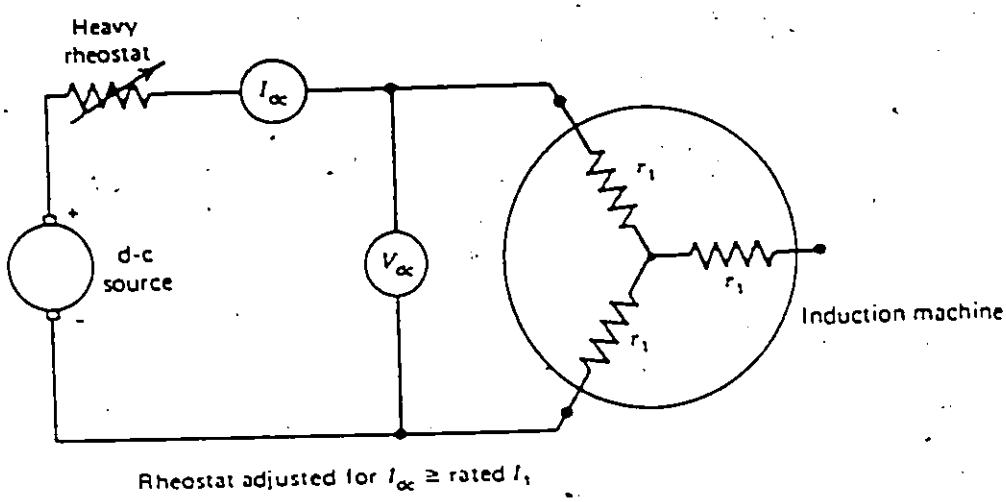

Figure 6.6: Set-up for D.C. Test

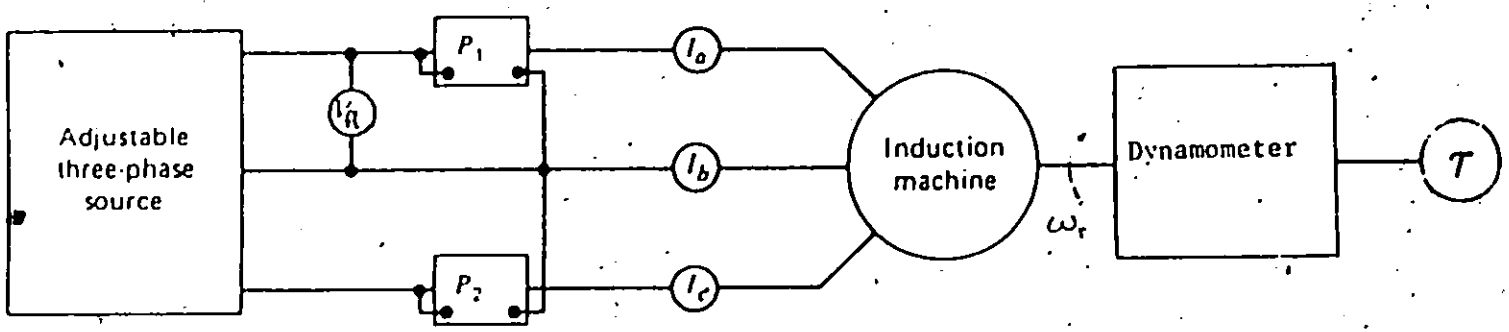

Figure 6.7: Set-up for Full-Load Test

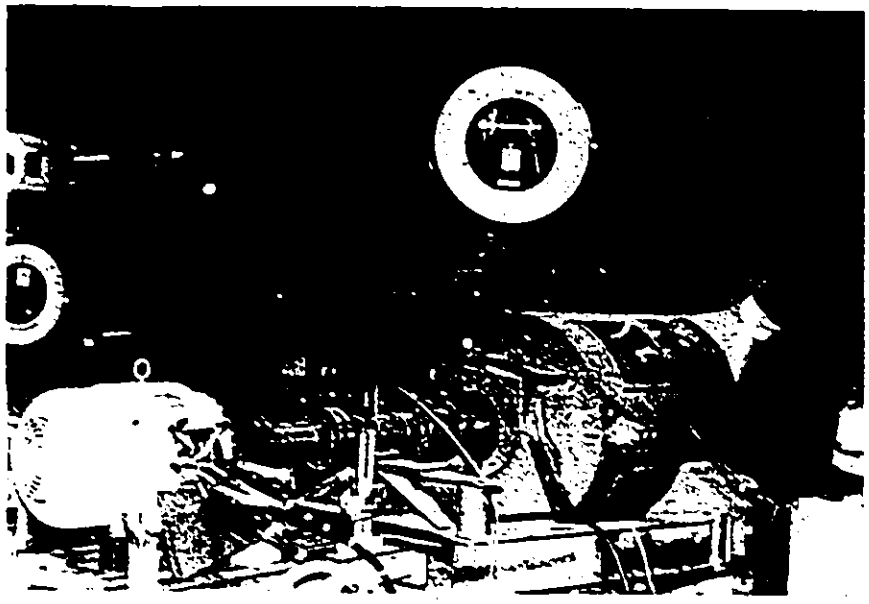

Plate 6.1: Set up for the full-load test of a squirrel-cage induction motor.

the rotor output torque was measured directly. The readings of the power input, speed, stator current, and temperature were noted. The following calculations were made from the result:

The output power,

$$P_o = \frac{\tau_o n_r}{9.545} \text{ Watts} \tag{6.17}$$

(Note τ_o is in N-m, and n_r is in r.p.m.)

$$P_{scufl} = 3I_{fl}^2 r_1' \tag{6.18}$$

where r_1' is r_1 corrected for skin effect and temperature.

$$I_{fl} = \frac{1}{3}(I_a + I_b + I_c)$$

$$P_{infl} = P_1 + P_2$$

$$P_{rcu} = s(P_{infl} - P_{scufl} - P_{(f+w)}) \tag{6.19}$$

Stray load loss was then determined as

$$P_{stray} = P_o - P_{infl} - (P_{rcu} + P_{scufl} + P_{(f+w)} + P_{core}) \tag{6.20}$$

6.4.1 Results and Comparison

The two proposed methods in sections 6.2.2 and 6.3.2 were used to predict the amount of stray load loss of the practical machine. The results compared with that as measured above and that predicted by the manufacturer at the design stage, using the nominal assignation method, are as shown in table 6.1.

Except for that obtained by the proposed method of section 6.2.2 all the stray load results in table 6.1 agree well. This observation

can not be well explained and neither can it be considered as general. This is because, as is elaborated in section 2.2.1, the input-output method of measuring stray load loss suffers accuracy problems: hence the measured result shown in the table can not be taken as reliable. In fact if stray load loss is to be measured as the difference of an electrical input power and a mechanical output power, then both have to be measured with an accuracy which cannot be achieved with the technique used in the experiment of section 6.4, particularly as far as mechanical power is concerned.

The results shown for the two proposed methods (columns B and C) do not agree because the calculation of that of column C in the table employed the measured efficiency, and hence may also be in error. The fact that the measured result compares closely with that shown in column A of table 6.1, whose prediction is based on nominal assignation together with some questionable empirical formulations, does not justify the latter because the former is unreliable.

Nevertheless, the two new techniques developed here for the prediciton of the stray load loss of an induction machine are theoretical. Such technique does not exist in the past works. The significance of a theoretical method of prediction is that it will enable many aspects of stray load losses in induction machines to be readily studied and therefore significantly enhance the accomplishment of the main objectives, which are understanding and reducing the loss. For the predictional problem of stray load losses to be resolved, and especially for the two proposed methods in this

Table 6.1: Comparison of Calculated and Measured Stray Load Loss

Full-load Loss Component	A	B	C	D
Stator copper loss (watts)	571	—	580	594
Stator iron loss (watts)	386	—	401	420
Rotor Conductor loss (watts)	435	—	477	405
Rotor Iron loss (watts)	—	—	—	—
Friction and Windage (watts)	138	—	121	128
Total Stray Full-load loss (watts)	405	669	375	450

A - Manufacturer's prediction at the design stage

B - Predicted by the method of section 6.2.2

C - Predicted by the method of section 6.3.2

D - Measured (section 6.4)

chapter to be adequately vindicated, there is a need to devise better methods for the experimental determination of stray load losses in induction machines. Hence, based on this fact two additional experiments have been developed in cooperation with Westinghouse (Canada) Limited during the course of this research. Unfortunately, their implementations are not yet completed. Some of the highlights of these additional experiments are as presented in appendix C.

CHAPTER 7

CONCLUSIONS

The correct understanding of the physical origin and components of stray load losses, and the developments of reliable methods of prediction and measurement of these losses are essential if induction machines are to be designed with minimum additional losses, namely stray load losses. The main aspects of the problem of these losses in induction machines, including aspects involving prediction and reduction, have been reviewed in detail. The questions of definition, origin, components, and effects have been researched. It was discovered that some of the commonly used terminologies in the subject area formed major obstacles to progress in definition. During the course of the investigation it was found that the principle effects of stray load loss are heating of various machine components, loss of output torque, acceleration and retardation effects, lowered efficiency, and, as a practical consequence of these, derating of the machine.

Several existing techniques that were proposed for measurement of stray load losses have been discussed. They all may be classified into two main categories: full-load, and light load tests. For one reason or another, none of these methods is found adequate for accurate determination of this loss.

A survey of the state of art of the prediction and calculational

problems has revealed that the empirical literature published on achievements in this aspect is subject to very large discrepancies reported between the calculated and measured results. It was found that, because of this, most manufacturers worldwide prefer at the design stage to account for stray load loss through a nominal assignation method based on empirical expressions. Universally these techniques are based only on the past experiences of the designers and have little rational analytic basis. Their only basis is the measured values determined by subtracting actual accounted results from predicted.

Various methods and means that have been suggested for the reduction of stray loss components in a machine have been investigated. It was found that successful reduction of losses has not been achieved.

A theory of analysis of squirrel cage induction machines has been developed. This theory precludes the introduction of the notions of belt and zig-zag reactances, or differential reactance, and does not view the air gap flux as the sum of linkage and leakage components. Squirrel cage windings are treated exactly the way they are configured with each bar or end ring segment represented by a lumped impedance. The highlight of the theory is that ultimately the machine ends up been represented by a set of linear periodic differential equations whose independent variables are the rotor mesh or bar currents, depending on the formulation.

The theory is conceptually simple and general in that the solutions to the differential equation are guessed. Hence, there is an infinite number of possible solutions out of which a suitable solution

technique has been developed.

The question of how to account for the effects of the actual and fictitious slot openings has been addressed. The technique used is based on the existing method which was originally developed by Carter [85]. For any instant the circumferential distribution, along the mean air gap radius, of the slot permeance factor can easily be developed.

Saturation was accounted for by a saturation factor. A means of developing the distribution of the saturation factor along the air gap periphery has also been devised. The ease with which these slot permeance and saturation factor distributions can be obtained made it easy to study how waveforms and harmonics create or influence stray load losses. It was found that the slot openings including those due to saturation (fictitious slot openings), reduce the magnitude of the fundamental of the air gap flux density waveform and augment the magnitude and change the phases of the harmonic components. The percentage of reduction and augmentation are constant with load for actual slot openings but vary with load for fictitious slot openings. Except for the fictitious slot openings, saturation does not affect the phases. It does reduce the magnitude of the fundamental component of the field waveform and creates saturation harmonics. The percentage of reduction and the magnitude of the saturation harmonics increase non-linearly with current, and hence with load. However, saturation reduces the magnitudes of the harmonic components in the field waveform. An additional effect of this is that the net effect of augmentation by the slot openings is limited.

During the course of this investigation an approximate means of separating the air gap flux density waveform into its fundamental, saturation, and other space harmonics has been developed. This separation enables harmonics to be accounted for in the developed model.

An expression for the electromagnetic torque in terms of the rotor and resultant air gap flux density distribution has been derived. Although the resulting expression is familiar, its derivation has never before been made without the assumption of a smooth air gap and linear magnetic circuits. Apart from the fact that this expression has enabled the concept of the development of synchronous and asynchronous torques to be easily derived, it also enables the net developed torque to be calculated once without having to calculate it for each harmonic component separately.

The theory developed, together with the ideas developed for the manipulation of the air gap waveforms with saturation, and the derived instantaneous and time-average electromagnetic torques, has been structured into an algorithm which is considered a model of the behaviour of squirrel cage induction machines. This algorithm has enabled the validity of the theory and the model to be verified through a study of the torque-speed characteristic of a practical machine. The predicted torque-speed curve has been compared with that measured by means of an accelerometer. The fact that the predicted torque compares well with the measured substantiates the theory and the developed model, hence enabling the new approach to be employed to the problem of theoretical prediction of stray load losses. The algorithm has also

been employed in carrying out brief studies of the influence of harmonics on the developed torques.

From a criticism of the ideas leading to the conventional equivalent circuit and the estimation of total load loss of an induction machine through the method of segregation, it is apparent that stray load losses occur as the result of the difference between the actual phenomenon in the machine and that represented by the method of segregation or the conventional model. Hence, on this basis, two new methods for predicting the amount of stray load loss have been developed for predicting this loss at the design, manufacturing, or utilization stage of an induction machine. Measurement of this loss has been conducted in the laboratory with the hope of substantiating the developed techniques. The fact that conclusive comparison could not be established between stray load loss predicted by these developed techniques and that measured through the input-output test suggests that further work, of an experimental nature, is required.

The concepts of useful and loss power flow in induction machines have also been discussed in detail; particularly as they relate to the machine equations representing the presented theory. Unlike stator copper loss, for example, stray load loss is neither distinct in terms of location nor unique in terms of the phenomena that lead to it. Part of stray load loss occurs in the stator and rotor conductors due to induced harmonic currents. Part occurs in the iron materials, especially the stator and rotor surfaces and the tooth body closest to the air gap, due to harmonics and leakage fluxes as hysteresis, eddy-

current and skin effect losses. Stray loss also exists as eddy current loss in the end region materials due to end-leakage flux. Other components, though not considered in the model are easily included. They may include eddy current loss in the iron material due to skew leakage flux, and additional losses due to manufacturing imperfection, especially the interbar current loss.

Finally, the advantage of the new model developed in this work has been found to be that it precludes the erroneous approximations characterizing the conventional one; hence it offers a better prediction of machine behaviours. In addition it lends itself easily to the study and the evaluation, even at the design stage, of stray load loss. As well, it still retains the simplicity and versatility of the conventional equivalent circuit. That is, it is not so mathematically complex as to require the solution of a set of differential equations or to involve an iterative approach. Furthermore, it lends itself easily to the study of the steady state performance of unbalanced machines, and machines fed with non sinusoidal supplies.

The specific original contributions claimed for this work are:

1) Insight into the problems of definition, origin, components, effects, measurement, prediction and reduction results from a comprehensive review of the subject of stray load losses in induction machine. The review also highlights the state of the art of the subject.

2) Presentation of a conceptually simple and general theory of squirrel cage induction machine which results in a set of linear periodic differential equations, having an infinite number of possible solutions.

3) Development of a new model which is based on the theory presented. As stated above, the new model has several advantages.

4) The procedure for the derivation of expressions for fictitious slot opening widths for any shape of slot (see sections 3.6.3).

5) Development of an approximate means of separating a saturated non sinusoidal waveform of an air gap flux density waveform into its fundamental, saturation, and other space harmonics.

6) The method of accounting for saturation in the model through the use of saturation factor distribution is an original contribution.

7) The derivation of a torque expression without making the assumption of a smooth air gap and a linear magnetic circuit. The expression was derived by introducing a conceptual current.

8) Invention of two theoretical methods suitable for predicting stray load loss at the design, manufacturing, and utilization stages.

7.1 Suggestions for Further Works

This research work, apart from revealing some other promising topics for further investigation, has particularly drawn attention to the need for experimental investigation of the subject of stray load losses in induction machines. This need was realised during the course of this research and was addressed. Although not yet fully implemented, two additional sets of experiments have been developed by the author in cooperation with Westinghouse (Canada) Limited (see Appendix C).

Immediate further work, therefore, should involve the completion of these experiments.

Other promising topics for further investigation are:

1) The development of other techniques for simultaneously solving the two machine equations (stator and rotor) such that the presence of harmonic power in the power system, from the air gap of the machine, if any, is reflected in the solution.

2) An extension of the developed model in this work to account for the effect of skewing and inter-bar currents loss.

3) The use of the developed algorithm in this work to comprehensively investigate parasitic torques.

4) Repetition of the investigation in this work for an unbalanced machine and induction machine fed with non sinusoidal supply.

REFERENCES

1. Jimoh, A. A., Findlay, R. D., and Poloujadoff, M., "Stray Losses in Induction Machines: Part I, Definition, Origin, and Measurement", IEEE Trans. on Power Apparatus and Systems, Vol. PAS-104, No. 6, pp. 1506-1512, June 1985.

2. Jimoh, A. A., Findlay, R. D., and Poloujadoff, M., "Stray Losses in Induction Machines: Part II, Calculation and Reduction", ibid., pp. 1500-1505, June 1985.

3. Olin, E. M., "Determination of Power Efficiency of Rotating Electric Machines. Summation of Losses Versus Input-Output Method", Trans. AIEE, 1912, vol. XXXI, part II, p. 1695-1719.

4. Schwarz, K. K., "Survey of Basic Stray Losses in Squirrel-Cage Induction Motors", Proc. IEE, 1964, 111, p. 1565-1574.

5. Alger, P. L., Angst, G., and Davies, E. J., "Stray Load Losses in Polyphase Induction Machines", Trans. AIEE, 1957, 78, p. 349-357.

6. Bird, B. M., "Measurement of Stray Load Losses in Squirrel-Cage Induction Motors", Proc. IEE, 1964, 111, p. 1697-1705.

7. Christofides, N., "Origins of Load Losses in Induction Motors with Cast Aluminum Rotors", ibid., 1965, 112, p. 2317-2332.

8. Morgan, T. H., Brown, T. E., and Schumer, A. T., "Reverse-Rotation Test for the Determination of Stray-Load Loss in Induction Machines", Trans. AIEE, 1939, 58, p. 319-324.

9. Odok, A., "Stray-Load Losses and Stray Torques in Induction Machines, ibid., 1958, 77, pt. II, p. 43-53.

10. Alger, P. L., "The Nature of Induction Machines", (Gordon and Breach, 1965).

11. Chalmers, B. J., and Williamson, A. C., "Stray Losses in Squirrel-Cage Induction Motors. Validity of Reverse-Rotation Test Method", Proc. IEE, 1963, 110, p. 1773-1777.

12. Barton, T. H., and Ahmad, V., "The Measurement of Induction-Motor Stray Loss and its Effect on Performance", Proc. IEE, 1958, 1050, p. 69-75.

13. Diamant, P., "The High Efficiency Induction Machine of the 1980's. Part One", Trans. IEEE, 1981, PAS-100, p. 4965-4968.

14. Bonnett, A. H., "Understanding Efficiency in Squirrel-Cage Induction Motors", Trans. IEEE, 1980, IA-16, p. 476-483.

15. "IEEE Standard Test Procedure for Polyphase Induction Motors and Generators", ANSI/IEEE Std 112-1983.

16. Alger, P. L., Campbell, G., Davies, E. J., "Discussion on Stray Load Losses in Squirrel-Cage Induction Motors", papers by Schwarz, K. K. [4], Bird, B. M. [6], Chalmers, B. J., and Williamson, A. C. [11], Proc. IEE, 1965, 112, p. 1750-1759.

17. Heller, B., and Hamata, V., "Harmonic Field Effects in Induction Machines", (Elsevier Scientific, 1977).

18. Koch, C. J., "Measurement of Stray Load Loss in Polyphase Induction Motors", Trans. AIEE., 1932, 51, p. 756-763.

19. Christofides, N., and Adkins, B., "Determination of Load Losses and Torques in Squirrel-Cage Induction Motors", Proc. IEE, 1966, 113, p. 1995-2005.

20. Bird, B. M., and Holgate, A., "Discussion on Determination of Load Losses and Torques in Squirrel Cage Induction Motors", by Christofides, N., and Adkins, B., Proc. IEE, 1967, 114, p. 1085-1088.

21. Gainstev, Y. V., "Errors in the Reverse Rotation Method for Determining Stray Losses in Squirrel-Cage Induction Motors", Elektrotekhnika, vol. 36, no. 2, 1965, p. 58-61.

22. Ware, D. H., "Measurement of Stray Load Losses in Induction Motors", Trans. AIEE, 1945, 64, p. 194-196.

23. Field, A. B., "Eddy Currents in Large Slot-Wound Conductors", Proc. AIEE, Vol. 24, p. 761-88, 1905.

24. Field, A. B., "Idle Currents", Journal IEE, 1906, Vol. 37, p. 83-93.

25. Taylor, H. W., "Eddy-Currents in Stator Windings", Journal IEE, 1920, Vol. 58, p. 279-300.

26. Gilman, R. E., "Eddy-Current Losses in Armature Conductors", 1920, Trans. AIEE, Vol. 39, p. 997-1056.

27. Gilman, R. E., "Eddy-Current Losses in Armature Conductors", 1924, ibid., Vol. 43, p. 246-51.

28. Lyon, W. V., "Heat Losses in the Conductors of A-C Machines", ibid., Vol. 40, 1921, p. 1361-95.

29. Lyon, W. V., "Heat Losses in the Stranded Armature Conductors", ibid., Vol. 41, 1922, p. 199-214.

30. Lammeraner, J. and Stafl, M., "Eddy Currents", (CRC Press, 1966).

31. Summers, I. H., "Reduction of Armature Copper Losses", Trans. AIEE, 1927, 46, p. 101-111.

32. Murkherji, K. B. C., "Stray Load Losses in a.c. Rotating Machinery, A Review of the State of the Art", ERA Report 7/T102, 1956.

33. Anderson, O. W., "Finite Element Solution of Skin Effects and Eddy Current Problems", IEEE Summer Power Meeting, Mexico City, paper A77 616-6, 1977.

34. Chari, M. V. K. and Csendes, Z. J., "Finite Element Analysis of the Skin Effect in Current Carrying Conductors", IEEE Trans. on Mag., Vol. MAG-13, No. 5, Sept. 1977, p. 1125-27.

35. Weiss, J., and Csendes, Z., "Efficient Finite Element Solution of Multipath Eddy Current Problems", ibid., Vol. MAG-18, No. 5, Nov. 1982, p. 1710-12.

36. Chari, M. V. K. and Bedrosian, G., "Electromagnetic Field Analysis of Eddy Current Effects in Rotating Electrical Apparatus and Machinery", ibid., p. 1713-15.

37. Rossmaier, V., "Berechnugn der durch unisolierte Kafige lenovgerufenen Zusatzverluste bei Asynchronmaschinen", Elektrotech. u. maschinenbau, 1939, 57, p. 249-55.

38. Alger, P. L., "Induced High-Frequency Currents in Squirrel-Cage Windings", Trans. AIEE, 1957, 76, pt. III, p. 724-29.

39. Subba Rao, V., and Butler, O. I., "Stray Losses of Polyphase Cage-Induction Motors with Particular Reference to the Condition of Imperfect Rotor-Bar-Iron Insulation", Proc. IEE, 1969, 116, p. 737-51.

40. Dreyfus, L., "Le Calcul des pertes par courants de foucault dans les joues non-magnetriques de serrange des totes des grandes turbo-generatrices", in "Comptes Rendus du Congres Internationale d'Electricite", 1932, Vol. 4, p. 273-80.

41. Winchester, R. L., "Stray Losses in the armature end iron of large turbine generators", Trans. AIEE, 1958, 74, p. 381-91.

42. Kant, M., "Etude due champ magnetique de la partie frontale d'un turbo-alternateur", Rev. Gen. Electr., 1966, 75, p. 913-20.

43. Hawley, R., Edwards, I. M., Heaton, J. M. and Stoll, R. L., "Turbogenerator end-region magnetic fields: Qualitative prediction by field plotting", Proc. IEE, 1967, 114 (8), p. 1107-14.

44. Douglas, J. F. H., "Reactance of End-Connections", Trans. AIEE, 1937, 56, p. 257-59.

45. Caldwell, Jr., B. H., "End-Winding Inductance of a Synchronous Machine", ibid., p. 455-61.

46. Harrington, D., "Forces in Machine End-Windings", ibid., 1952, 71 part III, p. 849-59.

47. Carpenter, C. J., "The application of the method of images to machine end-winding fields", Proc. IEE, 1960, 107A, p. 487-500.

48. Smith, R. T., "End Component of armature leakage reactance of round rotor generators", Trans. AIEE, 1958, 77, p. 636-47.

49. Honsinger, V. B., "Theory of End-Winding Leakage Reactance", ibid., 1959, 78, p. 417-26.

50. Honsinger, V. B., "Measurement of End-Winding Leakage Reactance", ibid., p. 426-31.

51. Ashworth, D. S., and Hammond, P., "The calculation of the magnetic field of rotating machine. Pt. 2 - The field of turbogenerator end-windings", Proc. IEE, 1961, 108A, p. 527-38.

52. Lawrenson, P. J., "The magnetic field of the end-windings of turbo-generators; ibid., p. 538-48.

53. Tegopoulos, J. A., "Determination of the magnetic field in the end zone of turbine generators", Trans. AIEE, 1963, 82, p. 562-72.

54. Reece, A. B. J. and Pramanik, A., "Calculation of the end region field of a.c. machines", Proc. IEE, 1965, 112 (7), p. 1355-68.

55. Stoll, R. L., and Hammond, P., "Calculation of the magnetic field of rotating machines Part 5. Field in the end region of turbogenerators and the eddy-current loss in the end plates of stator cores", Proc. IEE, 1966, 113, (11), p. 1793-1804.

56. Myerscough, C. J., "Calculation of magnetic fields in the end regions of turbogenerators", ibid., 1974, 121, p. 653-56.

57. Okuda, H., "Calculation of magnetic field distribution in the end zone of generator winding", Electr. Eng. Jpn., 1969, 89, No. 11, p. 27-33.

58. Sarma, M. S., Wilson, J. C., Lawrenson, P. J. and Joki, A. L., "End winding leakage of high-speed alternators by three-dimensional field determination", Trans. IEEE, 1971, PAS 90, p. 465-73.

59. Jacobs, D. A. H., Minors, R. H., Myerscough, C. J., Rollason, M. L. J., and Steel, J. G., "Calculation of losses in the end region of turbogenerators", Proc. IEE, 1977, 124, (4), p. 356-61.

60. Chari, M. V. K. and Silvester, P., "Analysis of turboalternators magnetic field by finite elements", IEEE Trans., 1971, PAS-90, p. 454-59.

61. Chari, M. V. K. and Sharma, D. K., and Kudlacik, H. W., "No load magnetic field analysis in the end region of a turbine generator by the method of finite elements", IEEE Winter Meeting, New York, Paper No. A76 230-3, 1976.

62. Okuda, H., Kawamura, T., and Nishi, M., "Finite-Element Solution of Magnetic Field and Eddy Current Problems in the End Zone of Turbine Generators", ibid., Paper No. A76141-2, 1976.

63. Howe, D., and Hammond, P., "Distribution of axial flux on the stator surface of the ends of turbogenerators", Proc. IEE, 121, No. 9, p. 980-90.

64. Baird, J., "Eddy-Current Losses in Induction Motor End-Turn Clamping Rings", Trans. AIEE, 1954, Part III, No. 12, p. 660-664.

65. Howe, D., and Hammond, P., "Examination of the axial flux in stator cores with particular reference to turbogenerators", Proc. IEE, 1974, 121, (12), p. 1536-41.

66. Tavner, P. J., Penman, J., Stoll, R. L. and Lorch, H. O., "The influence of winding design on the axial flux in laminated stator cores", ibid., 1978, 125, (10), p. 948-56.

67. Tavner, P. J., Hammond, P., and Penman, J., "Contribution to the study of leakage fields at the ends of rotating electrical machines", ibid., 1978, 125 (12), p. 1339-49.

68. Ming-Zheng, H., and McPherson, G., "Experimental Investigation of the Field and Stray Losses of the End Bells of an Induction

Motor", IEEE/PES 1983 Summer Meeting, Los Angeles, paper 83 SM 481-9, July 1983.

69. Dreyfus, L., "Die zusatzlichen Eisenverluste in Drehstromasynchronmotoren I.", Elektrotechnik und Maschinenbau, 1927, Vol. 45, p. 737-56.

70. Linkuous, C. E., "Effect of Skew on Induction Motor Magnetic Fields", Trans. AIEE, Vol. 74, 1955, p. 760-65.

71. Heller, B., and Joki, A. L., "Losses in Squirrel-Cage Motors due to Rotor Skew", Trans. IEEE, 1971, PAS-90, p. 557-63.

72. Behdashti, A., and Poloujadoff, M., "A New Method for the study of Inter-Bar Currents in Polyphase Squirrel-Cage Induction Motors", Trans. IEEE, 1979, PAS-98, p. 902-11.

73. Butler, O. I., and Mohammed, M. Z., "Change of Stray Loss of a Cage Induction Motor with Axial Variations of the Interbar Resistance", Proc. IEE, 1971, 118, p. 884-86.

74. Lindsay, J. F., "Modelling of Stray Losses in Induction Machines", IAS '75 Annual Meeting, paper 47C, p. 1045-48.

75. Lindsay, J. F., and Barton, T. H., "A Modern Approach to Induction Machine Parameter Identification", Trans. IEEE, 1972, PAS-91, No. 4, p. 1493-1500.

76. Bates, J. J. and Tustin, A., "Temperature rises in Electrical Machines as Related to the Properties of Thermal Networks", Proc. IEE, Vol. 103A, No. 11, 1956, p. 471-82.

77. Diamant, P., "The High Efficiency Induction Machine of the 1980's. Part One", Trans. IEEE, 1981, PAS-100, p. 4965-68.

78. Kato, K., Kohno, H., Urabe, K., and Takahashi, T., "Analytical and Experimental Study or Reducing High Frequency Pulsatoin Losses Created by the Existence of Armature Slots Using Magnetic Slot Wedges", Elect. Eng. in Japan, Vol. 102, No. 5, 1982, p. 103-11.

79. Chalmers, B. J., and Richardson, J., "Performance of some Magnetic Slot Wedges in an Open-Slot Induction Motor", Proc. IEE, 1967, 114, p. 258-60.

80. Kaga, A., Anazawa, Y., Akagami, H., Watabe, S., and Makino, M., A Research of Efficiency Improvement by Means of Wedging with Soft Ferrite in Small Induction Motors", IEEE Trans. on Mag., Vol. MAG-18, No. 5, Nov. 1982, p. 1547-49.

81. Anazawa, Y., Kaga, A., Akagami, H., Watabe, S., and Makino, M., "Prevention of Harmonic Torques in Squirrel Cage Induction Motors by Means of Soft Ferrite Magnetic Wedges", IEEE Trans. on Mag., Vol., MAG-18, No. 5, Nov. 1982, p. 1550-52.

82. Spooner, E., "Stray Loss in Solid-Rotor Induction Machines, Proc. IEE, 1982, 129, Pt. B., p. 181-89.

83. Oberrett, K., "13 Regeln fur minimale Zusatzverluste in Induktionsmotoren", Bull. Oerlikon, 1969, Nr. 389/390, p. 2-12.

84. Kostenko, M., Piotrovsky, L., "Electrical Machines", Volume II, MIR Publishers, Moscow, 1977.

85. Freeman, E. M., "The Calculation of Harmonics, Due to Slotting, in the Flux-Density Waveform of a Dynamo-Electric Machine", Proc. IEE, 1962, Vol. 109, Part C, No. 16, p. 581-588.

86. Carter, F. W., "The Magnetic Field of the Dynamo-Electric Machine", Journal IEE, 64, pp. 1115, November 1926.

87. Lee, C. H., "Saturation Harmonics of Polyphase Induction Machines", Trans. AIEE, Oct. 1961, p. ~~597~~-603.

88. Chalmers, B. J., and Dodgson, R., "Waveshapes of Flux Density in Polyphase Induction Motors Under Saturated Conditions", Trans. IEEE on Power Apparatus and Systems, Vol. PAS-90, No. 2, 1971, p. 564-569.

89. Veinott, C. G., "Theory and design of small induction motors", McGraw-Hill, New York, 1959.

90. Levi, E., "Polyphase Motors: A Direct Approach to Their Design", John Wiley & Sons, New York, 1984.

91. Liwschitz-Garik, M. and Whipple, C. C., "A-C Machines", Van Nostrand, Priceton, N.J., 1961.

92. Alger, P. L., and Wray, J. H., "Double and Triple Squirrel Cages for Polyphse Induction Motor", Trans. AIEE, Aug. 1953, p. 637-642.

93. Alger, P. L., Ivanes, M., and Poloujadoff, M., "Equivalent Circuits for Double-Cage Induction Motors", Electric Machines and Electromechanics, 1978, p. 137-145.

94. Williamson, S., and Begg, M. C., "Calculation of the Bar Resistance and Leakage Reactance of Cage Rotors with Closed Slots", Proc. IEE, Vol. 132, Pt. B, No. 3, May 1985, p. 125-132.

95. Gray, Clifford B., "Air-Gap Power flow and Torque Development in Electrical Machines - Can We Teach the Fundamentals?", Trans. IEEE on Power Apparatus and Systems, Vol. PAS-103, No. 4, April 1984, p. 874-879:

96. Alger, P. L., and Oney, W. R., "Torque-Energy Relations in Induction Machines", Trans. AIEE, April 1954, p. 259-264.

APPENDIX A

A FAST FOURIER TRANSFORM ALGORITHM

The fast Fourier transform of a real vector of length N, where N is any positive even integer, may be computed as follow:

Given a set of N (even) data points $A = (a_1, a_2, \ldots a_N)$ where $a_1, a_2, \ldots a_N$ are real numbers, then the cosine transformation and sine transformation are computed as

$$C_{K+1} = 2 \sum_{j=0}^{N-1} A_{j+1} \cos(2\pi jk/N) \tag{A.1}$$

and

$$S_{k+1} = 2 \sum_{j=0}^{N-1} a_{j+1} \sin(2\pi jk/N) \tag{A.2}$$

for $k = 0, 1, \ldots N/2$.

The foregoing therefore implies that if any waveform is represented as a vector A, then the set of sinusoidal components equivalent of that waveform can be computed using equations (A.1) and (A.2). The two sinusoidal waveform components (cosine and sine) represented by these two equations can be lumped together by treating (A.1) and (A.2) as real and imaginary components, respectively, of a complex of the transformation i.e.

$$A_k' = C_k + jS_k \tag{A.3}$$

The magnitude of the kth sinusoidal component of A represented by the complex equation (A.3) is, therefore,

$$|A_k'| = \sqrt{(C_k^2 + S_k^2)} \qquad (A.4)$$

and the corresponding phase is

$$\beta_k = \tan^{-1} \frac{S_k}{C_k} \qquad (A.5)$$

APPENDIX B

CALCULATION OF THE ROTOR BAR IMPEDANCE PARAMETERS

B.1 Resistances

1) Slot bar resistances:

For any harmonic ν the resistance of any of the regions in the slot of figure 4.14 is

$$R_{\nu i} = J_{R\nu i}\frac{1}{\gamma A_i} \; ; \; i=A,N,B \qquad (B.1)$$

where subscript i refers to a region in figure 4.14. $J_{R\nu i}$ is the "skin effect" constant (see B.3 below). The conductivity

$$\gamma = \frac{\gamma_{20}}{1 + \alpha(t-20)} \qquad (B.2)$$

where γ_{20} = conductivity of 20^oC

α = temperature coefficient

t = temperature in ^oC

and

$\gamma_{20} = 3.22 \times 10^7$ S/m ; $\alpha = 3.7 \times 10^{-3}\,{}^oC^{-1}$ for aluminium.

2) End-ring resistance

The resistance of an end-ring segment at any harmonic is

$$r_{er} = \frac{\pi D_{ring}}{\gamma Q_2 A_{ring}} K_{ring} \qquad (B.3)$$

where, K_{ring}, which accounts for the effect of wide resistance rings, is given by the expression [89]

$$K_{ring} = \frac{p}{2}\left(1 - \frac{D_i}{D_{ring}}\right)\frac{1 + (D_i/D_{ring})^p}{1 - (D_i/D_{ring})^p} \tag{B.4}$$

B.2 Reactances

1) Slot's self leakage reactances:

For any harmonic ν the self leakage reactances of the regions, A, N, B, and O in figure 4.14 are respectively

$$x_{\nu i} = J_{x\nu i} \cdot 2\pi f s_\nu \mu_o l K_{si} \; ; \; i = a, n, b, 0 \tag{B.5}$$

where $J_{x\nu i}$ is the "skin effect" constant (see B.3 below). K_{si} is the slot leakage constant for the region i. For the shapes in figure 4.14 the expressions for these constants are derived in reference [84] as

$$K_{sa} = 0.623 + h_A/3w_A$$

$$K_{sn} = h_N/3w_N$$

$$K_{sb} = 0.66$$

$$K_{so} = h_o/w_{o2}$$

2) End-winding leakage:

For one segment of a rotor cage ring, and for any harmonic ν, this is calculated using an expression derived by Liwschitz-Garik [91]:

$$x_{er} = 2\pi f s_\nu L_{e\nu} \tag{B.6}$$

where the end leakage inductance

$$L_{e\nu} = \frac{1}{2}\frac{\mu_o Q_2}{m_1 p^2}\frac{1}{3}[(l_b - l_c) + k\tau']\varepsilon_\nu \tag{B.7}$$

where

$$\tau' = D_{ring}/p$$

$$k = \begin{cases} 0.36 & \text{for } p = 2 \\ 0.18 & \text{for } p > 2 \end{cases}$$

$$\varepsilon_\nu = \frac{\sin^2(\alpha_{s2}/2)}{\sin^2(\alpha_{s\nu}/2)}$$

where

$$\alpha_{s\nu} = (2\nu/p)\alpha_{s2}$$

$$\alpha_{s2} = \pi p/Q_2$$

B.3 Skin-Effect

For regions A, N, and O in figure 4.14 the skin-effect factors, $J_{R\nu i}$ and $J_{x\nu i}$, are taken as unity while for region B they are calculated as [92].

$$J_{R\nu B} = \frac{\sqrt{(1.5x)}\,(\sinh\sqrt{(6x)} + \sin\sqrt{(6x)})}{\cosh\sqrt{(6x)} - \cos\sqrt{(6x)}} \tag{B.8}$$

and

$$J_{x\nu b} = \frac{\sqrt{(1.5x)}\,(\sinh\sqrt{(6x)} + \sin\sqrt{(6x)})}{x(\cosh\sqrt{(6x)} - \cos\sqrt{(6x)})} \tag{B.9}$$

where $x = x'_{\nu b}/R'_{\nu B}$.

$x'_{\nu b}$ and $R'_{\nu B}$ are the d.c. self leakage reactance and resistance respectively for region B and they are calculated from expressions (B.5) and (B.1) respectively when $J_{R\nu b} = 1$ and $J_{x\nu b} = 1$.

The reason for accounting for skin effect only in the top bar is because at high slip nearly all the current flows in the top bar only. At low slip, however, the current will flow chiefly in the bottom bar, but now the skin effect in all the bars will be small because of low frequency.

APPENDIX C

A BRIEF DISCUSSION OF THE DEVELOPED EXPERIMENTS

The need for experimental investigation of the subject of stray load losses in induction machines was realized during the course of this research and was addressed. Although not yet fully implemented, two additional sets of experiments have been developed by the author in cooperation with Westinghouse (Canada) Limited:

(i) A calorimetric method for studying stray load loss has been developed using a number of fine thermocouple probes conveniently located within the machine. In addition, search coil probes have been installed in the rotor of a machine prior to casting, figure C.1 and plates C.1(a) and C.1(b). When the whole set up is completed the aim will be to take readings from the probes through a computerized data acquisition system when running the motor under conditions such that the heat generating points due to stray load loss will be detected and determined from the readings.

The method is to devise a model accounting for transient and steady state temperature rise of various parts of the machine. With the several thermocouples located in the machine, this can be identified as a set of thermal sources (rotor iron, rotor cage, stator iron, stator windings) associated with several thermal capacitors, thermal resistances and an external temperature reference.

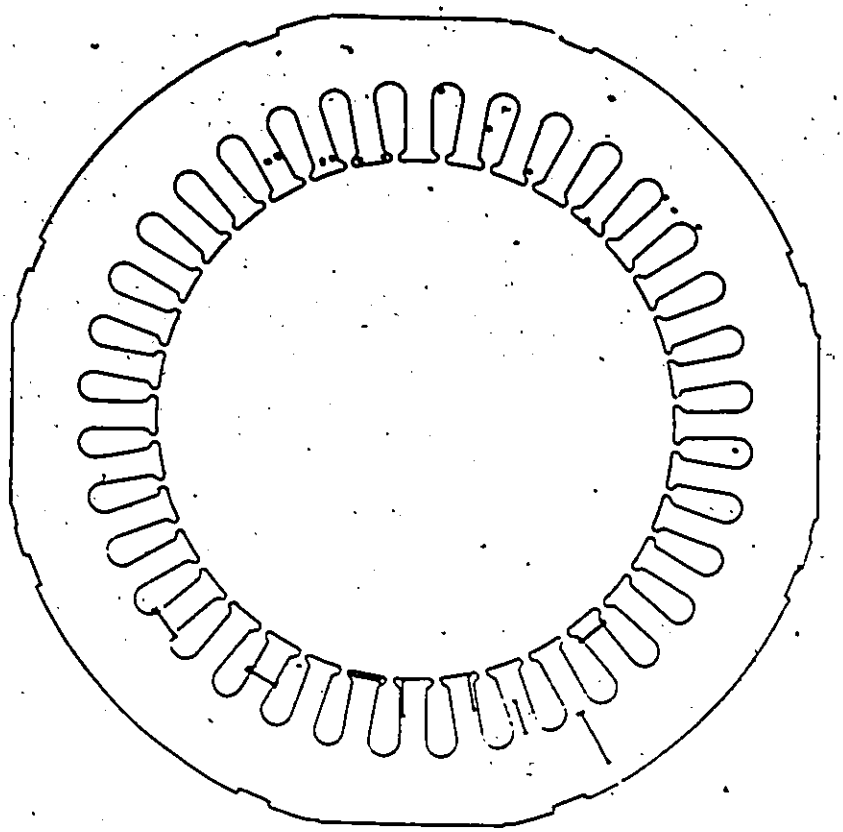

(a) Stator

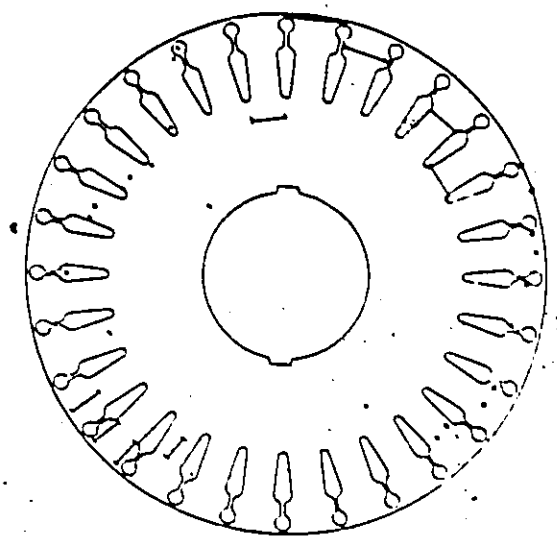

. - Thermocouples locations
⊢ - Search coils

(b) Rotor

Figure C.1: Instrumenting machine laminations for the Calorimetric method experiment

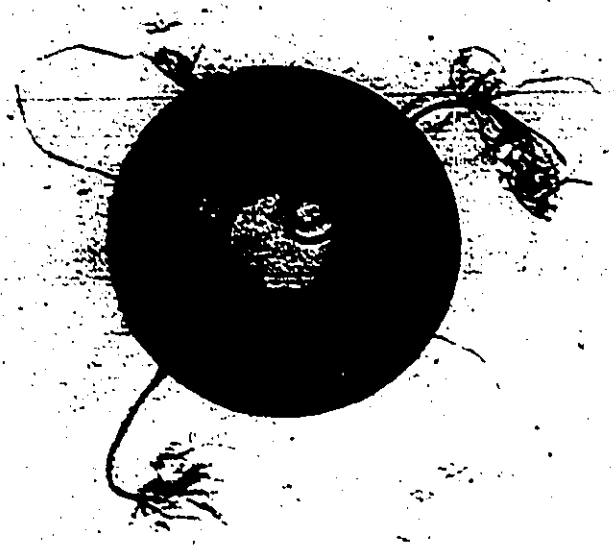

(a)

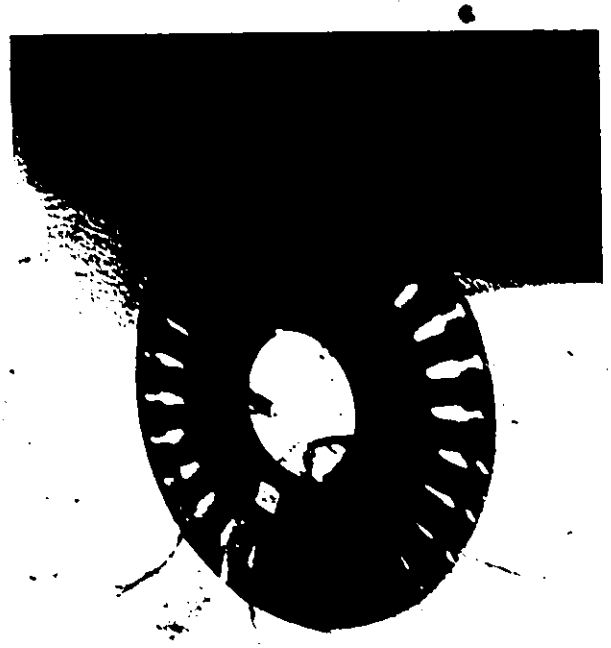

(b)

Plate C.1: Instrumented machine laminations for the Calorimetric method experiment

Since the measurements depend only upon losses, stray losses can be easily detected; they can even be separated into a few components. It is hoped that it will be possible to analyze losses not only for low values of slip, but for any value of slip, and any value of supply voltage, a fact which is of utmost importance for the development of a complete analysis.

(ii) As an additional benefit, a novel experimentation idea to study the inter-bar currents problem has been developed. This topic until now has been mainly a matter of conjecture. The technique would allow interbar current and voltage waveforms to be displayed on an oscilloscope. Like (i) above, skewed and unskewed motors are being studied. The investigative routine requires that fine copper wire probes be embedded in certain locations in the rotor, figure C.2 and plate C.2.

Stages which are involved in implementing these experiments are:

1) Experiment method and procedure development;

2) Instrumenting;

3) Manufacturing of the motor;

4) Performing the experiments; and

5) Analysis of results.

Stages 1 and 2 have been completed and stage 3 has been started. Due to both technical and economic problems this stage has been delayed. After completion it will only require to implement stages 4 and 5.

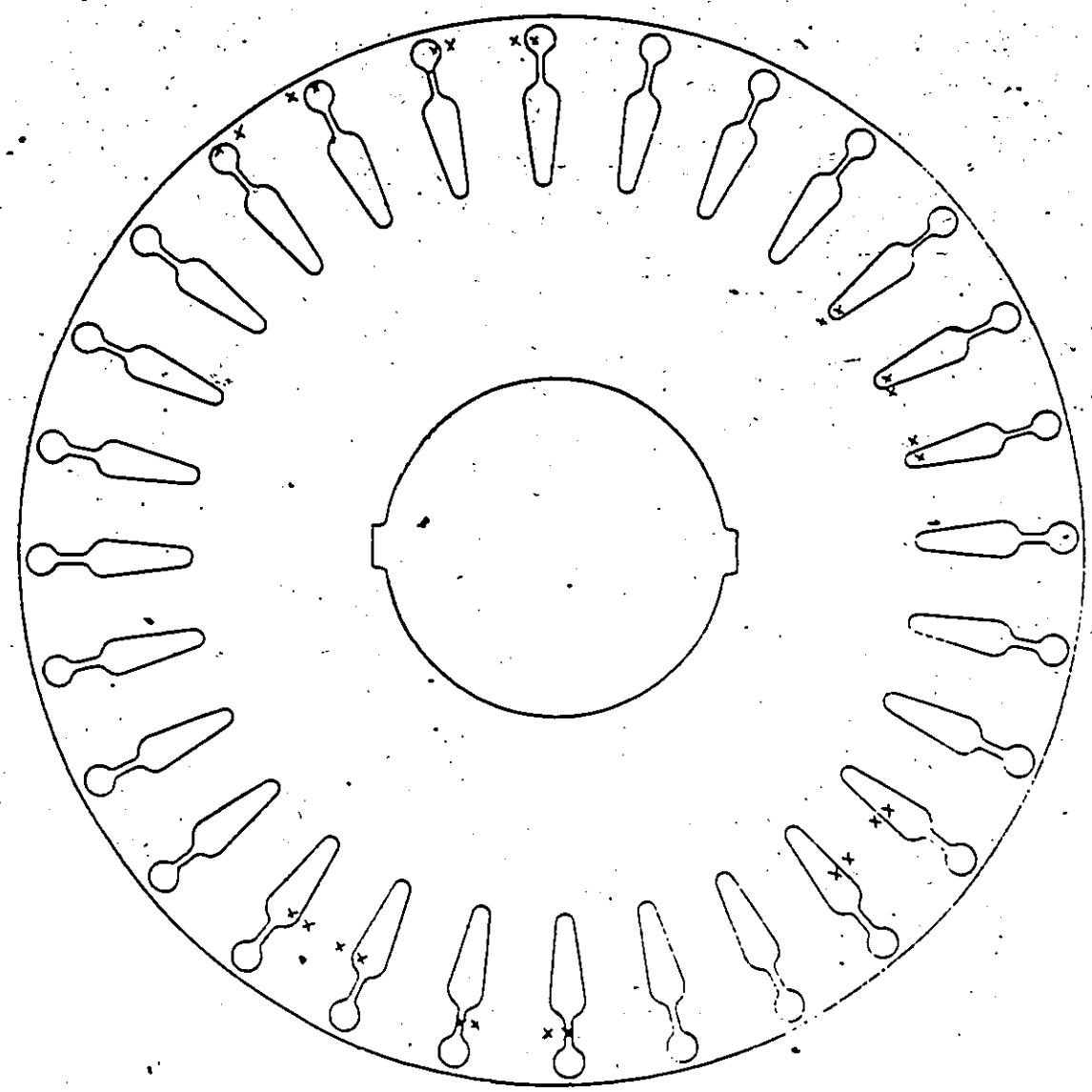

x - Copper wire probe locations

Figure C.2: Instrumenting a rotor lamination for a study of the inter- bar currents problem.

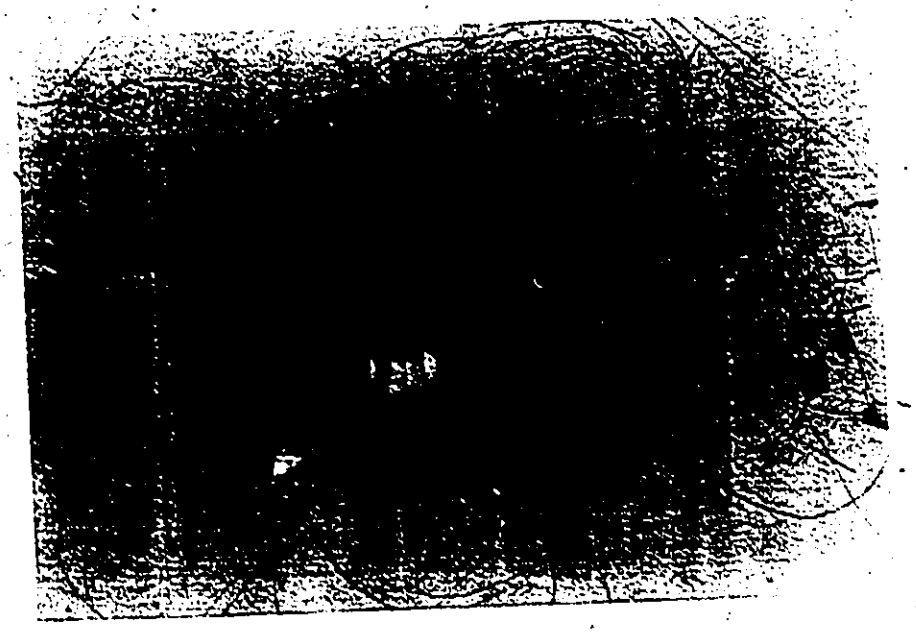

Plate C.2: Instrumented rotor lamination for a study of the inter-bar current problem